

Modelling hypothermia in patients undergoing surgery

Citation for published version (APA):

Severens, N. M. W. (2008). *Modelling hypothermia in patients undergoing surgery*. [Phd Thesis 1 (Research TU/e / Graduation TU/e), Mechanical Engineering]. Technische Universiteit Eindhoven.
<https://doi.org/10.6100/IR638063>

DOI:

[10.6100/IR638063](https://doi.org/10.6100/IR638063)

Document status and date:

Published: 01/01/2008

Document Version:

Publisher's PDF, also known as Version of Record (includes final page, issue and volume numbers)

Please check the document version of this publication:

- A submitted manuscript is the version of the article upon submission and before peer-review. There can be important differences between the submitted version and the official published version of record. People interested in the research are advised to contact the author for the final version of the publication, or visit the DOI to the publisher's website.
- The final author version and the galley proof are versions of the publication after peer review.
- The final published version features the final layout of the paper including the volume, issue and page numbers.

[Link to publication](#)

General rights

Copyright and moral rights for the publications made accessible in the public portal are retained by the authors and/or other copyright owners and it is a condition of accessing publications that users recognise and abide by the legal requirements associated with these rights.

- Users may download and print one copy of any publication from the public portal for the purpose of private study or research.
- You may not further distribute the material or use it for any profit-making activity or commercial gain
- You may freely distribute the URL identifying the publication in the public portal.

If the publication is distributed under the terms of Article 25fa of the Dutch Copyright Act, indicated by the "Taverne" license above, please follow below link for the End User Agreement:

www.tue.nl/taverne

Take down policy

If you believe that this document breaches copyright please contact us at:

openaccess@tue.nl

providing details and we will investigate your claim.

Modelling Hypothermia in Patients Undergoing Surgery

PROEFSCHRIFT

ter verkrijging van de graad van doctor aan de Technische Universiteit Eindhoven, op gezag van de Rector Magnificus, prof.dr.ir. C.J. van Duijn, voor een commissie aangewezen door het College voor Promoties in het openbaar te verdedigen op woensdag 5 november 2008 om 16.00 uur

door

Natascha Maria Wilhelmus Severens

geboren te Brunssum

Dit proefschrift is goedgekeurd door de promotoren:

prof.dr.ir. A.A. van Steenhoven
en
prof.dr.mr.dr. B.A.J.M. de Mol

Copromotor:
dr. W.D. van Marken Lichtenbelt

Copyright © 2008 by N.M.W. Severens

Cover design by Bregje Schoffelen, Oranje Vormgevers

All rights reserved. No part of this publication may be reproduced, stored in a retrieval system, or transmitted, in any form, or by any means, electronic, mechanical, photocopying, recording, or otherwise, without the prior permission of the author.

Printed by the Eindhoven University Press.

A catalogue record is available from the Eindhoven University of Technology Library

ISBN: 978-90-386-1430-4

Contents

1	Introduction	1
1.1	Clinical background of hypothermia	1
1.2	Physiological aspects of thermoregulation	2
1.3	Human thermal models	8
1.4	Goal and thesis outline	9
2	Passive model of bioheat transfer	13
2.1	Introduction	13
2.2	The passive part	15
2.2.1	Boundary conditions	16
2.2.2	Numerical methods	20
2.2.3	Numerical convergence	20
2.3	Submodels	21
2.3.1	Individual body characteristics	22
2.3.2	Heart lung machine	23
2.3.3	Forced-air heating	23
2.3.4	Circulating water mattress	24
2.3.5	Heat loss through wound with topical ice slush	24
2.4	Simulation with passive model	25
2.5	Discussion	27
3	Effect of forced-air heaters on perfusion and temperature distribution	29
3.1	Introduction	29
3.2	Materials and methods	30
3.2.1	Patients	30

3.2.2	Anesthesia	30
3.2.3	Protocol	31
3.2.4	Morphometric measurements	31
3.2.5	Temperature measurements	31
3.2.6	Skin perfusion measurements	32
3.2.7	Leg blood flow measurements	33
3.2.8	Statistics	33
3.2.9	Data analysis	34
3.3	Results	34
3.3.1	Patient characteristics	34
3.3.2	Core temperature	34
3.3.3	Mean skin temperature	35
3.3.4	Thigh temperature	35
3.3.5	Skin blood flow	37
3.3.6	Leg blood flow	37
3.4	Discussion	40
3.4.1	Perfusion	40
3.4.2	Temperature	42
3.5	Comparison of passive model and cardiac surgery measurements	43
3.6	Conclusion	45
4	Active model for cardiac surgery	47
4.1	Introduction	47
4.2	Interplay between temperature, metabolism and perfusion	48
4.3	Model formulation	49
4.4	Pharmacological models	50
4.4.1	Flow-limited versus diffusion-limited approach	52
4.4.2	A hybrid physiological model for propofol	54
4.4.3	Comparison of the pharmacological model to other models	58
4.5	Determining the vasoconstriction threshold	59
4.6	Vasoconstriction-propofol relation	60
4.7	Validation results	62
4.8	Discussion	66
5	Measurement of model coefficients of sympathetic vasoconstriction	69
5.1	Introduction	69
5.1.1	Physiology of the autonomous control of vasomotion	69
5.1.2	Control concept	70
5.1.3	Modelling the cutaneous sympathetic vasoconstrictor tone and amplification coefficients	70
5.2	Materials and methods	71
5.2.1	Subjects	71

5.2.2	Protocol	72
5.2.3	Temperature measurements	73
5.2.4	Skin perfusion	73
5.2.5	Forearm blood flow	74
5.2.6	ECG	74
5.2.7	Data analysis	75
5.2.8	Statistics	76
5.3	Results	77
5.3.1	Temperature	77
5.3.2	Perfusion	78
5.3.3	Relation perfusion/temperature	79
5.3.4	Experimentally determined amplification coefficients and sympathetic vasoconstriction tone	81
5.3.5	Discussion of results	85
5.4	Determination of proportionality constants of other body parts	86
5.5	Validity of the new model for healthy subjects	88
5.5.1	Sensitivity analysis of model coefficients	88
5.5.2	Dependent experiment	90
5.5.3	Independent experiments	91
5.6	Validity of the model for cardiac surgery under moderate hypothermic conditions	93
5.6.1	Aortic valve surgery	94
5.6.2	Coronary surgery	94
5.7	Discussion of model achievements	94
6	Additional applications of the computer model	99
6.1	Introduction	99
6.2	Cardiopulmonary bypass at 17°C	100
6.2.1	Protocol	101
6.2.2	Model adjustments for extreme cold	101
6.2.3	Results	102
6.3	Heat transfer during orthopedic back surgery	104
6.3.1	Experimental protocol	104
6.3.2	Simulation protocol	105
6.3.3	Results	106
6.4	Effect of changing temperature protocols	109
6.4.1	Cooling the head during deep hypothermic cardiac arrest	109
6.4.2	Comparison of old and new cardiac surgical procedures: moderate versus mild hypothermia	111
6.4.3	Influence of changing temperature protocols on afterdrop under moderate hypothermic conditions	112
6.5	Discussion	112

7	Conclusions and recommendations for further research	115
7.1	Conclusions	115
7.2	Recommendations for further research	117
A	Setpoint theory and its alternatives	131
A.1	Introduction	131
A.2	Concepts	132
A.3	Discussion	135
B	Properties of the passive part	137
B.1	Model properties of the different body parts	137
B.2	Convective heat transfer coefficients	139
B.3	Clothing parameters	141
B.4	Determination of the forced-air heat exchange coefficients	142
B.5	Evaporative heat losses from the wound surface	144
C	Measurement techniques	147
C.1	Laser Doppler flowmetry	147
C.2	Skin temperature	148
C.3	Ultrasound	150
C.4	Fat percentage	151
C.5	Plethysmography	151
C.6	Heart rate variability	151
D	Biological zero in laser Doppler flowmetry	153
D.1	Introduction	153
D.2	Literature	154
D.3	Measurements	155
D.4	Discussion	156
E	Leg blood flow calculations	159
E.1	Pulsatile flow	159
E.2	Non-pulsatile flow	163
	Samenvatting/Summary	165
	Dankwoord	169
	Publications	171
	Curriculum vitae	173

CHAPTER 1

Introduction

1.1 Clinical background of hypothermia

Thermal imbalances are common during surgeries that take place under general anesthesia. This often leads to peri- and postoperative hypothermia. Hypothermia is an abnormally low body temperature, affiliated with core body temperatures less than 36°C (Taguchi and Kurz, 2005). Hypothermia, even mild hypothermia (32-35°C), is most of the time associated with numerous adverse outcomes. In literature, it is reported that hypothermia increases the risk for wound infection (Knighton et al., 1986; Sessler, 1995), impairs immune function, causes haematological problems (Valeri et al., 1987; Cereda and Maccioli, 2004), decreases breakdown of drugs while the anesthetic effect stays equal (Sessler, 1995) and causes postoperative shivering, which is especially dangerous for patients that had heart surgery (Mort et al., 1996). Low environmental temperature and especially the pharmacological impairment of thermoregulatory defense mechanisms are the main causes of hypothermia.

On the other hand, during some procedures, like during resuscitation from cardiac arrest (cf. Merchant et al. (2006); Storm et al. (2008)) and cardiac surgery, hypothermia is deliberately induced, as hypothermia provides protection against cardiac and cerebral ischaemia (local oxygen deficiency, which can lead to tissue damage). A decrease in temperature lowers metabolism, which decreases oxygen demand of the cells. In this way, there is less chance to get tissue damage due to oxygen deficiency. At the end stage of a cardiac surgery, the body is rewarmed with help of the heart lung machine. The major thermal difficulty of rewarming is that heat is transferred to the core much faster than it can be dissipated to peripheral tissue. Due to the resulting unnatural distribution of body heat, patients often show an unwanted drop in core temperature when the heart lung machine is decoupled. This core temperature

drop is called afterdrop. Afterdrop adversely affects recovery and methods have to be found to minimize afterdrop as much as possible.

In this introductory chapter an overview is given of the physiology of thermoregulation under normal circumstances. Thereafter, the influence of anesthesia on thermoregulatory responses is explained. Then, actively induced hypothermia during cardiac surgery and the occurrence of afterdrop is discussed in more detail. Next, it is explained why a new human thermal model would help to gain more insight in the heat transfer processes during (cardiac) surgery and would help to improve intraoperative temperature protocols. Finally, the project goal is defined and an overview is given of the approach and layout of the thesis.

1.2 Physiological aspects of thermoregulation

Normal thermoregulation

Core body temperature of mammals is a carefully guarded physiological parameter. Humans, when healthy, maintain a core temperature of about 37°C with only small variations during the course of the day. The hypothalamus is the primary thermoregulatory control center in mammals. The thermal sensors, that are required for continuous monitoring of the thermal state of the body, are located in the core and skin. The skin surface, deep abdominal and thoracic tissue, spinal cord, and deep abdominal portions of the brain each contribute roughly 20 percent to the information input that arrives at the hypothalamus. The temperature of the hypothalamus itself also contributes roughly 20 percent of the information used in thermoregulatory control (Sessler, 1997). Values higher than the thresholds for warmth or lower than the thresholds for cold trigger thermoregulatory defenses. Values between the thresholds for vasoconstriction and sweating lie in the interthreshold-range. In this range, no thermoregulatory responses are activated. The interthreshold range is normally about 0.2°C. But it must be noted, that in physiology still different theories exist on body temperature control. In appendix A, an overview is given of the main points of view. The outputs from the thermoregulatory reactions counteract the temperature changes caused by external or internal disturbances. In this way a negative feedback system is formed.

Thermoregulatory responses

Thermoregulatory responses are predominantly under neural control; only in long-term adaptations hormonal processes play a role (Schmidt and Thews, 1989). Three neural systems are involved in thermoregulation: 1) the somatomotor system that controls the regulation of body pose and movement, 2) the sympathetic system and 3) the parasympathetic system (figure 1.1).

The somatomotor system activates shivering and behavioural responses. Behaviour response is the most effective thermoregulatory response. Behavioural responses include re-

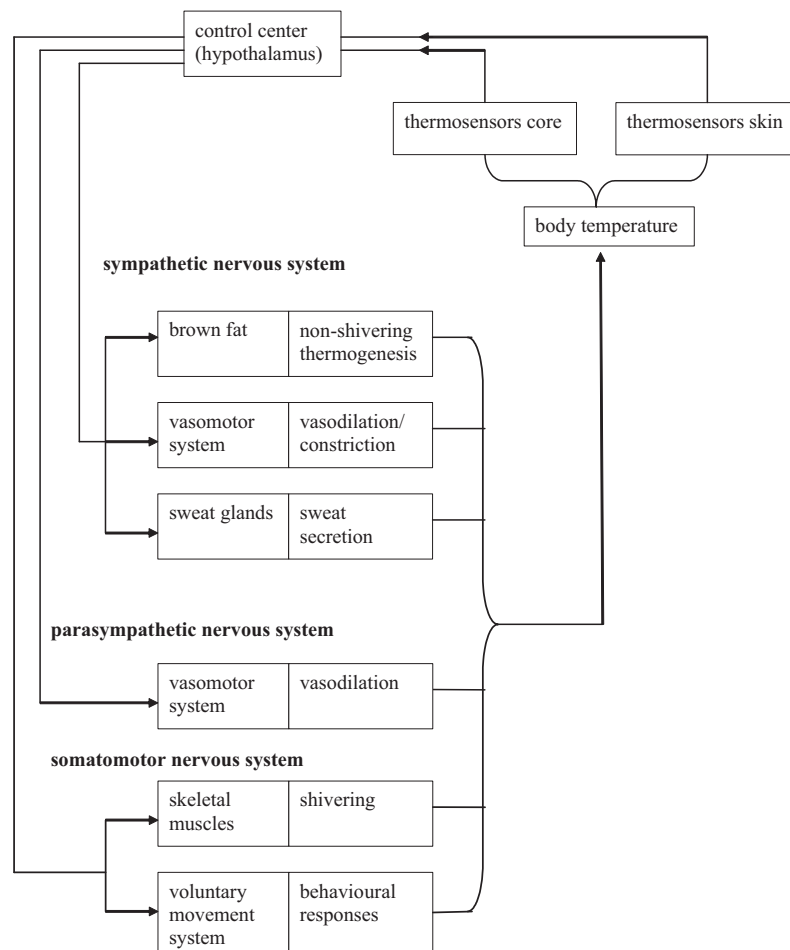


Figure 1.1: Sympathetic, parasympathetic and somatomotor nervous system for controlling thermoregulation.

sponses like dressing warmly, moving or adjusting the temperature of the surrounding. Shivering is an involuntary muscle activity that increases the metabolic heat production to two to three times the normal value.

Reactions activated by the sympathetic nervous system include non-shivering heat production (also called non-shivering thermogenesis), vasomotion and sweat secretion. Non-shivering thermogenesis is mediated by receptors on nerves that terminate on brown fat. Brown fat contains a protein (UCP-1) that enables the direct transformation of substrate into heat via mitochondrial uncoupling (Wijers et al., 2008). Vasomotion comprehends the vascular tone changes due to local alteration in smooth muscle constriction and dilation. Due to vasomotion, the resistance to blood flow in peripheral blood vessels is affected, which alters the amount of blood that arrives in the periphery and changes the amount of heat transport to that location. Consequently, this will influence the temperature of the periphery and therefore also the amount of heat exchanged with the environment. The effect of vasomotion is depicted in figure 1.2. In a warm environment vasodilation occurs. The diameter of the

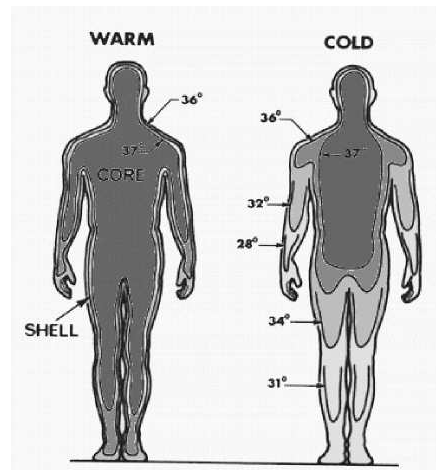


Figure 1.2: Body temperature distribution in warm and cold environment, after Schmidt and Thews (1989). Heat transfer to the periphery can be much increased or reduced by vasomotion, leading to increased or decreased heat transfer to the environment. Core temperature stays almost constant.

blood vessel's interior is widened. This provides an increase of blood flow to the periphery. As a result, skin temperature increases, which leads to an increase in heat transfer to the environment. The opposite mechanism, occurring in a cold environment, is called vasoconstriction and is defined as narrowing of the core-to-peripheral blood vessels by contraction of the blood vessels' muscular wall. By limiting the blood flow to the more peripheral parts, and consequently to the skin, heat is retained in the core while at the same time heat losses to the environment are reduced because of the smaller skin-to-environmental temperature gradient.

When the body is too warm, sweat excretion is an effective method to lose body heat in a dry environment. Evaporation of sweat requires a lot of heat that is withdrawn from the skin.

Most blood vessels are constricted and dilated by sympathetic stimuli. Parasympathetic stimulation generally has almost no effect on blood vessels, but does dilate vessels in certain restricted areas, such as in the blush area of the face (Guyton, 1976).

Thermoregulation is often represented using a system of thresholds, gains and maximum intensities. In those descriptions, the reaction threshold is represented by the temperature at which that response is triggered. The gain of a system describes the change in response intensity, for instance the vasoconstrictor tone, as temperature further deviates from the triggering threshold.

Thermoregulation during surgery with general anesthesia

Influence of anesthetics

Anesthesia causes substantial perturbation in the human heat balance. Nearly all patients administered anesthesia become hypothermic. Body core temperature decrease ranges between 1-3°C, depending on the type and amount of anesthesia, the surgery time and the ambient temperature and insulation (Sessler, 2000).

While under normal circumstances behavioural compensation contributes more than autonomic regulation, under peri-anesthetic conditions only (impaired) autonomic responses contribute. General anesthesia let the reaction thresholds, at which thermoregulatory reactions are triggered, shift to values that deviate much more from 37°C than under normal conditions. The interthreshold range that is defined as the body temperature range where no response is activated, may increase from about 0.2 to 4°C, see figure 1.3 (Sessler, 1995).

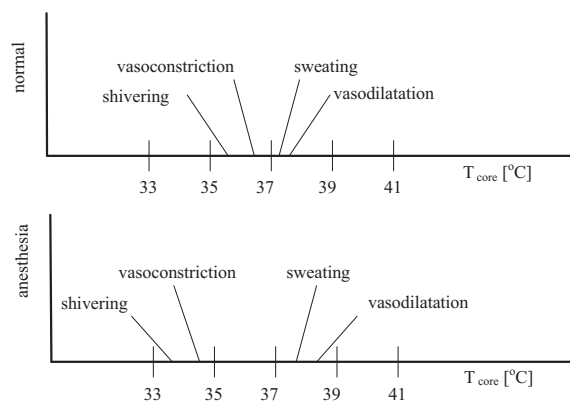


Figure 1.3: Thermoregulation in a normal person and anesthetized person.

Normally, anesthesia induced hypothermia develops with a typical pattern. During the first hour, core temperature decreases by 1-1.5°C. This drop is followed by a slower, linear decrease in core temperature for 2-3h. Thereafter, the core temperature will stabilize (Kurz et al., 1995a). The first drop is due to the induction of the general anesthesia. Administration of general anesthesia promotes vasodilation by two ways: 1) by shifting the vasoconstriction thresholds to lower values than normal, through which vasoconstriction is triggered at lower temperatures than normal (indirect effect) and 2) a lot of anesthetic agents contain vasodilators (direct effect). Vasodilation allows core heat to flow down the temperature gradient to the periphery. The second, slower linear decrease in core temperature results from the prevalence of heat loss over metabolic heat production. Metabolic heat production is reduced by 15-40% during general anesthesia (Matsukawa et al., 1995b, 1997; Sessler, 2000). The final stage is the core temperature plateau. This type of situation is reached when heat production equals heat loss. This situation can both exist with and without activation of thermoregulatory responses, but the latter situation is more rare.

Temperature manipulation during open heart surgery

During open heart surgery, often a heart lung machine is used. Surgeries performed with the help of a heart lung machine differ from other types of surgery in that enormous amounts of heat can be removed (cooling stage) or added (warming stage) to the body. In most open heart surgeries, hypothermia is deliberately induced because hypothermia offers protection to ischaemia of heart and cerebral tissue. Target core temperatures between 28 and 32°C are common for e.g. aortic valve replacements and coronary artery bypass grafts, whilst during surgery on the aortic arch the patient can be cooled to as low as 16-18°C (Tindall et al., 2008).

On nearing completion of the surgical procedure, the core temperature is restored to pre-bypass level by adjusting the temperature of the heat exchanging fluid. Typical time traces of core and peripheral temperatures during and after cardiac surgery are shown in figure 1.4. In the figure the different thermal stages of a cardiac surgery are visible: the administration of anesthesia preceding the cooling stage, the cooling stage with the heart lung machine, the warming stage with the heart lung machine and the postbypass stage.

Working principle heart lung machine

The principle of the heart lung machine (also known as pump-oxygenator or cardiopulmonary bypass pump) is quite simple, see figure 1.5. Oxygen-poor blood is withdrawn from the right upper atrium into a reservoir. From there, the blood is pumped through an artificial lung, also known as oxygenator. Here, the oxygen-poor blood comes into contact with the fine surfaces of the device itself. Oxygen gas is delivered to the interface between the blood and the device, permitting the blood cells to absorb oxygen. The oxygen-rich blood is actively pumped back into the patient through a tube connected to the arterial circulation. In modern heart lung machines, also shed blood that is spilled in the operating field around the heart is

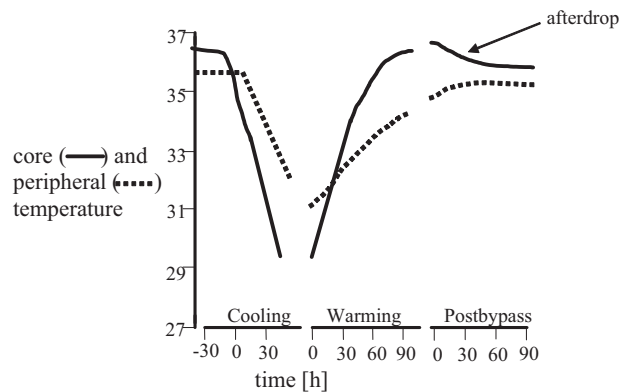


Figure 1.4: Typical core and peripheral temperature traces observed during aortic valve surgery in the Academic Medical Center in Amsterdam, The Netherlands, see also chapter 3 of this thesis.

collected and returned to the heart. In this manner, the patient's blood stores are preserved as much as possible throughout the operation.

The patient's body temperature can be controlled by cooling or heating the blood by means of the heat exchanger in the oxygenator. This allows the surgeon to use low body temperatures as a tool to preserve the function of the heart and other vital organs during the period of artificial circulation. Medication can be given through connectors in the system.

To initiate heart-lung bypass, the patient's clotting system must temporarily be deactivated by an anticoagulant, called heparin. Otherwise, the patient's blood would immediately clot when being exposed to the heart lung machine. To stop the heart beat, a cold cardioplegia solution is mixed with blood and infused into the coronary circulation. Also, cold saline is poured over the heart. The heart is then usually safe from tissue injury for 2 to 4 hours.

When the intervention of the heart has been completed, the heart beat is restored by increasing the arterial inflow temperature. When the patient's body temperature is at a normal level and the strength of the heart's own contractions is strong enough, the heart lung machine can be withdrawn. At this stage, the tubes are removed from the patient's circulation, and the anticoagulation medication is reversed.

Afterdrop

A drawback of rewarming with help of the heart lung machine is that heat is transferred to the core compartment (brain and trunk) more quickly than to the peripheral compartment (arms and legs), see also figure 1.4. At the end of the pump warming, even though core temperature is restored to pre-bypass levels, a considerable amount of mass of peripheral tissue remains at

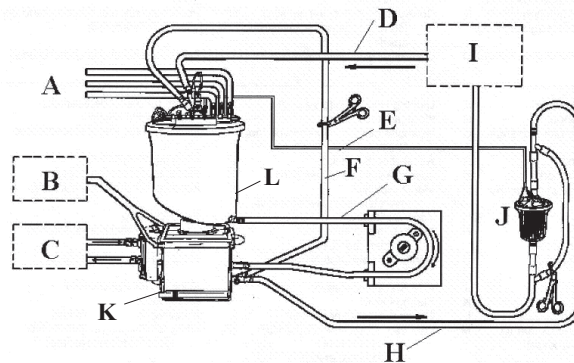


Figure 1.5: Heart lung machine circuit diagram. Components represent: A) Cardiomy lines, B) Oxygen/Air blender, C) Water heater/cooler, D) Venous line, E) Vent line, F) Re-circulation line, G) Pump loop, H) Arterial line I) Patient J) Arterial filter K) Membrane oxygenator L) Venous reservoir. Figure partly based on instruction manual of COBE Cardiovascular, Inc. Arvada, USA.

subnormal temperature. After disconnecting the pump, the body is allowed to self equilibrate. Since the vasoconstriction response that would occur under normal conditions is impaired by the administered anesthesia (Matsukawa et al., 1995a), heat redistribution takes place from the warm core to the colder periphery (Sessler, 2000). This causes 'afterdrop' which is a decrease in the temperature of the core organs (visible in the postbypass stage of figure 1.4).

Clinicians try to reduce afterdrop as much as possible e.g. by using forced-air heaters and circulating water mattresses, as afterdrop increases the risk of complications (Polderman, 2004) and causes thermal discomfort. In the postoperative period, when body temperature again increases, oxygen demand due to shivering, ventilatory requirements, and myocardial work may increase enormously. These variables increase the risk for cardiac arrest, myocardial ischemia and infarction (Cook, 1999).

In order to minimize afterdrop as much as possible, more insight in heat transfer mechanisms during surgery and the effect of different protocols should be gained.

1.3 Human thermal models

The understanding of the dynamic heat transfer in the patient-environment system and its effect on the transient physiological response is important for improving intraoperative temperature protocols. Many researchers (like Stolwijk (1971); Wyndham and Atkins (1968); Gagge (1973); Gordon (1974); Wissler (1985); Xu and Werner (1997); Fiala et al. (1999, 2001); Huizenga et al. (2001); Tanabe et al. (2002); Salloum et al. (2007); Wan and Fan (2008)) have contributed to the modelling of the physiological responses of humans during thermal transients. One reason for the development of a new mathematical human thermal

model is that all existing models focus on the dynamic physiological behaviour of the healthy human body, with intact thermoregulatory responses. Accordingly, these models are not suitable for predicting body temperature during anesthesia. Moreover, the models miss details that are essential for modelling cardiac surgeries. A model for simulating cardiac surgery should at least contain modules that account for the pharmacological-induced thermoregulatory impairment, the thermal influence of heart lung machine and equipment like forced-air heaters and heating mattresses.

Another reason for the development of a new thermo-physiological model is that this research field still leaves a lot of room for improvement. Modelling the body, the body properties and the heat interaction with the environment (passive part) has been extensively improved over time, where Stolwijk's (1971) work is often used as the basic approach. Modelling physiological responses (active part), on the other hand, is still less accurate. Thermal regulatory responses and person-to-person variations in thermoregulatory responses are not understood sufficiently well that they can be used to model exactly what occurs in the body. Various empirical relationships are used in the models to relate factors such as blood flows to various external conditions. A strategy that is often followed to derive such empirical relations is the use of an iteration scheme with which control parameters can be found that give the minimum difference between measurements and simulation (e.g. Gordon (1974) and Fiala et al. (2001)). This method is prone to errors, as small errors in the passive model can have major influence on the found control parameters. Other model makers like Tanabe et al. (2002) and Wan and Fan (2008) still use the same tentative values as proposed by Stolwijk (1971). It is quite likely that most models use relationships that are in fact only surrogates for the true control variables in the body and/or the relationships are only crude representations of the relationships actually employed by the body (Jones, 2002). Therefore, it is desirable to develop a thermal model that is based on physiological control variables that are directly derived from measurements. In this way, the active part is formulated independent from the passive part.

A benefit of having a thermal patient model is that it can be used to study the influences of different temperature protocols without directly exposing patients to conditions for which the result is unknown. In a later stadium, it is conceivable to use the model, in addition to using it as a study tool, for the development of an advisory monitoring system that can be used as an assist tool in the surgery room.

1.4 Goal and thesis outline

This thesis focuses on the development of a mathematical model that is able to describe heat transfer in humans during hypothermic surgery and that can be used to study the effect of different protocols on body temperature. With help of the model, especially the afterdrop effect occurring after cardiac surgery will be studied. To that end, more knowledge is needed about the effect of different protocols on thermoregulatory responses and temperature distribution in anesthetized persons.

Mathematical whole body temperature models are useful tools to quickly estimate the tem-

perature response of the body due to changes in environmental conditions. However, previously developed human thermal models are restricted to describing temperature responses of persons with an intact thermoregulatory system, and do not have enough detail for simulating (cardiac) surgeries. Those models are therefore not suitable for predicting temperatures of anesthetized patients with impaired thermoregulatory responses. Therefore, in this thesis heat transfer of patients undergoing hypothermic surgery is studied by means of numerical modelling and performing experiments. The model that was developed consists of three parts: 1) a passive part, which gives a simplified description of the human geometry and the passive heat transfer processes, 2) an active part that takes into account the thermoregulatory system as function of the amount of anesthesia and 3) submodels, through which it is possible to adjust the surgery (e.g. influence drugs and heart lung machine) and patient specific boundary conditions. Several experiments were performed on patients and volunteers in order to refine and validate the computational model.

The passive part of the human body, that describes the passive heat transfer processes in the body, is explained in chapter 2. Formulations are given for the heat losses that take place by means of convection, radiation, evaporation and respiration. Also the boundary conditions that were used to model cardiac surgery are described here.

Chapter 3 elaborates on experiments performed on two groups of aortic valve patients from which one group was warmed with forced-air heating and the other with only passive insulation. By simultaneously measuring core temperature, skin temperature, perfusion and deep peripheral temperature more insight is obtained in the effect and working principle of forced-air heaters. Moreover, the measured data also provides information that is useful for the formulation of an active model.

Thresholds at which thermoregulatory reactions are triggered depend on the amount of drugs in the blood. A pharmacological model was used to calculate the blood propofol (an often used anesthetic agent) concentration. With help of the measurements described in chapter 3, the threshold for vasoconstriction as function of the blood drug concentration was derived. As a first approach a stepwise model was used to model the intensity of the vasoconstriction response. The development of this active model and validation of the whole body model is described in chapter 4.

For the refinement of the vasoconstriction model, detailed local skin temperature and local tissue blood perfusion measurements were performed on volunteers, as described in chapter 5. Ten healthy male volunteers participated in an experimental study design. With help of laser Doppler flowmetry, skin perfusion at the toe, leg and arm was measured simultaneously with skin temperature and core temperature. Two methods were considered to model skin blood flow: the established relation of Stolwijk (1971) in which vasoconstriction and vasodilation are treated differently, and a newly proposed linear relation where vasoconstriction and vasodilation are implemented in a similar linear way. With help of the collected measurement data, physiological values for the proportional amplification coefficients for vasoconstriction of the toe, leg and arm and the transient vasoconstrictor tone were obtained. More detailed experiments were then performed on two subjects to find also physiological values for the

other body parts.

In chapter 6, validation studies were performed for different types of surgery like orthopedic back surgery and cardiac surgery under deep hypothermia involving circulatory arrest. Finally, the computer model was used to study different temperature protocols.

CHAPTER 2

Passive model of bioheat transfer*

2.1 Introduction

Engineering models describing the human thermal system have been the subject of many studies. The human thermal system is very complex, and simplifications have to be made to formulate a mathematical model. This has led to different modelling approaches with various assumptions and complexity and with widely varying numbers of variables involved.

Most human thermal models are split up in two systems: the controlled passive system and the controlling active system. The passive system gives a description of the human geometry in a simplified way and takes into account the heat production, the heat transport within the body and the heat exchange with the surroundings. The active system is normally described with control equations for thermoregulatory responses. For anesthetized persons, an extra model is required that takes into account the amount of anesthetic drugs. An overview of the model that was developed in this current work is shown in figure 2.1.

This chapter focusses firstly on the design of the passive model and the heat interactions that take place with the external environment. Secondly, a description is given of the sub-models that are needed to describe the body characteristics and the boundary conditions. The development of the active part is outlined in chapter 4.

Two main continuum approaches exist for modelling the passive model: mathematical models based on a simplified one-cylinder configuration and mathematical models based on multi-segments. Examples of one-cylinder models are the two node (core and shell) model of

*Parts of chapter 2 and 4 have been published in:

Severens N.M.W, Van Marken Lichtenbelt W.D., Frijns A.J.H., Van Steenhoven A.A., De Mol B.A.J.M and Sessler D.I. (2007). A model to predict patient temperature during cardiac surgery. *Phys Med Biol*, 52:5131–5145.

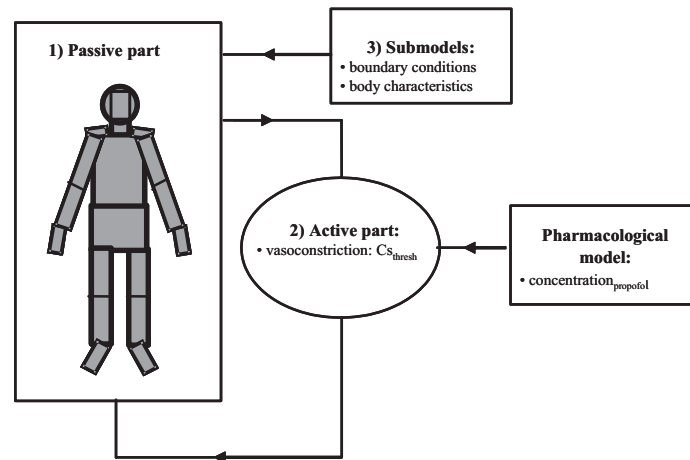


Figure 2.1: The human thermal model consists of three parts: 1) the passive part, 2) the thermoregulatory part, that is coupled to a pharmacological model and 3) a part that gives a description of the boundary conditions and body characteristics.

Gagge (1973), the multilayer model of Wyndham and Atkins (1968) and the three part model of Tindall et al. (2008)*. In contrast to the one-cylinder models, multisegmental models divide the body into more segments. Stolwijk (1971) was the first investigator who presented such an extensively detailed model. Later, Gordon (1974); Fiala et al. (1999); Huizenga et al. (2001); Tanabe et al. (2002); Salloum et al. (2007); Wan and Fan (2008) developed models that were based on the concepts of the Stolwijk model. Inherent in the continuum formulations is that local temperature inhomogenities caused by the larger vessels can not be predicted.

In contrast to the continuum approach, Kotte et al. (1996) developed an alternative model, in which vessels and tissue are separated. With help of vessel tracking by using MRA, discrete vasculature was modelled. Although this method provides an excellent description of local thermal behaviour in the tissue, large efforts need to be made to obtain MRA-images and translate them to a usable shape. Calculations with this model are much more time-consuming than using a lumped parameter approach. A recent model proposed by Salloum et al. (2007) combines the lumped approach to describe tissue properties with a detailed description of the arterial system including blood flow pulsation and heart rate.

For our purpose not much local details are required. Hence, a continuum model will provide abundant information for our application. The description of our passive model will therefore be based on a continuum approach, using the lumped heat-sink approach as proposed by Pennes (1948). Simulations performed by Van Leeuwen et al. (2000) showed that

*This model is published as:

Tindall M.J., Peletier M.A., Severens N.M.W., Veldman D.J. and De Mol B.A.J.M. (2008). Understanding post-operative temperature drop in cardiac surgery: a mathematical model. *Math Med Biol*, in press.

using a lumped heat-sink model has little effect on the qualitative nature in comparison to a discrete vessel description; only more local details are obtained. We therefore feel confident that the use of a continuum description for modelling the passive part will provide sufficiently accurate results for this study.

2.2 The passive part

As a starting point for the development of the passive part, the passive model of Fiala et al. (1999) was used. This model represents the human body using 10 body segments. In our model the number of body segments was increased to 19 body segments (figure 2.2): a sphere for the head and 18 cylinders representing trunk and limbs. In the Fiala model, shoulder, hands, feet, arms and legs were each modelled as one long segment. The leg segment therefore represented the right upper and lower leg as well as the left upper and lower leg. In contrast, in the current model the peripheral body parts were implemented separately. This makes the model more flexible for dealing with non-homogeneous boundary conditions on these body parts.

All segments consist of multiple concentric homogeneous layers, representing different tissue types like bone, fat, muscle and skin. Each tissue layer consists of one or more tissue nodes. The segments are divided into sectors (e.g. anterior, posterior and inferior, see figure B.1) on which asymmetric boundary conditions can be imposed.

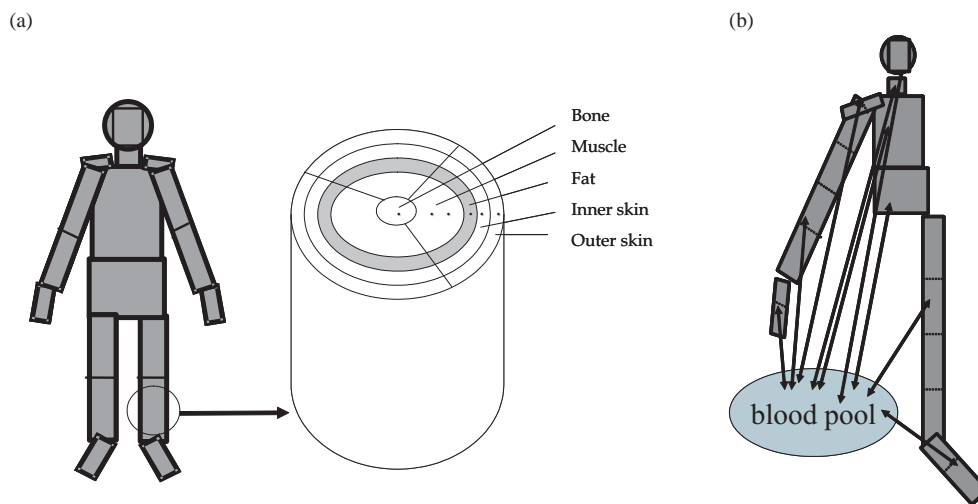


Figure 2.2: (a) Representation of our passive body model. The cylinder gives an impression how a body part (in this example the leg) is represented in the model. (b) Representation of the Fiala et al. (1999) model. Both models are based on a central blood pool.

Heat transfer in the tissue is modelled by the Pennes' bioheat equation (Pennes, 1948):

$$\rho c \frac{\partial T}{\partial t} = k \nabla^2 T + \rho_b c_b w_b (T_a - T) + \dot{q} \quad (2.1)$$

in which ρ , c and k are density, specific heat and thermal conductivity, respectively. T is the local tissue temperature and T_a the temperature of the perfusing blood. w is the volumetric perfusion rate, \dot{q} the metabolic heat production and subscript b describes a blood property. The Pennes' bioheat equation is applied to all tissue nodes using the appropriate material constants, adapted from Fiala et al. (1999). An extensive list of model properties is given in appendix B. The Pennes' equation is only solved in radial direction. The validity and utility of the Pennes' equation has been reviewed by Arkin et al. (1994); Wissler (1998); Van Leeuwen et al. (2000); Stańczyk et al. (2007). As not much detail is required, the Pennes' model will serve the purpose for the current thermal model.

The arterial blood temperature in the human model was calculated by assuming that the returning venous blood is mixed in a virtual mixing vessel, the central blood pool. The temperature of the mixed venous blood is the arterial temperature for the next time step. In some elements (viz. shoulders, arms, hands, legs and feet), counter current heat exchange takes place between arteries and veins. In that case, the local temperature T_a in those segments equaled the arterial temperature after counter current heat exchange. Hence, the arterial blood temperature can be different in various body segments. The counter current coefficients (h_x) are based on Fiala et al. (1999) (see appendix B, table B.1), but it must be noted that in literature no reliable data exists for these coefficients. Fiala et al. determined the values by trial and error procedures in which the coefficients were adjusted to obtain agreement between local skin temperature as predicted and measured. Although no independent verification of those values was possible because of lack of experimental data, it was observed that changing the coefficients to extreme values of $0.5h_x$ and $2h_x$ changes the core and skin temperature with maximally 0.1°C with respect to the original values. Hence, it is expected that no big errors are introduced in the model predictions by the inaccuracy of h_x .

2.2.1 Boundary conditions

The Pennes' equation accounts for all the heat exchanging processes that take place in the body, but not the exchange between the body and the environment. Therefore, boundary conditions are needed that take into account the heat exchanging mechanisms between the body and the environment. A distinction is made between the heat exchange mechanisms that take place from the body surface, the heat losses due to respiration and the losses due to conduction.

Heat exchange with body surface

At the body surface, heat exchange takes place by convection, radiation and evaporation, see figure 2.3. The net heat loss through a skin part is the equivalent of the sum of contributions

passing through that surface:

$$q''_{\text{skin}} = q''_{\text{convection}} + q''_{\text{radiation}} + q''_{\text{evaporation}} \quad (2.2)$$

with q'' the heat transfer rate per surface area [Wm^{-2}].

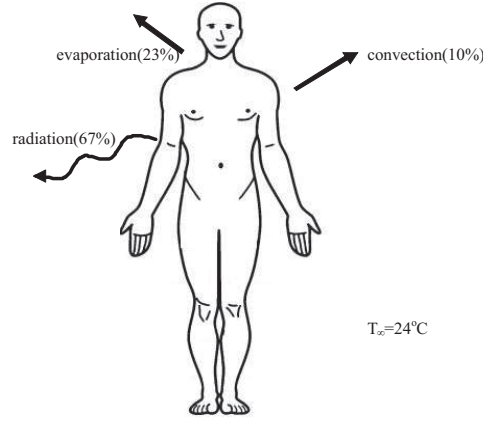


Figure 2.3: Heat exchanging mechanisms between body surface and environment.

- **Convection**

The convective heat flux is modelled by:

$$q''_{\text{convection}} = h_{c,\text{mix}}(T_{\text{skin}} - T_{\infty}) \quad (2.3)$$

where $h_{c,\text{mix}}$ is a combined-convection coefficient, T_{skin} the surface temperature of the segment and T_{∞} the temperature of the surroundings. The mixed convection coefficient was taken from Fiala et al. (1999) and yielded:

$$h_{c,\text{mix}} = \sqrt{a_{\text{nat}} \sqrt{T_{\text{skin}} - T_{\infty}} + a_{\text{frc}} \nu_{a,\text{eff}} + a_{\text{mix}}} \quad (2.4)$$

where a_{nat} , a_{frc} and a_{mix} are regression coefficients and $\nu_{a,\text{eff}}$ is the effective relative air speed. In appendix B table B.1, values for the regression coefficients are given. In addition, relation (2.4) is compared with alternative models in section B.2.

- **Radiation**

Radiative heat flux per surface area between two diffuse-gray surfaces is described by:

$$q_{\text{radiation}} = \frac{\sigma(T_1^4 - T_2^4)}{\frac{1-\varepsilon_1}{\varepsilon_1 A_1} + \frac{1}{A_1 F_{12}} + \frac{1-\varepsilon_2}{\varepsilon_2 A_2}} \quad (2.5)$$

with σ the Stefan Boltzmann constant ($\sigma = 5.67 \cdot 10^{-8} \text{Wm}^{-2}\text{K}^{-4}$), F_{12} the geometric view factor and ε the emissivity. The first and third terms in the denominator

of equation (2.5) can be considered to account for the surface resistances to radiation, whilst the second term accounts for the spatial resistance. Fiala et al. (1999) introduced sector view factors, ψ_{sr} that were defined with help of a finite element-method, that account for the spatial radiative resistance between the human body and the surrounding. Equation (2.5) was then rewritten, for a certain sector sr, as:

$$q''_{\text{radiation,sr}} = \frac{\sigma \psi_{sr} (T_{\text{skin}}^4 - T_{\infty}^4)}{\frac{1}{\varepsilon_{\text{skin}}} + \frac{1}{\varepsilon_{\infty}} - 1} \quad (2.6)$$

where the ψ_{sr} values were taken from Fiala et al. (1999) (see table B.2). Subscripts skin and ∞ represent skin and ambient properties, respectively. Rearranging equation (2.6) gives:

$$q''_{\text{radiation,sr}} = h_r (T_{\text{skin}} - T_{\infty}) \quad (2.7)$$

where the radiative heat transfer coefficient (h_r) is represented by:

$$h_r = \frac{\sigma \psi_{sr}}{\frac{1}{\varepsilon_{\text{skin}}} + \frac{1}{\varepsilon_{\infty}} - 1} \frac{(T_{\text{skin}}^4 - T_{\infty}^4)}{(T_{\text{skin}} - T_{\infty})} \quad (2.8)$$

• Evaporation

Even in cold conditions, evaporation of moisture takes place. In the superficial cutaneous layer, where sweat glands are located, moisture is always present. It is assumed that the vapour pressure at this location is equal to the saturation value, given by the Antoine equation:

$$p_{\text{outer skin,sat}} = 100e^{18.965 - \frac{4030}{T_{\text{outer skin}} + 235}} \quad (2.9)$$

with $p_{\text{outer skin,sat}}$ in Pa and the temperature in °C.

Active sweat production during hypothermic surgery is not likely. Therefore, only the normal evaporation process was implemented. Assuming that no moisture accumulates, the evaporative energy transport through the outer skin (with a moisture permeability $\frac{1}{R_{E,\text{skin}}}$ of $0.003 \text{ Wm}^{-2}\text{Pa}^{-1}$) to the skin surface equals the energy transport from the skin surface to the environment with the evaporative coefficient U_E :

$$q''_{\text{evaporation}} = U_E(p_{\text{skin,surf}} - p_{\infty}) = \frac{p_{\text{outer skin,sat}} - p_{\text{skin,surf}}}{R_{E,\text{skin}}} \quad (2.10)$$

in which $U_E [\text{Wm}^{-2}\text{Pa}^{-1}]$ depends on the evaporative resistance of clothing and the mass transfer resistance through the air near the skin, for more details and clothing values see section B.3, Fiala et al. (1999) and McIntyre (1980).

From (2.10) follows that the vapour pressure at the skin surface ($p_{\text{skin,surf}}$) is equal to:

$$p_{\text{skin,surf}} = \frac{U_E p_{\infty} + \frac{p_{\text{outer skin,sat}}}{R_{E,\text{skin}}}}{U_E + \frac{1}{R_{E,\text{skin}}}} \quad (2.11)$$

where p_∞ represents the vapour pressure of the ambient air given by $p_\infty = \phi p_{\text{sat}}$, with ϕ the relative humidity and p_{sat} the saturated vapour pressure at a certain ambient temperature.

Combining equation (2.10) and (2.11) leads to the following relation describing evaporation during (hypothermic) surgery:

$$q''_{\text{evaporation}} = U_E \left(\frac{U_E p_\infty + \frac{p_{\text{outer skin, sat}}}{R_{E, \text{skin}}}}{U_E + \frac{1}{R_{E, \text{skin}}}} - p_\infty \right) \quad (2.12)$$

Respiratory heat losses

Although most heat is exchanged through the body surface, heat exchange with the environment normally also occurs by means of respiration. During cardiac surgery, no respiration takes place when the heart lung machine is switched on, but during the anesthesia stage and after disconnecting the pump, respiratory heat losses take place. It is assumed that heat losses when artificial breathing is applied are comparable to normal respiratory heat losses. The model for respiratory heat losses was based on the description of Fanger (1973). The total respiratory heat loss is the sum of the evaporative heat loss and convective heat losses:

$$q_{\text{respiration}} = E_{\text{respiration}} + C_{\text{respiration}} \quad (2.13)$$

where the evaporative heat loss ($E_{\text{respiration}}$ [W]) is given by:

$$E_{\text{respiration}} = 3.44 \int \dot{q} dV (2.77 \cdot 10^{-2} + 6.5 \cdot 10^{-5} T_\infty - 4.91 \cdot 10^{-6} p_\infty) \quad (2.14)$$

and the dry heat loss ($C_{\text{respiration}}$) is represented by:

$$C_{\text{respiration}} = 1.439 \cdot 10^{-3} \int \dot{q} dV (32.6 - 0.934 T_\infty + 1.96 \cdot 10^{-4} p_\infty) \quad (2.15)$$

with \dot{q} representing the metabolic heat production and V the volume of the body.

Please note: the dimensions of the constants in the empirical equations are not mentioned for better readability throughout the thesis.

The total respiratory heat loss $q_{\text{respiration}}$ is distributed over body elements of the pulmonary tract where the following distribution coefficients are employed: 20%, 25%, 14%, 11% and 30% for the inner face muscle, the outer face muscle, inner muscle band of the neck, the outer muscle band of the neck and the lung, respectively.

Conduction

During surgery the mattress, covered with a cotton drape on which the patient lies, and the sterile surgical drape that covers the patient, provide extra thermal insulation. In the simulation, clothing parameters were enclosed with insulation values of 0.9 clo for the mattress, 0.78 clo for the cotton draping and 0.83 clo for the sterile cover respectively (Bräuer et al. (2004b)). In appendix B, section B.3 the details of the clothing model are given.

2.2.2 Numerical methods

The partial derivatives of the Pennes' bioheat equation with respect to the radius were approximated by a central difference scheme. On the interface between two adjoining tissue layers, boundary conditions are used that impose continuity of temperature and heat flux across the interface at distance r_{ifc} , using the method of Schuh (1957):

$$\begin{aligned} \lim_{r \uparrow r_{\text{ifc}}} T &= \lim_{r \downarrow r_{\text{ifc}}} T \\ \lim_{r \uparrow r_{\text{ifc}}} q'' &= \lim_{r \downarrow r_{\text{ifc}}} q'' \end{aligned} \quad (2.16)$$

The time derivative in the Pennes' equation was discretized with the Crank-Nicolson method. This method is a linear combination of the explicit and implicit Euler scheme with weighing factors $\vartheta = \frac{1}{2}$. For $\vartheta = \frac{1}{2}$, the method is second order convergent in both Δt and Δr .

An infinite family of solutions exists to the set of time-dependent partial differential equations that are solved. By prescribing the initial condition and boundary conditions, a unique solution is obtained. Hence, it should be realized that proper knowledge of initial and boundary conditions is of high importance for the predictive value of the model.

2.2.3 Numerical convergence

Number of grid points

Janssen (2007) performed a detailed analysis in which he compared results obtained with the discretized Pennes' equation to known analytical solutions of a sphere with properties that resemble biological materials. Temperature errors between numerical and analytical solutions were found to be of the order of typically 0.05°C .

For our passive body model, standard calculations were performed with the 19 segments model using 261 nodes in total (for the node distribution, see table B.3) with a time step of 1 minute. Under thermoneutral conditions, where no thermoregulatory responses are expected, increasing the amount of nodes twofold, fourfold and eightfold led to convergent results in which core temperature changed less than 0.07°C and mean skin temperature changed less than 0.02°C . These values are of the same order of magnitude as the maximum feasible accuracy found by Janssen. Using more nodes than the standard value will therefore not lead to an improved accuracy, but will only increase calculation time.

Number of segments

In order to show the flexibility and the accuracy of the model for the number of segments, the model geometry of Fiala (with 10 body segments) was compared to our body geometry (19 segments), see the schematic presentation in figure 2.2. The total size of the leg parts, and all the tissue properties are kept constant (see for details table B.1 and B.3). For comparing the two geometries, simulations were performed under identical conditions for both the 10 and 19 segmental-models: the passive naked body was exposed to a temperature of 30°C for 60

minutes, thereafter a stepwise change in temperatures takes place to a temperature of 20°C. Temperatures stays at 20°C for another 60 minutes. Simulation results are found in figure 2.4.

It is seen that changing the number of segments (while keeping other properties like length constant) gives, under symmetrical simulation conditions, identical mean results. This is in line with the expectations that the model results are independent of the number of peripheral segments as long as the total sizes and the tissue properties are the same and the boundary conditions are mirror symmetrical. From this, it is concluded that the number of segments in the body model can be extended or reduced for different circumstances, without affecting the model's predictions.

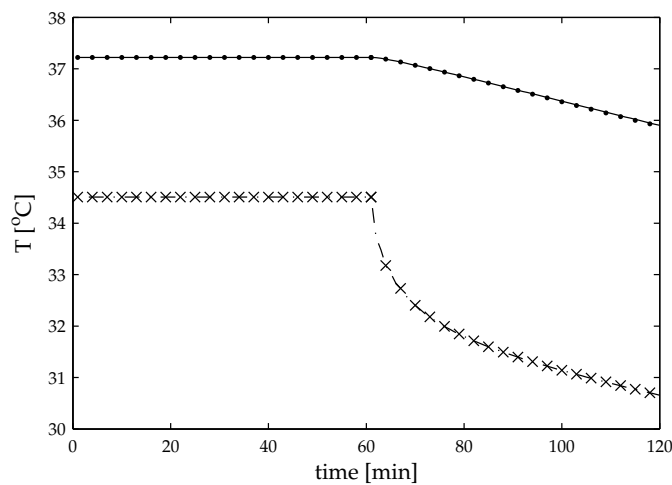


Figure 2.4: Core and mean skin temperature responses to a stepwise change in temperature (from 30°C to 20°C at $t=60$ min) of a passive model built up of 10 segments and 19 segments. On top of the figure the core temperature results of the 10 segments (\cdot) and 19 ($-$) segments model are given. At the bottom the mean skin temperature of the 10 segments (\times) and 19 segments model ($- \cdot$) are shown.

2.3 Submodels

An advantage of the current model is the submodel section, which makes the model very flexible. With help of the newly developed submodels, body characteristics and boundary conditions can be adapted. In this way, an accurate representation of the followed surgical procedures can be used in the simulation. In this section an overview is given of the methods that were used to account for individual body characteristics and the most important submodels for prescribing boundary conditions of a cardiac surgery like the heart lung machine,

forced-air heating, circulating water mattress and wound heat loss. When simulating other types of surgery, simulations can also be run without the model of the heart lung machine.

2.3.1 Individual body characteristics

Contrary to the original model of Fiala et al. (1999), individual subject characteristics were accounted for. The standard geometry was scaled in such a way that body composition data in the model agreed with the body composition of the persons from the measurements. Previous simulations have shown that predictions of a group can be improved by adopting individualized body characteristics (Van Marken Lichtenbelt et al., 2007).

We developed a module that accounts for body shape and body sizes (height, weight, percentage of body fat). There are two basic body shapes: 'apples' and 'pears'. Apple shaped people carry most of their excess body fat around their abdomen and middle, surrounding internal organs, such as the heart. Apple shaped people have higher risk of diabetes, stroke, high blood pressure and gall bladder disease. Pear-shaped people carry their excess fat on their hips and thighs. Pear-shaped people do not seem to have as high risk of developing above conditions as 'apples' do. As the fat distribution of apple and pear shapes is different, this will affect the heat production and flow. Therefore, distinction will be made between those two groups.

We use the following criteria (see table 2.1) for determining if a person is apple-shaped (Lean et al., 1995). If a person does not fulfill these criteria, the body is considered pear-shaped.

Table 2.1: Criteria for determining apple shaped persons.

Women	Men
waist-to-hip ratio > 0.8 and waist circumference > 80 cm	waist-to-hip ratio > 0.95 and waist circumference > 94 cm

To incorporate the difference in size, length and body fat, the model is adopted in the following way. The standard model represents an average man with a body mass of 73.5 kg, a height of 1.71 m and a fat percentage of 14%. The actual body size of the patient is scaled relative to the standard model, by introducing a scaling factor λ_1 given by:

$$\lambda_1 = \frac{H}{H_0} \quad (2.17)$$

where H is the actual length of the person and H_0 is the length of the standard person. As it is expected that the size of all body elements in adults scale linearly with the body, except for the head, all element lengths are scaled with the factor λ_1 . The head is scaled with $\sqrt{\lambda_1}$, which is arbitrarily chosen but more realistic than scaling with λ_1 . The thickness of the inner and outer skin layer is kept constant, since the thickness of the skin is relatively

constant in a population. Next, for determining the thickness of the core and muscle layer another scaling factor λ_2 is introduced. The fat layer in the face, neck, shoulder, thorax and abdomen is scaled with λ_3 , whilst the fat layer in the arms and legs are scaled with $0.7\lambda_3$ for apple-shaped people and with a factor λ_3 for pear shaped people. In a population, it is seen that when body weight and size changes, the thickness of the fat layer in hands and feet does not change. Therefore, it was chosen to keep the fat layer thickness in hands and feet always at the standard value. Then, the values for λ_2 and λ_3 were iteratively chosen in such a way that the body mass M_{body} and the fat mass M_{fat} correspond to the mean characteristics of the simulated subjects. A constraint in adapting λ_2 and λ_3 is that all tissue layers have a minimum thickness of 1 mm, in order to prevent negative tissue radii. Typically, values for λ_2 and λ_3 are between 0.8 and 1.2. Finally, all tissue layer thicknesses and segment sizes were calculated with help of the found values of λ_1 , λ_2 and λ_3 . In this way, the body segment lengths and radii of the desired person can be obtained.

2.3.2 Heart lung machine

During cardiac surgery, the heart lung machine functions as a substitute for the heart (pump) and the lungs (gas exchange). Apart from these functions, the heart lung machine is also used as a heat exchanger, with which the temperature of the blood can be controlled. The heart lung machine is the most important method for both cooling and rewarming of the human body during cardiac surgery. The heat exchanger of the heart lung machine was implemented in the model by using the information given by the manufacturer (COBE Cardiovascular, Inc. Arvada, USA). The effectiveness of the heat exchanger for an average flow rate of 5 l min^{-1} was $\varepsilon = 0.7$ (manual COBE Cardiovascular, Inc. Arvada, USA). However, in the tube between the heat exchanger and the arterial cannulation site, additional heat loss takes place. Therefore, the effectiveness in the model ε^* was set to an arbitrary value of 0.5. Effectiveness then yields:

$$\varepsilon^* = \frac{T_{\text{b,out}} - T_{\text{b,in}}}{T_{\text{w,in}} - T_{\text{b,in}}} \quad (2.18)$$

where $T_{\text{b,out}}$ is the outgoing blood temperature, $T_{\text{b,in}}$ is the ingoing blood temperature and $T_{\text{w,in}}$ is the ingoing water temperature (temperature of the water reservoir). On the next time step, $T_{\text{b,out}}$ was used as blood pool temperature instead of the venous mixing vessel temperature. When a patient is on pump (i.e. connected to the heart lung machine), no respiration takes place and the artificial respirator device is switched off. Hence, respiratory heat losses, $q_{\text{respiration}}$ as given by equation (2.13), are omitted in this situation.

2.3.3 Forced-air heating

Forced-air warming systems consist of a power unit incorporating an electrical heater and a fan to generate an air flow that is delivered downstream to a blanket, see figure 2.5. The heat exchange between a forced-air heating blanket and the patient's skin is given by:

$$q_i'' = h_{\text{fa}}(T_{\text{skin},i} - T_{\text{fa}}) \quad (2.19)$$



Figure 2.5: U-shaped model forced-air blanket, that is often used during surgery.

The heat exchange coefficient h_{fa} defines the efficiency of all the heat exchange mechanisms (radiation, convection and conduction) between the blanket and the patient. From experiments (see for details appendix B, section B.4) performed with an U-shaped model forced-air blanket (Bair Hugger, model 560 Cath Lab Blanket, Arizant Healthcare Inc.) a h_{fa} was found of $16.4 \pm 0.3 \text{ Wm}^{-2}\text{K}^{-1}$ at an outlet air temperature of 43°C (Bertens et al., 2006).

2.3.4 Circulating water mattress

Circulating water mattresses are active intraoperative warming/cooling systems that are connected to a water-pumping system. A water mattress consist of two layers of foam incorporating a tube system, through which the water flows. Circulating water mattresses are placed under the patient and exchange heat by conduction. Heat transfer between the circulating water mattress and the patient's skin (parts of the head, neck, shoulder, thorax, abdomen, arms, hands, legs and feet) was given by:

$$q_i'' = h_{mat}(T_{skin,i} - T_{mat}) \quad (2.20)$$

with a heat transfer coefficient h_{mat} of $121 \text{ Wm}^{-2}\text{K}^{-1}$ (Bräuer et al. (2004a)).

2.3.5 Heat loss through wound with topical ice slush

During open heart surgery, the thorax is opened. Extra heat loss takes place through the opened thorax by means of evaporation, convection and radiation. Ice-cold fluid (saline 0°C) is poured in the open thorax to cease the heart beat. In order to calculate the influence of

the open thorax on the heat balance, an extra element was implemented in the model. This brings the total number of elements to 20. This element consists of 2 layers: a lung layer and a fluid layer. The angle of the segment is estimated to be 75° . Naturally, the anterior part of the existing lung element is reduced by 75° .

It is assumed that heat transfer only takes place in radial direction, and not from the azimuthal plane. Heat exchange between the upper layer in the open thorax element and the surroundings takes place by means of convection, radiation and evaporation. The convective heat flux was given by:

$$q''_{\text{convection}} = h_{c,\text{mix}}(T_w - T_\infty) \quad (2.21)$$

where $h_{c,\text{mix}}$ is the convection coefficient given by equation (2.4), T_w the surface temperature of the open thorax element and T_∞ the temperature of the surroundings. The radiative heat flux was described by:

$$q''_{\text{radiation}} = \frac{\sigma\psi(T_w^4 - T_\infty^4)}{\frac{1}{\varepsilon_w} + \frac{1}{\varepsilon_\infty} - 1} \quad (2.22)$$

where σ is the Stefan-Boltzmann constant, ε the emission coefficient and ψ a view factor. These values were taken equal to the normal values for the thorax, see table B.2. The evaporative heat flux from the wound surface yields:

$$q''_{\text{evaporation,water}} = 0.54 \frac{D}{L} \left(\frac{g\beta_c(\rho_w - \rho_\infty)L^3}{\nu D} \right)^{1/4} (\rho_w - \rho_\infty)\lambda_{\text{H}_2\text{O}} \quad (2.23)$$

with $\lambda_{\text{H}_2\text{O}}$ denoting the latent heat of vaporization of water [Jkg^{-1}], ρ the mass concentration of water vapor [kg m^{-3}], D the mass diffusivity of the air-water vapor mixture [m^2s^{-1}], ν the kinematic viscosity [m^2s^{-1}], L the characteristic length of the plane surface [m], g the gravitational acceleration [m s^{-2}] and β_c representing the composition expansion coefficient of the air/water vapor mixture [m^3kg^{-1}]. Subscripts w and ∞ denote properties at the wound surface and environment, respectively. A detailed derivation of equation (2.23) is given in appendix B, section B.5.

To study the effect of heat loss due to the open thorax, heat fluxes of a person with and without open thorax were explored at an environmental temperature of 30°C (figure 2.6). The simulations were run for a time period where the heart lung machine was not switched on.

The contribution of the opened thorax to the total heat balance was small: 2.3 W heat loss took place through the wound, while the total heat loss was 77.6 W. Hence, it is justified to ignore the heat loss through the open thorax in further simulations.

2.4 Simulation with passive model

Under general anesthesia hypothermia occurs. In order to verify the passive model, simulations are compared with an experiment performed by Kurz et al. (1995a). They demonstrated that core temperature drop in anesthetized persons develops with a typical pattern and will reach a plateau after about four hours. After that, core temperature does not decrease further.

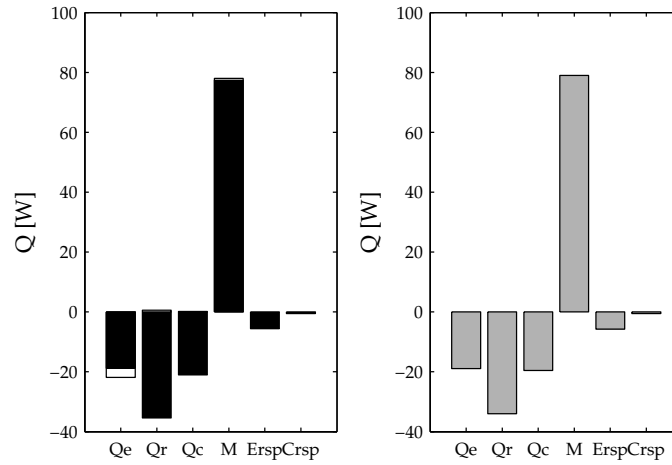


Figure 2.6: Left: Heat flows in a person with opened thorax at a thermoneutral temperature of 30°C . White parts represent the heat fluxes through the opened thorax part. Black parts give the heat flows through the 19 other elements. Right: Heat flows under thermoneutral conditions with closed thorax. In the figures from left to right evaporative heat loss (Q_e), radiative heat loss (Q_r), convective heat loss (Q_c), metabolic heat production (M), evaporative respiratory heat loss (E_{rsp}) and dry respiratory heat loss (C_{rsp}) are given, respectively.

This plateau is typically $1\text{-}3^{\circ}\text{C}$ lower than the normal temperature, see figure 2.7(a). In their study protocol nine healthy males (1.75 ± 0.04 m, 74 ± 11 kg and $18 \pm 4\%$ fat) were administered general anesthetic drugs and exposed to a room temperature of 22°C for six hours. The first two hours propofol was administered with a dose rate of $150 \mu\text{gkg}^{-1}\text{h}^{-1}$. Thereafter the drug dose was decreased.

With help of the passive model, a simulation was performed where a passive, minimally clothed body, lying on a bed, was exposed to an environmental temperature of 22°C . It is observed that core temperature continuously decreases for more than six hours, see the solid line in figure 2.7(b).

In order to simulate the same situation with a passive anesthetized body, another simulation was run in which the typical metabolic heat production, that occurs during anesthesia, is taken into account. For this, a metabolic reduction of 30% is taken, based on values reported in literature (cf. Matsukawa et al. (1995b, 1997); Sessler (2000)). In the right hand side of equation (2.1), the term \dot{q} is reduced by 30%. The result of the simulation with the anesthetized passive model is illustrated by the black circles in figure 2.7(b).

It is seen that by modelling only the passive part, the core temperature drop after six hours is much bigger than the drop observed by Kurz et al.. This effect is enhanced, when the anesthesia induced reduction of metabolism is taken into account. The influence of the metabolic rate reduction is quite large; in this specific case core temperature is reduced by an additional 1.5°C at $t=6$ hours. Simulating an anesthetized passive body exposed to an ambient

temperature of 22°C resulted in a temperature drop of 7°C, while Kurz et al. report under approximately similar conditions a 3.5°C core temperature drop and observed a distinct vasoconstriction response. This stresses that using only a passive model is not sufficient to capture the temperature response of anesthetized persons and that efforts are needed to formulate an active model for describing thermoregulation during anesthesia.

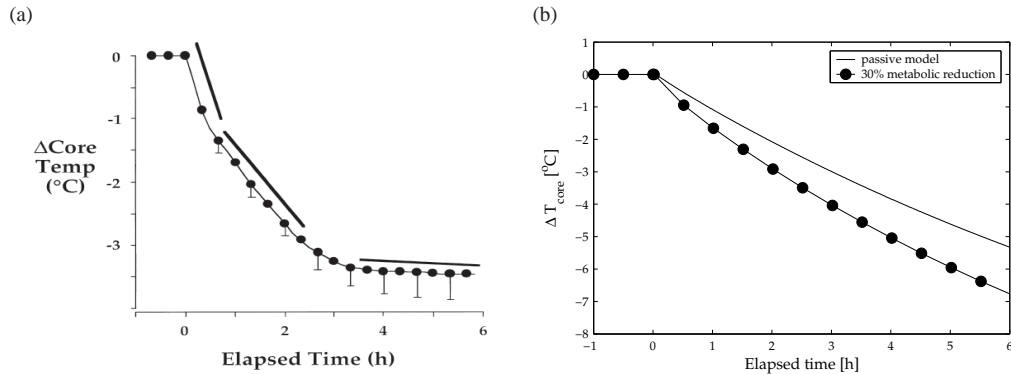


Figure 2.7: (a) Typical pattern of hypothermia during general anesthesia. Figure taken from Kurz et al. (1995a). (b) Simulation: core temperature of the passive anesthetized minimally clothed body after exposing the body to an environmental temperature of 22°C for 6 hours.

2.5 Discussion

In this chapter, a description is given of the development of the passive part of the human thermal model, that was based on the model of Fiala et al. (1999). Secondly, the submodels that were used to account for specific boundary conditions of the surgery and the patient's body characteristics were described. The passive part gives a description of the human geometry and the heat interaction between the body and the environment. The human body was described using a multi-segmental, multi-layered representation, for which we elaborated and adjusted the passive model formulated by Fiala et al. (1999). Internal heat flows in the body are modelled using the Pennes' equation. Heat exchanging processes at the surface, i.e. convection, radiation, evaporation and respiration are also taken into account. For the purpose of using the model to simulate cardiac surgeries, special submodels are formulated to account for heat exchange by the heart lung machine, usage of forced-air heaters, a circulating water mattress and heat loss through the opened thorax. Furthermore, a module is designed that accounts for individualized body shape and body size of the simulated subject.

In order to model the passive part, simplifications and assumptions were made and most model parameters were taken from literature. A simplification in the model is the assumption that the body segments are either perfect cylindrical or spherical shapes and the tissue layers are perfect circles. Besides that, the model is build up in such a way that the separate body

parts are only connected via a central blood pool. Under predominantly homogeneous environmental conditions, like in this thesis, this simplification will not introduce much errors, but in extreme, non-homogeneous conditions a more sophisticated model is needed to link the body parts.

Parameter values and empirical relations are mainly taken from existing literature, like the counter current heat exchange coefficients, the relations for convective heat transfer, respiratory heat losses and the clothing model. The sensitivity of inaccuracies in the counter current heat exchange coefficient on core and mean skin temperature were found to be small ($<0.1^{\circ}\text{C}$) when the values in literature would deviate 100%. The convective heat transfer coefficient relation that was used was compared to other relations found in literature and to the basic engineering method for convective heat loss around cylinders. The model, that was used, was in the same range as the other models and is therefore considered appropriate. No verifications were performed on the equations for modelling respiratory heat losses, but as can be seen in figure 2.6 the respiratory heat losses contribute only little to the total heat loss. Hence, small errors in the respiratory heat loss equation will not lead to large deviations in the total model. The clothing model as proposed by Fiala et al. (2001) accounts for heat transfer and evaporative resistances of clothing. In this model no distinction is made between external flow and the effect of clothing ventilation, which can cause up to 50% reduction in thermal insulation and up to 88% reduction in evaporative resistance (Wan and Fan, 2008). In future models, this part needs to be elaborated by a more detailed model.

During surgical incisions, extra heat losses take place from the wound surface. During cardiac surgery, cold saline is poured in the open thorax. It was shown that the contribution of the open wound to the total heat balance was small during cardiac surgery (about 3%) in contrast to other interventions with a surgical incision, like was shown in the rabbit study of Roe (1971). For future simulations concerning open-heart surgery, heat losses through the surgical incision are therefore ignored.

By simulations, it was shown that it is not possible to capture the typical pattern of hypothermia during general anesthesia as demonstrated by Kurz et al. (1995a) with only a passive model. Using a passive anesthetized passive model, where anesthesia induced reduction of metabolic rate is taken into account, even augments the difference. This indicates that for correct modelling of temperatures during anesthesia, efforts have to be made to also formulate an active model. For this, measurement data of patients administered general anesthesia are needed. In the next chapter, measurements are described of patients that undergo cardiac surgery. In a later stadium, it is explained how, with help of this data, the active model is developed and validated.

CHAPTER 3

Effect of forced-air heaters on perfusion and temperature distribution during and after open-heart surgery*

3.1 Introduction

In the previous chapter, it was ascertained that for the development of a reliable numerical human thermal model proper data sets are required of patients during hypothermic surgery. Additionally, more information is needed about the used protocols during surgery and the resulting temperature and perfusion responses of anesthetized patients. To that end, an experimental measurement protocol was developed in which two patient groups were followed during cardiac surgery. In one group forced-air warming was used, in the other group passive insulation was applied.

Forced-air warmers are often used to reduce hypothermia in the peri- and postoperative period. Effectiveness of forced-air heating to improve core temperature is reported for the postoperative stage (Bräuer et al., 2004), during off-pump coronary bypass surgery (Kim et al., 2006) and in anesthetized hypothermic volunteers (Taguchi et al., 2004). Nowadays, forced-air heaters are also often used peri-operatively during cardiac on-pump interventions. Heat is transferred to the periphery by forced-air heaters while the core is rewarmed by the heat exchanger in the heart lung machine. Covering the inadequately warmed periphery with forced-air heaters during systemic rewarming reduces afterdrop (Hohn et al., 1998; Rajek et al., 2000). One explanation is that forced-air warming increases peripheral temperature.

**This chapter is an extended version of:*

Severens N.M.W, Van Marken Lichtenbelt W.D., Van Leeuwen G.M.J., Frijns A.J.H., Van Steenhoven A.A., De Mol B.A.J.M, Van Wezel H.B. and Veldman D.J. (2007). Effect of forced-air heaters on perfusion and temperature distribution during and after open-heart surgery. *Eur J Cardiothorac Surg*, 32(6):888–895.

This reduces the core-periphery gradient and consequently reduces afterdrop. Measurements and analysis of Rajek et al. (2000) did not support this explanation. Instead they think that forced-air heaters do not prevent redistribution, but preserve the total body heat content. It is of interest to assess how forced-air heaters change body temperature distribution.

Body temperature distribution depends strongly on blood-borne heat transfer. Under anesthesia, thermoregulation is impaired. This leads to alterations in blood flow, with corresponding changes in temperature distribution (Matsukawa et al., 1995a). Only few studies with animals have been performed that assess perfusion during extracorporeal circulation (Rudy et al., 1973). To our knowledge, no study on peripheral heat flow during human extracorporeal circulation has been published. Therefore, we simultaneously measured perfusion and temperature distribution during and after cardiac surgery. In this way, information is provided about the amount of convective heat flow to the periphery. Ultimately, this will help to explain how forced-air heaters favour core temperature.

Additionally, the surgery protocol is simulated with help of the passive thermal model, that was developed in the previous chapter, and compared to the measured temperature values. Later, in chapter 4, the data will also be used for further development of the active model.

3.2 Materials and methods

3.2.1 Patients

With approval from the Academic Medical Center (AMC) Medical Ethical Committee and written informed patient consent, 15 patients undergoing elective aortic valve replacement were studied. Patients were followed during surgery and the first three hours after surgery at the intensive care unit (ICU). We enrolled patients aged between 40 and 80 without severe left ventricular dysfunction. Patients were randomly assigned into one of two protocols: a test group ($n=8$) that was rewarmed with forced-air heaters and a control group ($n=7$) that was rewarmed with only passive insulation.

3.2.2 Anesthesia

Calcium channel blockers and long acting nitrates were given until the evening before surgery. Beta-adrenoceptor blocking agents were continued until the morning of surgery. Lorazepam 2-3 mg was given for premedication 2 hours before surgery. Anesthesia was induced with sufentanil 3 μg kg^{-1} (Sufenta[®], Janssen-Cilag, Tilburg, The Netherlands) and propofol 50-100 mg (Fresenius Kabi, Den Bosch, The Netherlands). Pancuronium bromide 0.1 mg kg^{-1} (Pavulon[®], Organon, Oss, The Netherlands) was given for muscle relaxation. Morphine 10-30 mg was given as a slow bolus injection. Anesthesia was maintained with a continuous infusion of propofol 2-5 mg $\text{kg}^{-1}\text{h}^{-1}$ and/or isoflurane at 0.5 MAC. The lungs were ventilated with air/oxygen ($\text{FiO}_2=0.5$). Following the induction of anesthesia, a flow directed pulmonary artery catheter (Edwards Lifesciences, Irvine, CA, USA) was inserted

into the right internal jugular vein. Dexamethasone and α_2 -adrenoceptor agonists were not used in any of the participating patients.

3.2.3 Protocol

Temperature in the operating theatre was kept at $20 \pm 1^\circ\text{C}$. In the test group, the blanket was mounted along the body by sticking the blanket on the surgery table with tape. The sterile cover was positioned over the patient and covered also the forced-air heater. Forced-air heaters in the test group were used after fastening the aortic valve (28 ± 18 minutes after the onset of rewarming) and active heating was continued until skin closure. The inlet air temperature of the forced-air blankets (see figure 2.5) was set to a maximal temperature of 43°C . The patients in the control group were solely covered with a sterile sheet.

Both patient groups were cooled to a nasopharyngeal temperature of 30°C . Thereafter, patients were rewarmed to a nasopharyngeal temperature of 33°C and depending on the state of the surgery, fully rewarmed (when the aortic valve was already fastened) or kept for a few minutes at this temperature till the aorta valve was fastened. Patients were rewarmed to a nasopharyngeal temperature of $37\text{--}37.5^\circ\text{C}$ and a rectal temperature of minimally 36.3°C . Non-pulsatile bypass flow was kept at $2.4 \text{ l min}^{-1}\text{m}^{-2}$. Arterial inflow temperature was maximum 4°C warmer than the venous return temperature. Subsequently the heart lung machine was decoupled and the patients were transferred to the ICU. The arterial cannulation site was the ascending aorta in all patients. The venous cannulation site was the right atrium.

3.2.4 Morphometric measurements

Before surgery, the patient's body characteristics were measured: height, weight and fat percentage. Fat percentage was determined by measuring skinfold thickness at four positions: at the m. biceps brachii, m. triceps brachii, subscapular and suprailiacal (Durnin and Womersley, 1974). Body surface area (BSA) was calculated according to Dubois and Dubois (1916):

$$BSA = 0.007184W^{0.425}H^{0.725} \quad (3.1)$$

with weight W in kg and height H in cm.

3.2.5 Temperature measurements

Core temperatures were measured at regular intervals from the nasopharynx, in the rectum (oesophageal/rectal temperature probe, Philips 21090A), and from the pulmonary artery (Thermodilution Paceport Catheter: 931HF75, Edwards Lifesciences). In the operating room, the nasopharyngeal temperature was used as an estimator for the core temperature. At the ICU the pulmonary artery temperature was used to assess core temperature. Transient thigh temperature was determined at the skin and at deeper thigh tissue with a needle thermocouple (MT Needle microprobe 23 ga. Physitemp Instruments Inc. New Jersey) containing three sensors. Tissue thigh temperature was measured at 8-, 18-, and 38-mm depth. The needle

was inserted perpendicular to the skin surface slightly lateral from the anterior mid-upper right thigh.

For calculating mean thigh temperature, the regression method as proposed by Belani et al. (1993) was used. This regression assumes that tissue temperature is radially symmetrical. We used the skin temperature at the posterior thigh (at r_{thigh}) and thigh temperatures at 8, 18 and 38 mm below the skin. Similarly to Belani et al., it was assumed that the temperature in the leg at $r = 0$ was equal to the nasopharyngeal temperature. The parabolic regression equation was formulated as:

$$T(r) = a + br^2 \quad (3.2)$$

with $T(r)$ representing temperature, r the radial position and a and b regression constants. Average tissue temperature in the thigh was then calculated by:

$$\overline{T}_{\text{thigh}} = \frac{1}{\pi R^2} \int_0^R 2\pi(a + br^2)rdr = a + \frac{1}{2}bR^2 \quad (3.3)$$

Skin temperature measurements were performed using wireless thermistors (iButtons type DS192H, Maxim/Dallas Semiconductor Corp., USA, see also Van Marken Lichtenbelt et al. (2006)) at the forehead, lower arm, finger tip, foot dorsum, lower leg and upper leg. Because chest skin temperature could not be measured we modified the seven-point system of Hardy and Dubois (1938) to a six-point system according to:

$$T_{\text{skin}}^* = (0.07T_{\text{forehead}} + 0.14T_{\text{posterior forearm}} + 0.05T_{\text{hand}} + 0.19T_{\text{anterior thigh}} + 0.13T_{\text{anterior calf}} + 0.07T_{\text{foot}})/0.65 \quad (3.4)$$

Equation (3.4) does not provide a mean skin temperature that can be compared to other studies, but can be used to identify and compare changes in transient mean skin temperatures of the two groups in this study.

3.2.6 Skin perfusion measurements

Skin perfusion was continuously measured using a commercially available laser Doppler flowmetry device (Perimed PF4001, with a 780 nm laser diode and 0.25 mm fibre separation) under the right big toe. Sample rate was set to 4 Hz using a time constant of 0.2 s. All measurements were performed using a standard probe (Probe 408, Perimed AB), which was calibrated with PF 1000 calibration equipment (Perimed AB). Laser Doppler results were analyzed as a running average of 50 seconds epochs, to filter out motion artefacts. No attempts were made to compensate for the biological zero value. Arguments for that are outlined in appendix D.

In order to make individual data comparable and to easy see the effect of forced-air heating on perfusion, the perfusion result data are related to local temperature data using a power-law equation (see also, Janssen et al. (2007)), that is given by:

$$\frac{w_b}{w_{b,0}} = C \frac{T - T_0}{10^{\circ\text{C}}} \quad (3.5)$$

where C is a constant that will be determined by fitting equation (3.5) to local toe perfusion and temperature data. w_b is the current perfusion value, $w_{b,0}$ a reference perfusion value, and T and T_0 are current and base line temperature, respectively.

For each experiment a base line value for T_0 and $w_{b,0}$ was determined. Because the period at the ICU was relatively stable, the mean perfusion value during the last 10 minutes of that measurement period was used as base line value $w_{b,0}$. Subsequently, all perfusion values w_b were divided by $w_{b,0}$. From all temperatures (T) the base line temperature T_0 was subtracted. T_0 was the mean temperature during the last 10 minutes.

3.2.7 Leg blood flow measurements

Leg blood flow was determined in 12 patients by ultrasound measurements (Siemens Sono-line Antares) in the right femoral artery one cm before the bifurcation in the groin area. The femoral artery was visualized in B-mode. The diameter of the vessel was measured in systole and diastole. Subsequently, Doppler mode was used to record centerline velocity in the vessel during two heartbeats. Measurements were performed at four defined points in time, and repeated two times at these time points: 1) just before entering the surgery room 2) at the coolest point during the bypass cooling 3) just after surgery as the patient has arrived at the ICU and 4) about three hours after surgery.

Methods for calculating the leg blood flow are outlined in appendix E. The flow at the first measurement period was considered to be the base line value Q_0 . For each patient the flow at each measurement moment was normalized with the individual base line value Q_0 . Leg blood flow results are thus presented as relative changes in relation to the individual neutral state (Q/Q_0).

At the same points in time when leg blood flow was measured also cardiac output was determined by thermodilution measurements in the pulmonary artery. During the bypass period, pump flow rate was used instead of cardiac output.

3.2.8 Statistics

Results are presented as mean with standard deviation. Differences between the groups at different time points were analyzed with an unpaired t-test. For determining the effect of using forced-air heaters on afterdrop, a summary measure, which reveals the real clinical relevance, is used (Matthews et al., 1990). As summary measure for defining afterdrop, the core temperature of the moment of going off-pump minus the minimal postbypass core temperature, was used. For comparison of the gender and vasoactive medication between the two groups, Fisher's exact test was used with two-tailed probability. Leg blood flow at the four time points are compared with a paired t-test. Differences were considered to be statistically significant when $P < 0.05$. For determining C in equation (3.5), linear regression after log-transformation was used. Data fitting was performed using nonlinear regression analysis (Statgraphics Plus 5.1).

3.2.9 Data analysis

The beginning of the bypass was the designated time zero for cooling. As the duration of cooling/warming differed among patients, the start of fully warming was defined as the designated time zero of warming, and the moment of decoupling the heart lung machine was defined as the zero time for the postbypass period.

One needle did not work properly in one patient in the control group, so deep tissue temperatures in that group are based on $n=6$. Four patients of the control group were covered with forced-air heaters at the ICU (24, 30, 60 and 64 minutes after arrival at the IC). Two persons in the test group were given a heating screen at the ICU (62 and 200 minutes after arrival at the IC). Only statistical differences before giving additional heating equipment at the ICU were studied.

For three patients $w_{b,0}$ was not determined as no stable base line value for skin perfusion was observed. These data sets were excluded in the analysis.

Leg blood flow data of one patient taken at measurement moment four was excluded, because we observed an extreme increase in heart rate.

3.3 Results

3.3.1 Patient characteristics

Subject characteristics of the control and test group are shown in table 3.1. No significant differences were found in morphometric characteristics of the two groups.

Table 3.1: Subject characteristics. Values are given as mean values \pm standard deviation.

Subject characteristics	Control group	Test group	P
Gender [M/F]	5/2	2/6	0.13
Weight [kg]	80.8 \pm 10.9	78.6 \pm 12.0	0.72
Height [cm]	172 \pm 4	167 \pm 11	0.28
Age [y]	69.1 \pm 15	57.9 \pm 11	0.12
BMI [kgm ⁻²]	27.3 \pm 3.0	28.2 \pm 3.6	0.61
Fat [%]	31.8 \pm 5.9	36.0 \pm 5.4	0.17
BSA [m ²]	1.93 \pm 0.14	1.94 \pm 0.16	0.90

3.3.2 Core temperature

In figure 3.1, core temperatures are given during surgery and the first period at the ICU. Twenty minutes after weaning from bypass, core temperatures in the test group were slightly

higher than in the control patients ($P=0.07$). This difference lasted till patients were 50 minutes at the ICU ($P=0.09$). No differences were seen in nasal and rectal temperature between

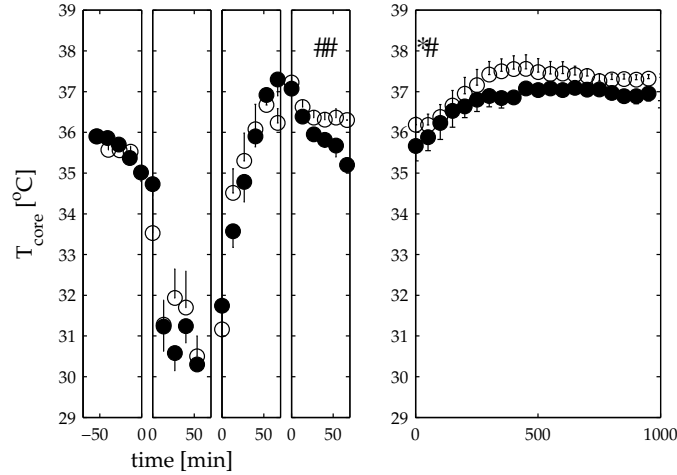


Figure 3.1: Core temperature during and after cardiac surgery. ● control group, ○ test group. From left to right the anesthesia stage, the cooling stage, the rewarming stage, the postbypass phase and the period at the ICU are shown, respectively. Significant differences ($P < 0.05$) are indicated with *, results with $P < 0.10$ are marked with #. Differences are only investigated when n is minimally 6 and 7 in the control and test group respectively. Values are given as means with standard deviation.

both groups at the end of rewarming, see table 3.2. Core temperature afterdrop, defined as the core temperature of the moment of going off pump minus the minimal postbypass core temperature, was significantly lower in the test group ($P=0.04$). A trend was visible to a longer lasting afterdrop for the control group ($P=0.21$). Afterdrop duration is the period from the end of bypass until the minimum postbypass core temperature is reached.

3.3.3 Mean skin temperature

In figure 3.2, the mean skin temperature is shown. Mean skin temperature of the test group was significantly higher 30-80 minutes after decoupling from the heart lung machine. Mean skin temperature of patients from the control group, that obtained forced-air heaters at the ICU, is indicated with a different symbol. An increase in mean skin temperature was clearly visible after that time point.

3.3.4 Thigh temperature

No significant difference was found in skin temperature of the thigh, $T_{\text{skin,thigh}}$ (figure 3.3(a)) between the two groups during anesthesia, cooling and warming. In the postbypass stage

Table 3.2: Temperature and afterdrop characteristics. Values are given as mean values \pm standard deviation.

Temperature and afterdrop characteristics	Control group	Test group	P
Nasopharyngeal temperature at the coolest point [°C]	29.4 \pm 0.6	29.7 \pm 1.4	0.61
Nasopharyngeal temperature at the end of rewarming [°C]	37.2 \pm 0.4	37.4 \pm 0.5	0.41
Rectal temperature at end of rewarming [°C]	36.6 \pm 0.2	36.5 \pm 0.5	0.63
Afterdrop [°C]	1.8 \pm 0.7	1.2 \pm 0.2	0.04*
Afterdrop duration [min]	73 \pm 24	59 \pm 14	0.21
Cooling time [min]	38 \pm 16	38 \pm 17	1.0
Warming time [min]	64 \pm 10	66 \pm 19	0.81
Bypass time [min]	102 \pm 19	105 \pm 30	0.82

*Significant different result (P<0.05)

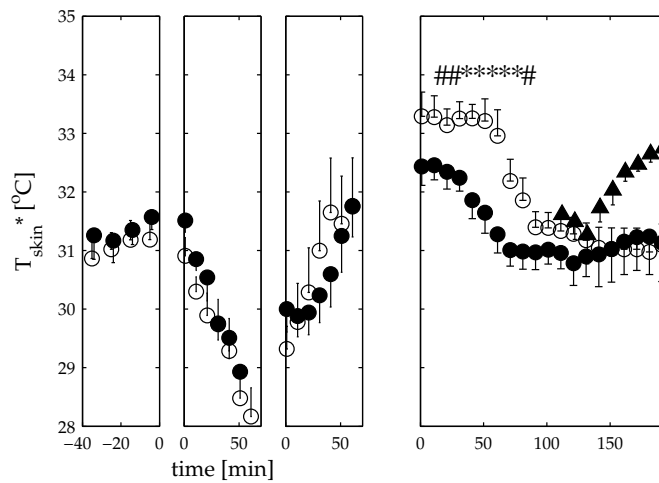


Figure 3.2: Mean skin temperature with standard deviation. ● control group, ○ test group, ▲ patients in control group who got forced-air heaters at the ICU. Significant differences (P<0.05) are marked with *, and results with P<0.10 are marked with #. Results are based on n=8 in test group and n=7 in control group. The figure consists of four parts, from left to right: anesthesia, cooling, warming and postbypass (operating theatre and ICU).

there was a tendency that the skin temperature of the thigh in the test group was higher than in the control group. The thigh temperature (T_{thigh}) at 8 mm depth (figure 3.3(b)) differed significantly prior to cooling and during the first 10 minutes of cooling. About 25 minutes before cooling T_{thigh} at 18 mm depth was significantly lower in the test group (figure 3.3(c)) which lasted till the moment cooling started. After approximately 50 minutes of rewarming thigh temperature at 38 mm depth was warmer in the control group than in the test group (figure 3.3(d)). This difference was observed till approximately 10 minutes after going off pump. The 95% confidence intervals at 25 minutes after decoupling the heart lung machine (where temperature differences were largest) are $-1.26^{\circ}\text{C} \leq T_{\text{test}} - T_{\text{control}} \leq 0.26^{\circ}\text{C}$ and $-1.44^{\circ}\text{C} \leq T_{\text{test}} - T_{\text{control}} \leq 0.09^{\circ}\text{C}$ at 18 and 38 mm depth, respectively. This indicates that clinically relevant improvement in deep thigh temperature at that time point can be excluded. The first three hours at the ICU no significant differences were found in thigh temperature at 8, 18 and 38 mm (not shown in a figure). Finally, no difference in mean thigh temperature as calculated with the parabolic regression method of Belani et al. (1993) was found at the operating theatre and ICU.

3.3.5 Skin blood flow

Typical curves of skin temperature under the toe and skin perfusion are given in figure 3.4. Skin perfusion is given in dimensionless perfusion units (PU). In figure 3.5 average values of the sampling distribution of the relative perfusion ($w_b/w_{b,0}$) are plotted against the change in temperature ($\Delta T = T - T_0$). The data with $\Delta T < 7^{\circ}\text{C}$ was used to fit the value of the unknown constant C in equation (3.5). The resulting fit and the average values are given in figure 3.5. The best fit revealed that $C=15.8\pm 1.7$, which means that at 10°C in local temperature coincides with a 16-fold increase in skin perfusion.

In figure 3.6 a typical example of a patient is shown before and after being covered with a forced-air blanket. The perfusion-temperature curve shows a shift to the right when forced-air heating is applied. This means that the perfusion was the same as in the situation without forced-air heaters whilst the local skin temperature of the toe increased $2.5\text{-}3^{\circ}\text{C}$. This effect was also visible in patients in the control group, to whom forced-air blankets were supplied at the ICU. Hence, we conclude that under these circumstances the forced-air heater did not change the amount of skin perfusion. Only skin temperature was affected by forced-air blankets.

3.3.6 Leg blood flow

Arterial blood supply into the right femoral artery was determined for 12 patients at four defined points in time, when no forced-air heating was used (figure 3.7). The base line value Q_0 (taken at the first measurement time point) equalled $0.22\pm 0.06 \text{ l min}^{-1}$ (range $0.13\text{-}0.32 \text{ l min}^{-1}$). Schmidt and Thews (1989) suggest that about 10% of the resting blood flow (about 5 l min^{-1}) is supplied to the legs. This amounts to approximately 0.25 l min^{-1} per leg, which is in agreement with the value found by us.

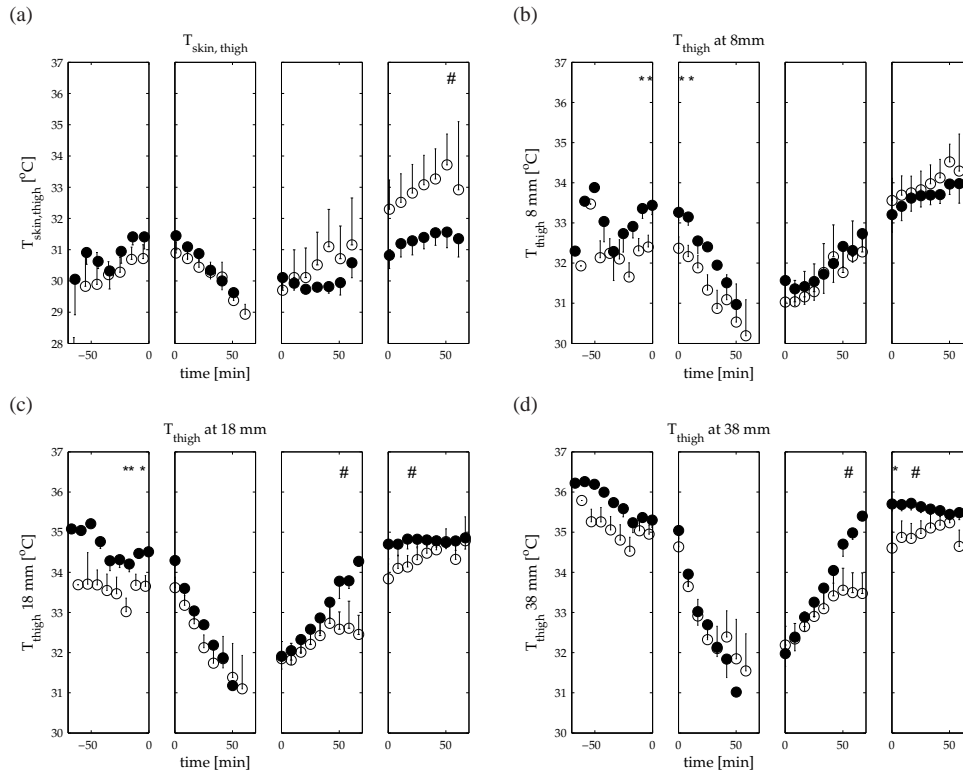


Figure 3.3: Thigh temperature measured at skin, 8, 18 and 38 mm depth during and after surgery with standard deviation. ● control group, ○ test group. Figures consist of four parts, from left to right: anesthesia, cooling, warming and postbypass. Differences are only investigated when the number of patients is minimally 5 and 7 in the control and test group, respectively. Significant differences ($P < 0.05$) are marked with *, results with $P < 0.10$ are marked with #.

Before entering the surgical room and during bypass cooling, no significant difference in leg blood flow was observed. Just after surgery, the leg blood flow decreased significantly ($P = 0.02$) and was still significantly reduced ($P = 0.02$) when the patients were at the ICU for three hours. No significant difference was observed between the last two measurement time points. From these results, it is concluded that leg blood flow through the femoral artery after surgery reduced to about 70% of the pre- and perioperative value.

Mean cardiac output or bypass flow was $2.4 \pm 0.4 \text{ l min}^{-1} \text{ m}^{-2}$. Individual changes in cardiac output/bypass flow were small over the four measurement points (mean fluctuation was 6.8%).

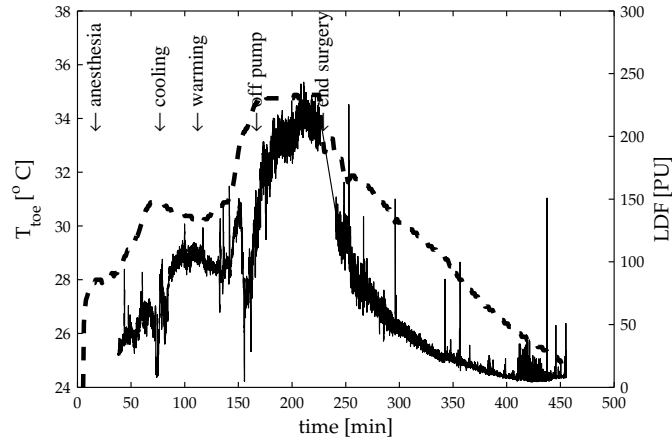


Figure 3.4: Toe temperature and perfusion as a function of time. The dotted line shows temperature and the solid line the Laser Doppler signal (LDF) in arbitrary perfusion units.

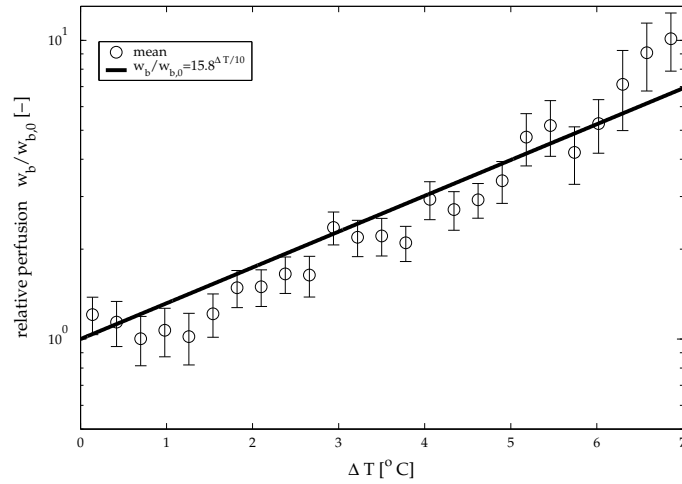


Figure 3.5: Mean relative perfusion and standard deviation of all patients versus relative temperature marked with \circ . Included is the best fit for equation (3) (solid line). Best fit was found for $C=15.8\pm 1.7$. Results are based on $n=12$.

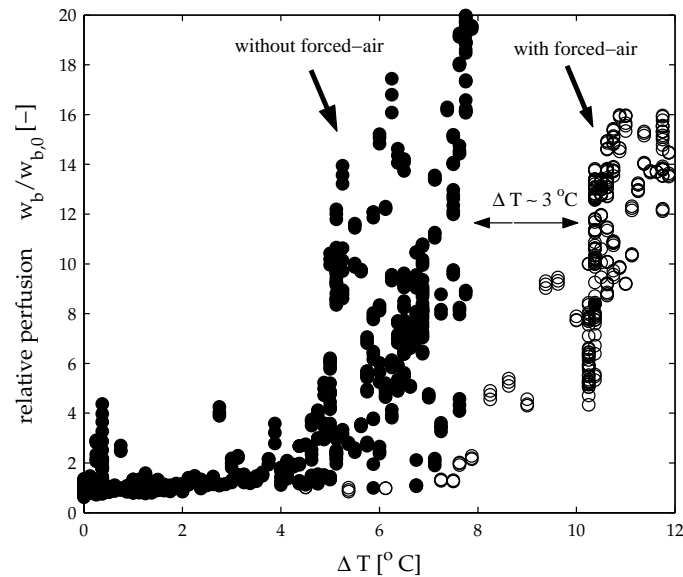


Figure 3.6: Example of a skin perfusion-temperature curve of one patient without and with forced-air heating. • denotes time points at which no additional blankets are used, ○ gives results when a forced-air blanket is used perioperatively.

3.4 Discussion

In this survey the reduction in afterdrop by using forced-air heaters was confirmed. A new approach in explaining the effectiveness of forced-air heaters was the simultaneous assessment of transient temperature distribution and peripheral perfusion in patients undergoing cardiac surgery. Two groups were studied: patients who were perioperatively rewarmed with and without forced-air blankets. Important findings in this study are that by using forced-air blankets no clinically relevant improvements in deep tissue temperature in the thigh can be expected, but only in skin and superficial tissue temperatures. Usage of forced-air heaters results in higher local skin temperature, but nonetheless does not lead to higher peripheral perfusion rates. Our data show that the extra heat from forced-air warming especially ends up in the core, and not in the deep periphery.

3.4.1 Perfusion

Local temperature and skin perfusion data were used to establish a relationship for skin temperature and perfusion in the toe during cardiac surgery, when no forced-air heating was used. Our data showed that a 10°C increase in skin temperature of the toe leads to a 16-fold increase in skin perfusion.

Usage of forced-air heaters resulted in higher local toe skin temperature (temperature increase

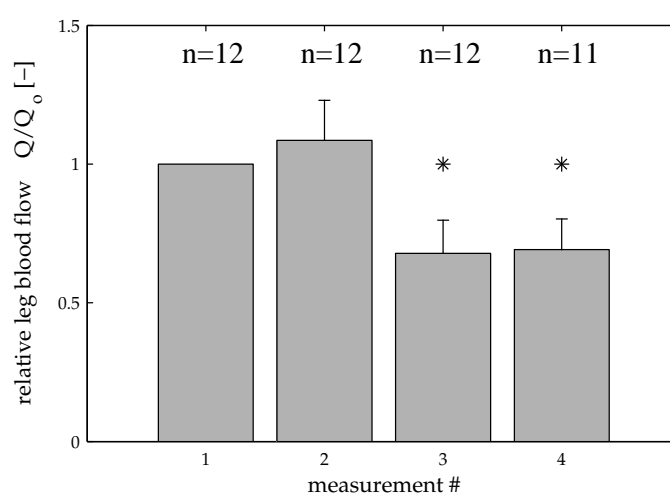


Figure 3.7: Relative change in blood flow through the right femoral artery obtained with ultrasound measurements. The first measurement is used as base line value (Q_0). Values are represented as mean with standard deviation. Measurements are performed at four moments in time: 1) just before entering the surgery room 2) at the coolest point during the bypass cooling 3) just after surgery as the patient has arrived at the ICU and 4) about three hours after surgery. The number of patients is indicated on top of each bar. The third and fourth measurements differed significantly ($P < 0.05$) from the first and second values.

of typically 2.5-3°C), but did not accompany with higher perfusion according to equation (3.5). Apparently, perfusion did not improve by cutaneous heating. If equation (3.5) would have held, perfusion could be advanced by applying forced-air heaters. In that case forced-air heaters had been even more effective in reducing afterdrop.

Ultrasound measurements pointed out that leg blood flow during the first hours after cardiac surgery was reduced to approximately 70% of the blood flow measured prior and during surgery. This decrease in postoperative blood flow coincided with the decrease in skin perfusion, that was observed under the toe at the ICU. Low skin perfusion suggests a high resistance in the vascular bed of the periphery. This leads to a lower leg blood flow. At about equal cardiac output (fluctuation 6.8%) this means that less blood leaving the heart is distributed to the periphery compared to the core.

3.4.2 Temperature

Afterdrop magnitudes of $1.8 \pm 0.7^\circ\text{C}$ (range 0.7-3.1°C) were found in the control group, and $1.2 \pm 0.2^\circ\text{C}$ (range 1.0-1.6°C) in the test group. This was slightly larger than in previous studies (Rajek et al., 2000, 1998). Rajek et al. (2000) reported an afterdrop of $1.2 \pm 0.2^\circ\text{C}$ for the control group and $0.5 \pm 0.2^\circ\text{C}$ for the test group. Patients in our study were cooled to lower temperatures (average 29.6°C) than Rajek's patients (31.8°C) and rewarmed to higher nasopharyngeal temperatures (37.3°C vs. 37.1°C). This might explain the larger afterdrop in our study. Rajek's previous study (Rajek et al., 1998) supports this explanation. Here afterdrop magnitudes of $1.5 \pm 0.4^\circ\text{C}$ were found for patients with passive covers who were cooled till $30.8 \pm 1^\circ\text{C}$ and were rewarmed till core temperatures of 37.5°C. Also the fact that we used another type of heating blanket (tube model vs. a cardiac blanket that covered the legs) could have caused the different outcomes.

Only marginal differences were observed between the thigh temperatures in the two groups. Skin temperature and thigh temperature at 8 mm depth of the test groups tended to be warmer in postbypass stage. Unexpected were the results that at the end of the rewarming stage and beginning of the postbypass stage deep thigh temperatures (at 18 and 38 mm depth) were higher in the group without additional forced-air heaters. The 95% confidence intervals, at 25 minutes after decoupling the heart lung machine, show that clinical relevant improvements, when using forced-air heaters, can be excluded at the deep peripheral tissue. This indicates that the extra heat of forced-air warmers does neither penetrate to the deeper peripheral tissue by means of conduction, nor by heat redistribution by the blood. Thigh tissue temperature in the control group was over the total measurement period slightly higher. It is remarkable that forced-air heaters did not compensate, or reverse this. It is expected that heat provided by forced-air heaters only causes a clinical relevant temperature rise at the skin and at superficial situated tissue but not at the deeper tissue. Average thigh temperatures as calculated according to equation (3.3) did not show significant differences between the groups, which agreed with the results of Rajek et al. (2000).

There are three mechanisms by which adding heat to peripheral skin can favour core temperature: 1) direct conduction through peripheral tissue, which would reduce the core-

periphery gradient, 2) blood-borne convection of heat from the skin, which would result in a higher blood pool temperature and 3) blood-borne convection of heat from the deeper peripheral tissue. The fact that forced-air warmers reduced afterdrop, but did not warm the deep peripheral tissue, indicates that the effectiveness of forced-air warmers in reducing afterdrop is especially explained by blood-borne convection from the skin. Forced-air heaters favour skin temperature by convective heat transfer. Moreover, heat loss from the patient's body to the surrounding is reduced. We think that the major part of the extra heat of forced-air warming is transported from the capillary network in the skin to the venous system through the superficial veins of the lower extremities (Van De Graaff, 1995). From there, the heat is transported via direct connections to the heart. This leads to a higher mixed blood pool temperature in the test group than in the control group. The slightly warmer blood is redistributed over the body. Core organs are better perfused than peripheral organs under current circumstances. Indeed, our leg blood flow measurements underline this thought, as we observed that postoperative leg blood flow was reduced significantly compared to pre- and peri-operative flow. In this way, the decrease in core temperature drop and the unchanged deep peripheral temperature in the test group, can be explained.

3.5 Comparison of passive model and cardiac surgery measurements

With help of the developed passive model from chapter 2 (without active thermoregulation or any adjustments for the thermal effects of anesthetics), simulations were run to mimic the temperature response of the passively covered patients as presented in section 3.2.3. In short: 7 patients (mean body characteristics: weight 80.8 kg, height 172 cm, fat percentage 31.8%) were cooled with help of a heart lung machine to a nasopharyngeal temperature of 30°C. Towards the end of surgery, they were rewarmed to a nasopharyngeal temperature of 37-37.5°C. Bypass flow was kept at 2.4 l min⁻¹m⁻². The fluid-blood gradient was near 1°C. During cooling, a circulating water mattress was used with a temperature of 30°C. During rewarming and in the postbypass stage, the mattress temperature was approximately 36°C. No forced-air heater was used. The surrounding temperature was 20°C. Simulations were run for a subject with the group average body characteristics. Core (nasopharyngeal) and mean skin temperature data from the aortic valve surgery were compared to the passive simulation results.

As can be seen in figure 3.8 the general trends of core and mean skin temperature are predicted well by the passive model, but the quantitative behaviour is somewhat different. Especially, in phase 1 and 4, core temperatures of the simulation are higher than the measured values. This is mainly due to omitting the effect of the anesthesia, which lets the metabolic rate decrease by approximately 30% (Matsukawa et al., 1997), see also section 2.4. In figure 3.9 the temperature results are shown in case the anesthesia induced decrease of 30% in metabolic rate is implemented in the model. As can be seen, model predictions with de-

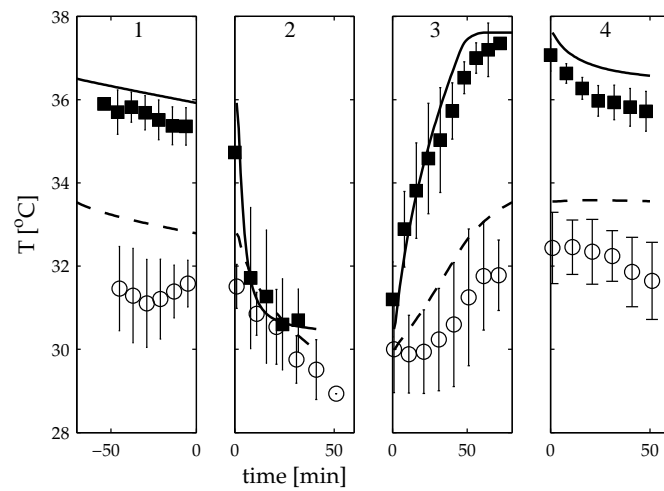


Figure 3.8: Comparison of passive model simulations and measurements without forced-air heating. The surgery consist of four stages: 1. anesthesia stage 2. cooling with heart lung machine 3. warming with help of heart lung machine 4. postbypass stage. ■ and ○ represent experimentally assessed core and mean skin temperature, respectively. — and — — represent the core and mean skin temperatures following from the passive model simulation, respectively.

creased metabolism indeed considerably improve the resemblance with the measurements. The skin temperature is mainly determined by external influences. The model is quite sensitive to the imposed boundary conditions. Probably, skin temperature predictions will improve, in case experimental boundary conditions (e.g. surrounding temperature, clothing insulation, air flow etc.) are assessed in more detail.

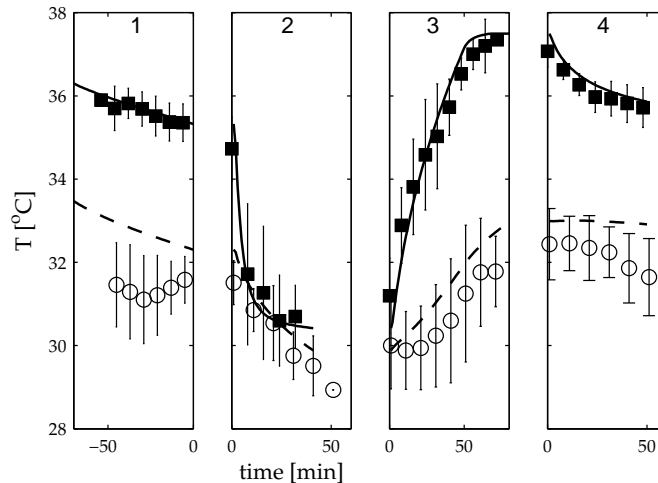


Figure 3.9: Comparison of passive model simulations with 30% decreased metabolism and measurements without forced-air heating. The surgery consist of four stages: 1. anesthesia stage 2. cooling with heart lung machine 3. warming with help of heart lung machine 4. postbypass stage. ■ and ○ represent experimentally assessed core and mean skin temperature, respectively. — and — — represent the core and mean skin temperatures following from the passive model simulation, respectively.

3.6 Conclusion

Our measurements confirm that afterdrop is reduced by using forced-air heating. Current measurements reveal that using forced-air heaters does not lead to clinically relevant improvements in deep peripheral temperature, but only in skin and superficial peripheral temperature. Laser Doppler flowmetry measurements point out that forced-air heating does not improve skin blood flow proportionally to the increase in skin temperature. We think that the increase in temperature of the venous blood that returns to the heart especially favours core organs. Indeed, the measured significant decrease in postoperative leg blood flow suggests that less warmed blood leaving the heart flows to the legs in the last stage of the surgery. We therefore conclude that the majority of extra heat from forced-air heaters is directly transported from the skin capillaries to the heart, and from there mainly redistributed to core organs, and not so much to the periphery.

Comparison of the passive model, that was developed in chapter 2, to the measurement data of this chapter resulted in the conclusion that with help of the passive human thermal model the qualitative behaviour of patients during cardiac surgery can be predicted. However, it is expected that the quantitative predictions can be much more improved by formulating an active model, that depends on the drug concentration in the blood. Based on the passive model results of section 2.4 and the previous section, it is concluded that there is an aim for a detailed active part for the human thermal model that accounts for the impaired thermoregulation and metabolism of the body during anesthesia. Accordingly, the next chapter focusses on the formulation of the active part of the model.

CHAPTER 4

Active model for cardiac surgery*

4.1 Introduction

Autonomous thermoregulation by the body occurs in several ways: during cold, the defense mechanisms are vasoconstriction, shivering and non-shivering thermogenesis while in the heat vasodilatation and sweating are the protective mechanisms. When a person is anesthetized, thermoregulation is impaired in a dose dependent way and the interthreshold range (where no thermoregulatory responses take place) may increase from 0.2°C to 4°C. However, once the thermoregulatory response is triggered, the maximum intensities of the reactions are normal (Sessler, 1995). The gain of sweating is well preserved during anesthesia (Washington et al., 1993), while the gain of vasoconstriction is reduced by at least a factor of two (Kurz et al., 1995b). However, the vasoconstriction gain is still so high that this reduction can be ignored.

Consequently, during surgery, patients commonly develop hypothermia due to the inhibitive effect of anesthetics on thermoregulation and the exposure to the cold environment of the operating room.

In this chapter, a model is derived to describe drug-dose-dependent thermoregulation during anesthesia. The thermoregulatory model that is developed to simulate a cardiac surgery under hypothermic conditions, confines to the vasoconstriction response. During general anesthesia, non-shivering thermogenesis does not occur (Sessler, 1997) while shivering is prohibited by muscle relaxants.

* Parts of chapter 2 and 4 have been published in:

Severens N.M.W, Van Marken Lichtenbelt W.D., Frijns A.J.H., Van Steenhoven A.A., De Mol B.A.J.M and Sessler D.I. (2007). A model to predict patient temperature during cardiac surgery. *Phys Med Biol*, 52:5131–5145.

4.2 Interplay between temperature, metabolism and perfusion

Under thermoneutral conditions, tissue perfusion and metabolism are at a basal perfusion rate ($w_{b,0}$) and basal metabolic rate (q_0). Under non-neutral conditions, perfusion rates and metabolic rates vary with temperature. The interplay between metabolism and temperature was modelled according to the Q_{10} relation. This relation states that for every 10°C reduction in tissue temperature, there is a corresponding reduction in cell metabolism by a factor Q_{10} (Gordon, 1974; Fiala et al., 1999; Dennis et al., 2003; Janssen et al., 2005):

$$\frac{q_i}{q_{i,0}} = Q_{10}^{\frac{T_i - T_{i,0}}{10^\circ\text{C}}} \quad (4.1)$$

with q_i representing the metabolic heat production in element i . For Q_{10} mostly the value 2 is used. Induction of general anesthesia decreases metabolic heat production. In literature metabolic rate decreases are reported between 15 and 40% (Matsukawa et al., 1995b, 1997; Sessler, 2000). Hence, as a first approach, a 30% reduction in metabolic rate is used in the model. In section 4.7, the sensitivity of the model to the variability/uncertainty of this metabolic reduction is studied in more detail. The metabolic rate reduction leads to the following expression:

$$q_{i,\text{anes}} = 0.7q_i \quad (4.2)$$

In non-neutral conditions, blood flows vary with changes in regional metabolic rates. This is accounted for by calculating the change in the factor $\Delta\beta_i = \rho_b c_b \Delta w_{b,i}$ [$\text{Wm}^{-3}\text{K}^{-1}$] as a function of the change in metabolism Δq_i . For this relation, a proportionality constant $\mu_b = 0.932$ [K^{-1}] was obtained from Fiala et al. (1999):

$$\Delta\beta_i = \mu_b \Delta q_i \quad (4.3)$$

Blood vessels in the skin and in skeletal muscles can also be innervated by sympathetic neural stimulation (Stolwijk and Hardy, 1966; Daanen, 1997). When body temperature is lower than the vasoconstriction threshold, perfusion is lowered by the normal local temperature effect and via a central vasoconstriction tone. The expression for skin and muscle blood flow was modelled according to the formulation proposed by Stolwijk (1971):

$$\frac{\beta_i}{\beta_{i,0}} = f \cdot Q_{10}^{\frac{T_i - T_{i,0}}{10^\circ\text{C}}} \quad \text{with} \quad Q_{10} = 2 \quad (4.4)$$

and

$$f = \frac{1}{1 + a_{cs,i} Cs} \quad \text{for the inner skin layer and skeletal muscles} \quad (4.5)$$

in which $a_{cs,i}$ is the distribution factor for vasoconstriction and Cs is the vasoconstriction signal. As a first approach, the values for a_{cs} are based on Fiala et al. (2001) (see table 4.1). Later, in chapter 5 measurements are described to determine physiological based values for those coefficients. As can be seen in equation (4.4), skin and muscle blood flow of a segment are affected by the local temperature T_i as well as a centrally mediated vasoconstriction signal Cs . According to Schmidt and Thews (1989), the vasoconstriction tone in the muscle is

Table 4.1: Values for a_{cs} , based on Fiala et al. (2001).

Body part	a_{cs}
head	0.0300
face	0.0330
neck	0.0250
shoulder	0.0100
thorax	0.0005
abdomen	0.0205
hand	0.1100
arm	0.1945
leg	0.2000
foot	0.3765

less than in skin.

In case body temperature is lower than the threshold for vasoconstriction, a certain vasoconstriction tone is generated and in case body temperature is higher than the vasoconstriction threshold, the centrally mediated vasoconstriction tone is absent. For the implementation of this concept, it is required to have a drug-dose-dependent threshold for vasoconstriction and a gain and maximum intensity of the vasoconstrictor tone. To formulate a drug-dose-dependent relation, information is required about the starting point of vasoconstriction as a function of the blood drug concentration.

4.3 Model formulation

Opioids and intravenously injected anesthetics lower the threshold for vasoconstriction in linear proportion to increased plasma concentration (Sessler, 1997). During cardiac surgery a mixture of anesthetic drugs is administered to the patient. The simplest way to study the relation between drug concentration and vasoconstriction, is to directly relate measured drug concentration from blood samples to vasoconstriction threshold. An alternative for taking blood samples is to use pharmacokinetic models to assess the drug concentration in the blood. An advantage of using such a model is that it can be used to predict unknown situations. Therefore, a pharmacological model will be used to provide information about the momentary drug concentration in the blood. For the development of a vasoconstriction model, the anesthetic protocol of the measurement series outlined in chapter 3, was used, with propofol as the main anesthetic agent.

For reducing model complexity, the following simplifications were made: propofol concentration is linearly related to the overall drug concentration and represents the overall drug concentration, other drugs do not affect propofol and the temperature effect on blood propofol concentration (Sessler, 1995) is omitted in the model.

In order to relate the blood propofol concentration to the momentary body temperature

at the time point where the vasoconstriction threshold is reached, measurement data of the 15 patients, involved in the protocol outlined in chapter 3, were analyzed. For all patients, the time for the start of vasoconstriction was appointed. At this time the standardized core temperature was calculated from the measurements (according to equation (4.28)). With help of the pharmacological model, the momentary blood propofol concentration at that time can be obtained. An overview of the approach to formulate a dose-dependent relation for calculating the vasoconstriction, is given in figure 4.1.

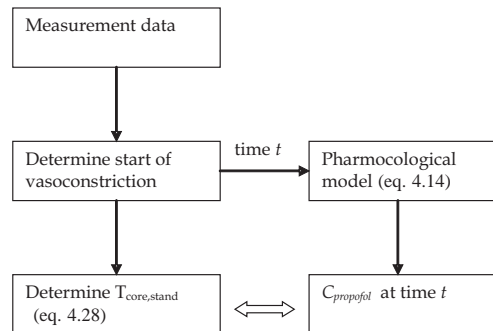


Figure 4.1: Approach to derive a linear relation between propofol concentration and vasoconstriction threshold. From measurement data of all individual patients of chapter 3, the starting time of vasoconstriction was determined. At that time, the standardized core temperature was determined. With the help of the pharmacological model, also the blood propofol concentration at that time was calculated. Then, the standardized core temperature and the drug concentration in the blood were used to derive a relation that couples these two quantities.

4.4 Pharmacological models

Development of pharmacokinetic models has generally followed three approaches. The model-independent approach, the compartmental approach and the physiological approach. The model-independent approach does not try to make any physiological connection in contradiction to the compartmental and the physiological approach. Instead, the model-independent models consist of an empirical set of mathematical equations, that represent the situation of interest. The usual model formulation takes place by selecting a best fit relation using a statistical criterion. This limits the application field of the model, as the selected model does not extend beyond the information contents of the available experimental data.

The compartmental approach assumes that the drug distributes into typically two or three compartments. Those compartments usually represent a particular region of the body, an organ, a group of tissues, or body fluids. The compartments are assumed to be well-mixed.

Consequently, no spatial variations exist in a compartment. With help of this type of models, it is easier to relate fitted parameters to physiological processes. For instance clearance can be related to renal function. Nevertheless, the compartments in these classical compartment models do not represent real physical spaces, and their meaning has been misinterpreted by many authors. Consequently, these models should be viewed as semi-mechanistic models (Aarons, 2005).

In physiological models, the movement of the drug is based on blood flow rate through a particular organ or tissue and includes consideration of the rates of the mass transport processes within these regions. The advantages of a physiological approach are (1) they are parameterized in real physiological quantities (e.g. blood flows, tissue volumes), (2) they embody considerable *a priori* knowledge, like the blood flow connectivity of body tissues and elimination sites and (3) they lend themselves for use when drug dose or model parameters differ from those initially studied, e.g. animal to man kinetic scale-up. Drawbacks of physiological modelling are the following. (1) Assumptions regarding kinetics are needed to complete the models, while simple assumptions are often made without evidential support. (2) For the estimation of unknown model parameters and tissue kinetics, data from several tissues and blood must be fit simultaneously. This creates considerable problems of data weighting and multiparameter estimation. (3) Assumed values of physiological parameters may be in error if not actually measured. Often, data of relevant tissues and organs is not available and hard to obtain.

Verotta et al. (1989) proposed a linear system approach to flow models that preserves the advantageous features of physiological flow models, but eliminates the disadvantageous ones. Their idea was to estimate model parameters by physiological hybrid modelling. This means that each submodel is treated as a hybrid of the complete model for which only its inputs and outputs are of interest. The structure and origin of the input function is irrelevant as long as it provides a good fit for the *in vivo* measured data. This results in a nonparametric model instead of the usual tissue specific parameters like blood flow and volume. The model only gives the function response of the isolated compartment to a certain input. The function can be used to estimate some of the usual tissue-specific parameters (blood flow, volume, tissue clearance) if desired. Estimation of these nonparametric model parameters is less complex than determining all tissue specific parameters, but it is still possible to give predictions about blood and tissue kinetics when drug doses or model parameters differ from the initially studied parameters. By using the methodology of Verotta et al. (1989) undesirable assumptions regarding intratissue distribution need not to be made, whilst no concessions are made in descriptive and predictive power.

In literature only limited availability of studies on human *in vivo* physiological propofol data was found. One of the few found work on propofol modelling was done by Upton and Ludbrook (1997). They described a simple, but flexible six-compartmental hybrid physiological model for calculating blood propofol concentrations in sheep. As this was the only model that extensively described all the used relations and parameter values, this model is used for modelling anesthesia concentration in current human body model.

Because body size and weight are comparable for sheep and human, no large differences exist in propofol kinetics and dynamics between sheep and humans. Indeed, Ludbrook and Upton (1997) found close agreement between human and sheep data. Hence, it seems justified to use the sheep model for current application.

4.4.1 Flow-limited versus diffusion-limited approach

The Upton and Ludbrook model assumes that the transport of propofol through the capillary wall is flow-limited for the venous mixing compartment, the lung, the well-perfused organs and the poorly perfused organs. The brains are represented by the flow-limited capillary compartment and the transport to the brain core happened with diffusion limitation (see figure 4.2). Before using this model, the flow and diffusion limitation approach of the model is evaluated with help of established solute transport theory, as described by Fournier (1999). Drug particle transport to tissue depends on the blood flow rate, the resistance that the blood gives for the solute transport and the permeability of the capillary wall. For a flow-limited approach to be valid, the transport of drugs should be limited by the blood supply. For diffusion-limitation, the diffusion over the capillary is the limiting step.

Solute flux from the blood to the capillary wall at position r_c , and across the capillary wall to the beginning of the tissue space at $r_c + t_m$ is represented by:

$$N = 2\pi r_c \Delta z K_0 (C - \bar{C}|_{r_c+t_m}) \quad (4.6)$$

with t_m the wall thickness of the capillary, N the transport rate over the capillary wall [mol s^{-1}], r_c the inner radius of the capillary, Δz the axial distance in the capillary, K_0 the overall mass transfer coefficient [ms^{-1}], C the mixing cup solute concentration in the capillary and $\bar{C}|_{r_c+t_m}$ the concentration at the outer capillary wall in the tissue domain [mol m^{-3}]. K_0 depends on the resistance to the solute transport rate (k_m) and on the resistance of the capillary wall (P_m):

$$K_0 = \frac{1}{\frac{1}{k_m} + \frac{1}{P_m}} \quad (4.7)$$

The solute transport rate is related to the Sherwood number by:

$$k_m = \frac{\text{Sh}D}{D_c} \quad (4.8)$$

with D representing the solute diffusivity [m^2s^{-1}] and D_c the inside diameter of the capillary (capillary characteristics are summarized in table 4.2). When both the concentration field ($\frac{z}{D_c} > 0.05\text{ReSc}$) and the hydrodynamic flow ($\frac{z}{D_c} > 0.05\text{Re}$) are fully developed the Sherwood number (Sh) equals 3.66. For capillary blood flow, the Re-number is $\text{O}(10^{-3})$, the Sc-number $\text{O}(10^3)$ and L/D_c is $\text{O}(10^2)$, so both criteria are fulfilled.

The diffusivity D of propofol is estimated using the Stokes-Einstein equation:

$$D = \frac{RT}{6\pi\mu a N_A} \quad (4.9)$$

with R denoting the ideal gas constant ($8.314\text{Jkg}^{-1}\text{mol}^{-1}$), T the temperature [K], a the propofol radius, μ the solution viscosity ($1.2 \cdot 10^{-3}\text{kg m}^{-1}\text{s}^{-1}$) and N_A Avogadro's number ($6.023 \cdot 10^{23}$ molecules/mol). The radius of the solute was estimated by (Fournier, 1999):

$$a = \left(\frac{3MW}{4\pi\rho N_A} \right)^{1/3} \quad (4.10)$$

For propofol, having a molecular weight of $MW=178.2 \text{ gmol}^{-1}$, density ρ equal to the density of water ($1 \cdot 10^6 \text{ gm}^{-3}$) this results in $a_{\text{propofol}} = 0.4 \cdot 10^{-9} \text{ m}$. Implementing this value in equation (4.9) gives a diffusivity of $D = 4.73 \cdot 10^{-10} \text{ m}^2 \text{ s}^{-1}$. Eventually this results, when using equation (4.8), in $k_m = 1.73 \cdot 10^{-4} \text{ ms}^{-1}$.

Table 4.2: Capillary characteristics based on Fournier (1999); Janssen (2007).

Property	Symbol	Value
Inner diameter	D_c	$10 \mu\text{m}$
Length	L_z	$0.1 \cdot 10^{-2} \text{ m}$
Wall thickness	t_m	$0.5 \mu\text{m}$
Blood velocity	U	$0.05 \cdot 10^{-2} \text{ m s}^{-1}$
Pore fraction	ε	0.01
Wall pore radius	r	3.5 nm
Tortuosity	τ	2

The permeability of the capillary wall P_m with wall thickness t_m for solute propofol is given by Fournier (1999):

$$P_m = \frac{D_m \varepsilon}{t_m \tau} \quad (4.11)$$

where D_m is the effective diffusivity of the solute in the membrane, ε is the pore fraction and τ is the tortuosity. The Renkin equation relates the bulk diffusivity (D) to the effective diffusivity D_m by:

$$D_m = D \left(1 - \frac{a}{r} \right)^2 \left[1 - 2.1 \left(\frac{a}{r} \right) + 2.09 \left(\frac{a}{r} \right)^3 - 0.95 \left(\frac{a}{r} \right)^5 \right] \quad (4.12)$$

Implementing the solute radius, the wall pore radius and the solute diffusivity results in $D_m = 2.84 \cdot 10^{-10} \text{ m}^2 \text{ s}^{-1}$. The permeability, calculated with equation (4.11) is then equal to: $P_m = 2.83 \cdot 10^{-6} \text{ ms}^{-1}$.

With help of equation (4.7) it can be shown that $K_0 \approx P_m$. In other words, the blood offers little resistance to the solute transport in comparison to that of the capillary wall.

From this result follows that solute transport depends mainly on two factors: 1) the total permeability of the capillary wall ($2\pi r_c P_m z$) and 2) the blood flow rate ($\pi r_c^2 U$). The ratio

Θ between those factors is used to define whether the solute transport can be considered flow limited or diffusion limited. Θ is given by:

$$\Theta = \frac{2P_m z}{r_c U} \quad (4.13)$$

When $\Theta \ll 1$ the transport is diffusion-limited and when $\Theta \gg 1$ the transport can be considered flow-limited.

Implementation of the values in equation (4.13) leads to $\Theta = 2.23$. This means that the propofol transport is indeed closer to being flow-limited than to being diffusion limited. As a first estimate, a predominantly flow limited model for most organs seems acceptable.

Experiments performed by Gredell et al. (2004) revealed that propofol diffuses extremely slowly in rat brain tissue *in vitro*, its diffusion coefficient being approximately $D_t = 0.02 \cdot 10^{-10} \text{m}^2 \text{s}^{-1}$. It was shown (Fournier, 1999) that the ratio $\frac{D_t}{D}$ and $\frac{D_m}{D}$ are of the same order of magnitude. When implementing D_t in equation (4.11) this leads to $P_m = 2 \cdot 10^{-8} \text{ms}^{-1}$. Implementing this value in equation (4.13) gives $\Theta = 0.016$, which is $\ll 1$. From this, it follows that propofol transport in the brain is diffusion limited, under the assumption that propofol diffusion in rat brain tissue and human brain tissue are comparable.

From this analysis, it can be concluded that using a flow limited model for most compartments and a diffusion limited approach for describing the brain compartment, as was chosen by Upton and Ludbrook (1997), is justified.

4.4.2 A hybrid physiological model for propofol

In the pharmacological model of Upton and Ludbrook (1997), the body is divided into compartments which represent individual organs and tissue groupings. An overview of the model is shown in figure 4.2.

Transport into or out of a compartment is described by a mass balance around that compartment. A lumped model is used, which means that the concentration in a compartment is homogeneous and that the physical variables describing the transport processes in the compartment are only time dependent. The general mass balance equation in a lumped compartment model yields:

$$V_i \frac{dC_i}{dt} = x_{\text{in}} + \sum Q_i C_i - x_{\text{out}} \quad (4.14)$$

where V_i is the volume of the compartment [l], C_i is the propofol concentration in the compartment [mg l^{-1}], Q_i is the flow rate [l min^{-1}] and x_{in} and x_{out} denote the injected and excreted drug rates, respectively. The concentration of drugs in the venous mixing compartment is taken as the representative of the blood propofol concentration.

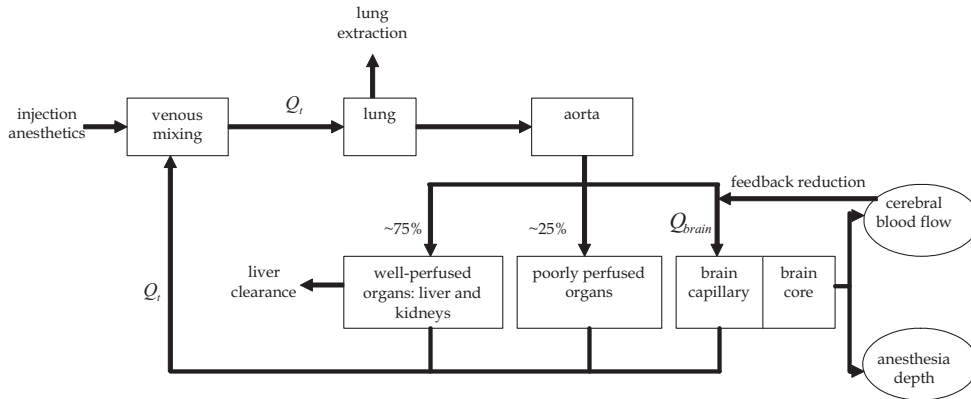


Figure 4.2: Overview of the compartmental propofol model, based on Upton and Ludbrook (1997). The concentration of drugs in the venous mixing compartment is taken as the representative value of the blood propofol concentration.

Detailed mass balances in the compartments

In the pharmacological model, the venously injected concentration propofol C_{inj} is given by:

$$C_{inj} = \frac{R_{propofol}}{Q_t} \quad (4.15)$$

where R is the dose rate of propofol and Q_t the cardiac output (symbols and standard values are summarized in table 4.3). The mass balance in the venous mixing compartment is denoted by:

$$V_{mix} \frac{dC_{pa}}{dt} = Q_t(C_{inj} - C_{pa}) + Q_1 C_1 + Q_2 C_2 + Q_{brain} C_{b,cap} \quad (4.16)$$

with V_{mix} representing the venous mixing compartment, C_{pa} the pulmonary artery concentration, Q the flow and C tissue concentration. Subscripts 1 and 2 represent rapidly perfused and slowly perfused tissue, respectively. $C_{b,cap}$ is the brain capillary concentration and Q_{brain} is the flow in the brain.

Before lung extraction the mass balance in the lung is given by:

$$V_{lung} \frac{dC_{lung}}{dt} = Q_t(C_{pa} - C_{lung}) \quad (4.17)$$

Herein is V_{lung} the apparent volume of the lung and C_{lung} the arterial concentration before lung extraction.

Lung extraction (E_{lung}) is empirically described by (Upton and Ludbrook, 1997):

$$\frac{1}{E_{lung}} = 0.007C_{pa} + 0.013 \quad (4.18)$$

Table 4.3: Variables of the standard propofol model.

Parameter	Description	Value
R_{propofol}	Dose rate propofol	$[\frac{\text{mg}}{\text{min}}]$
Q_t	Cardiac output	$5.6 \frac{1}{\text{min}}$
Q_1	Flow in rapidly perfused tissue	$\frac{1}{\text{min}}$
Q_2	Flow in slowly perfused tissue	$\frac{1}{\text{min}}$
$Q_{b,0}$	Base line cerebral flow	$0.04 \frac{1}{\text{min}}$
V_{mix}	Hypothetical venous mixing compartment	0.255 l
V_{lung}	Apparent volume of the lung	3.607 l
$V_{b,\text{cap}}$	Apparent volume of brain capillary space	0.143 l
$V_{b,\text{core}}$	Apparent volume of the brain core	0.035 l
V_1	Volume rapidly perfused tissue	15.67 l
V_2	Volume slowly perfused tissue	570 l
E_{lung}	Lung extraction	[-]
Cl_{liver}	Hepatic clearance	$1.12 \frac{1}{\text{min}}$
Ps	Membrane permeability of the brain	$0.032 \frac{1}{\text{min}}$
C_{pa}	Pulmonary artery concentration	$[\frac{\text{mg}}{\text{l}}]$
C_{lung}	Lung concentration	$[\frac{\text{mg}}{\text{l}}]$
C_{art}	Arterial concentration	$[\frac{\text{mg}}{\text{l}}]$
$C_{b,\text{cap}}$	Brain capillary concentration	$[\frac{\text{mg}}{\text{l}}]$
$C_{b,\text{core}}$	Brain core concentration	$[\frac{\text{mg}}{\text{l}}]$
Q_{red}	Percentage reduction in cerebral blood flow	%
A_{inc}	Percentage increase in anesthesia	%

After lung extraction, the propofol concentration in the blood C_{art} is given by:

$$C_{\text{art}} = C_{\text{lung}} \frac{100 - E_{\text{lung}}}{100} \quad (4.19)$$

Cerebral blood flow is linearly reduced by a percentage Q_{red} with increasing propofol concentration in the brain core ($C_{\text{b,core}}$):

$$Q_{\text{red}} = 19.82C_{\text{b,core}} \quad (4.20)$$

Anaesthetic drugs can reduce cerebral blood flow to only 50% of the base line value (Drummond and Shapiro, 1994). So Q_{red} is maximal 50. Brain blood flow Q_{brain} is then given by:

$$Q_{\text{brain}} = Q_{\text{b,0}} \frac{100 - Q_{\text{red}}}{100} \quad (4.21)$$

The mass balances in the brain capillary and brain core are given by:

$$V_{\text{b,cap}} \frac{dC_{\text{b,cap}}}{dt} = Q_{\text{brain}}(C_{\text{art}} - C_{\text{b,cap}}) + \text{Ps}(C_{\text{b,core}} - C_{\text{b,cap}}) \quad (4.22)$$

and

$$V_{\text{b,core}} \frac{dC_{\text{b,core}}}{dt} = \text{Ps}(C_{\text{b,cap}} - C_{\text{b,core}}) \quad (4.23)$$

Ps is the membrane permeability of the brain and $V_{\text{b,cap}}$ and $V_{\text{b,core}}$ denote the apparent volumes of the brain capillary space and brain core, respectively.

The blood flows to the rapidly (Q_1) and poorly (Q_2) perfused compartments are calculated according to:

$$Q_1 = 0.75(Q_t - Q_{\text{brain}}) \quad (4.24)$$

and

$$Q_2 = 0.25(Q_t - Q_{\text{brain}}) \quad (4.25)$$

The mass balance equations in the rapidly and poorly perfused tissue yield:

$$V_1 \frac{dC_1}{dt} = Q_1(C_{\text{art}} - C_1) - \text{Cl}_{\text{liver}}C_1 \quad (4.26)$$

and

$$V_2 \frac{dC_2}{dt} = Q_2(C_{\text{art}} - C_2) \quad (4.27)$$

with Cl_{liver} representing the liver clearance.

A parameter study was performed in which flows and volumes of the compartments were changed by 20%. From this parameter study, it was observed that the most sensitive parameter in the propofol model was cardiac output. Therefore, the cardiac output value in the model was replaced by the actual value of cardiac output for the individual patients.

4.4.3 Comparison of the pharmacological model to other models

For testing the model, results obtained with the sheep model of Upton and Ludbrook (1997) are compared to two other models: the PBPK model developed by Levitt and Schnider (2005) and the NONMEM model of Schnider et al. (1998). Both models are human models. PBPK stands for physiological based pharmacokinetic model, which means that it is tried to represent the body in terms of realistic human parameters. The model uses 13 compartments. The NONMEM model is a 6-parameter compartmental model (see also the beginning of section 4.4 for explanation of the model types).

Because only limited experimental data was available, the PBPK model and the NONMEM model were both fitted and evaluated by applying it to the same experimental data of Schnider et al. (1998). This means that it can be expected that the PBPK and NONMEM model are greatly dependent and show large similarity. Drawback of the descriptions of the PBPK and NONMEM model in literature is that not all details and values of the models are described, but the descriptions still offer possibilities to compare the predictions of current used model to other (human) models.

We compared two simulation results of the modified Upton and Ludbrook model to the PBPK model and the NONMEM model. This data set was not used to derive the PBPK and NONMEM model. The first test case involved a male (weight 77 kg and height 177 cm) for which a sedation protocol was used with an 1-hour constant infusion of $100 \mu\text{g kg}^{-1}\text{min}^{-1}$ propofol, followed by a 9-hour washout period. Figure 4.3 shows the predictions of the three models.

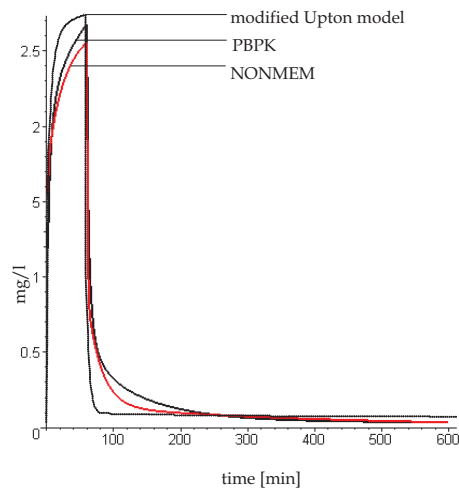


Figure 4.3: Validation of the compartmental propofol model. Model concentration versus time for a 1-hour constant infusion of $100 \mu\text{g kg}^{-1}\text{min}^{-1}$ followed by a 9 hour washout.

It is seen that the peak concentration and the concentration during the washout period obtained by the modified Upton and Ludbrook model are of the same magnitude as the PBPK

and NONMEM model, but the time constant of the reaction is somewhat higher.

The second test case involved a protocol for a 5-day constant infusion of $100 \mu\text{g kg}^{-1}\text{min}^{-1}$ for a male (weight 77 kg and height 177 cm). Again, the results of the modified Upton and Ludbrook model are compared to predictions of the PBPK model and the NONMEM model, see figure 4.4. It is seen that the adapted model results lay between the PBPK and the NON-

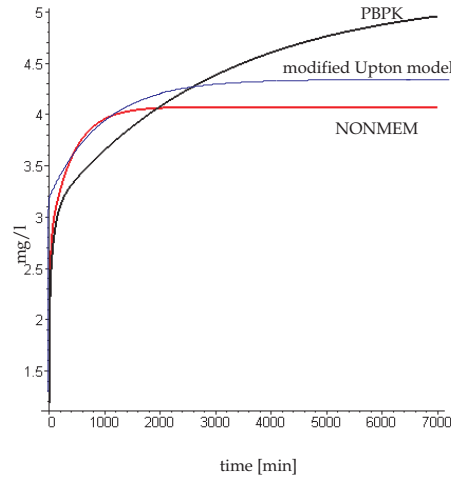


Figure 4.4: Validation of the compartmental propofol model. Model concentration versus time for a 5 day constant infusion of $100 \mu\text{g kg}^{-1}\text{min}^{-1}$.

MEM model.

Overall, the modified Upton and Ludbrook model gives results in the same range as the other models available in literature. We therefore consider this simple model to be suitable for developing a dose-dependent vasoconstriction model and for further simulations.

4.5 Determining the vasoconstriction threshold

Cheng et al. (1995) demonstrated that the cutaneous contribution of mean skin temperature to vasoconstriction is linear. Therefore, it is possible to use the measured skin and core temperatures at each threshold to calculate a core-temperature threshold that would have been observed had skin been at a standardized temperature (Matsukawa et al., 1995a):

$$T_{\text{core,stand}} = T_{\text{core,obs}} + \left(\frac{\beta}{1 - \beta} \right) (T_{\text{skin,obs}} - T_{\text{skin,stand}}) \quad (4.28)$$

Relation (4.28) was used for calculating the standardized core temperature at which vasoconstriction was triggered in the measurements. Here, $\beta = 0.2$ and $T_{\text{skin,stand}} = 35.7^\circ\text{C}$

for vasoconstriction (Matsukawa et al., 1995a). Subscripts stand and obs denote standardized and observed (measured) temperatures, respectively. β is the fractional contributions of mean skin temperature to the threshold of vasoconstriction. The start of vasoconstriction was defined as the moment in time when $T_{\text{finger}} - T_{\text{forearm}}$ showed a sustained decrease. An example is given in figure 4.5.

Chest skin temperature was not measured for the aortic valve patients in the previous chapter.

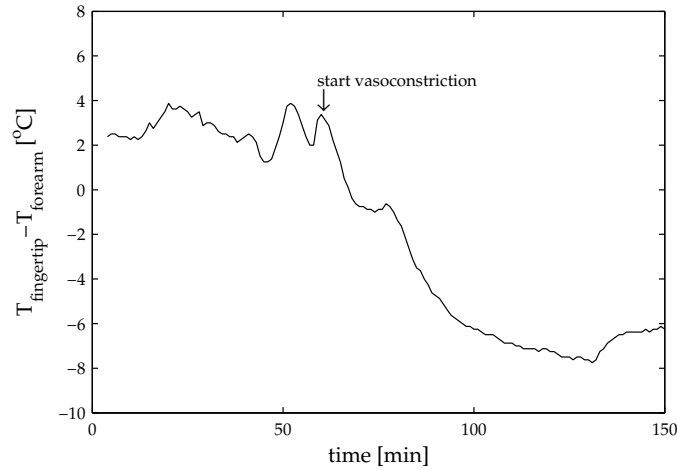


Figure 4.5: Typical example to illustrate the definition that was used to appoint the start point of vasoconstriction: time point where $T_{\text{fingertip}} - T_{\text{forearm}}$ shows a sustained decrease.

Hence, we used the same modified Hardy-Dubois' six-point formula as in chapter 3:

$$T_{\text{skin,obs}} = (0.07T_{\text{forehead}} + 0.14T_{\text{posterior forearm}} + 0.05T_{\text{hand}} + 0.19T_{\text{anterior thigh}} + 0.13T_{\text{anterior calf}} + 0.07T_{\text{foot}})/0.65 \quad (4.29)$$

4.6 Vasoconstriction-propofol relation

At the point in time at which vasoconstriction started, the amount of propofol concentration in the blood was calculated with the help of the pharmacological model. For the simulations with the model, the propofol protocol was employed according to the measurement series described in chapter 3. This protocol comprised a bolus injection of approximately 100 mg propofol in 1 minute, followed by continuous injection of about $5 \text{ mg kg}^{-1} \text{ h}^{-1}$ during the actual surgery.

At the same time point, the standardized core temperature was determined with equation (4.28). Painful stimulation, as produced by surgery, increases the threshold for vasoconstriction by approximately 0.4°C (Belani et al., 1993). To determine the vasoconstriction threshold at zero concentration propofol, the measurement data of Matsukawa et al. (1995a)

were used. Given that vasoconstriction thresholds are linearly related to drug concentration (Matsukawa et al., 1995a) and taking into account the increased threshold during pain, the following equation for the vasoconstriction threshold ($T_{\text{core,stand},0}$) was found using linear regression analysis (Statgraphics Plus 5.1):

$$T_{\text{core,stand},0} = 36.69^{\circ}\text{C} - 0.82C_{\text{propofol}} \quad (4.30)$$

with $R^2 = 0.82$.

Ultimately, the following vasoconstriction model is used:

- If $T_{\text{core,stand}}(t) < T_{\text{core,stand},0}(t)$ then $C_s(t) = 200$ for the inner skin layer, 75 for muscle.
- If $T_{\text{core,stand}}(t) > T_{\text{core,stand},0}(t)$ then $C_s(t) = 0$.

The choice of setting the C_s -value to 200 is made on the basis of figure 4.6 and equations (4.4)-(4.5). The distribution factor for vasoconstriction, a_{cs} , varies roughly between 0.03 and 0.3, with a mean value of 0.1. In case the tissue temperature decreases by 5°C , it is seen that a five time increase in C_s -value, i.e. $C_s = 1000$ instead of 200, changes the relative perfusion value by maximal 10%, which means that $\frac{\beta_i}{\beta_{i,0}}$ is about constant. The ratio of muscle constriction to skin vasoconstriction (75 and 200, respectively) is based on data presented by Schmidt and Thews (1989).

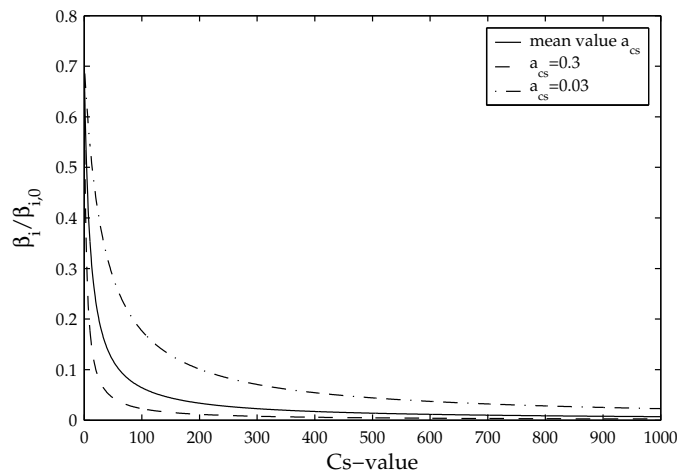


Figure 4.6: Effect of magnitude C_s on the relative perfusion value for a_{cs} -values of 0.03, 0.3 and 0.1 (mean a_{cs} value). The effect is studied for a ΔT of -5°C .

4.7 Validation results

After adding the vasoconstriction model with the coupled propofol model to the passive model, the validity of the model was tested by comparing the model results to measurement results of three surgical procedures. Firstly, data from the aortic valve surgery without forced-air heating (see chapter 3) was compared to model predictions. This data was also used to derive equation (4.30). Thereafter, an independent data set was used from a coronary artery bypass graft surgery performed by Rajek et al. (2000). Thirdly, data was used from the aortic valve surgery in which forced-air heating was used (see chapter 3). The latter data was also used to deduce equation (4.30). Thereafter, the model's sensitivity to reductions in metabolic rate was studied.

Aortic valve surgery at 30°C

Core (nasopharyngeal) and mean skin temperature data from the aortic valve surgery were compared to simulation results. 7 patients (mean body characteristics: weight 80.8 kg, height 172 cm, fat percentage 31.8%) were cooled with help of a heart lung machine to a nasopharyngeal temperature of 30°C. Towards the end of surgery, they were rewarmed to a nasopharyngeal temperature of 37-37.5°C. Bypass flow was kept at $2.4 \text{ l min}^{-1} \text{ m}^{-2}$. The fluid-blood gradient was near 1°C. During cooling, a circulating water mattress was used with a temperature of 30°C. During rewarming and in the postbypass stage, the mattress temperature was approximately 36°C. No forced-air heater was used. The surrounding temperature was 20°C. Simulation results are based on average body characteristics of the patient group. The calculated and measured core temperature trends agree very well (figure 4.7). The skin temperatures initially deviated 2°C, but eventually the simulation follows the pattern of the measured skin temperature quite well. In the anesthesia stage (stage 1), a sawtooth profile for core temperature is observed caused by the stepwise model.

Coronary artery bypass surgery at 32°C

Next, a simulation was run with similar surgical conditions as used in the study of Rajek et al. (2000). 10 patients (mean body characteristics: weight 77.9 kg, height 171 cm, fat percentage 32.3%) were cooled to a nasopharyngeal temperature of 32°C. Bypass flow was set to $2.5 \text{ l min}^{-1} \text{ m}^{-2}$. Towards the end of the surgery, patients were rewarmed to a nasopharyngeal temperature of 37°C. The initial fluid-blood gradient was near 3°C. During rewarming and during the postbypass stage, a circulating water mattress was used at 39°C. No forced-air heater was used. The surrounding temperature was kept near 21°C. The simulation and the measurements agree again reasonably well, see figure 4.8. In the anesthesia stage (stage 1) again a sawtooth profile for core temperature is observed as the standardized core temperature is around the threshold temperature for vasoconstriction.

The initial temperature differences between the simulation and the experimental results of the coronary artery bypass surgery were larger than for the aortic valve surgery. Unfortu-

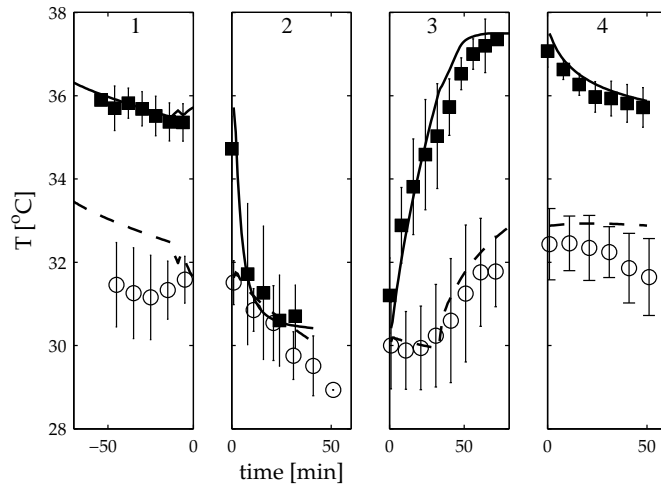


Figure 4.7: Aortic valve surgery. Simulations consist of four stages: 1. anesthesia stage 2. cooling with heart lung machine 3. warming with help of heart lung machine 4. post-bypass stage. ■ and ○ represent experimentally assessed core and mean skin temperature, respectively. — and - - represent the core and mean skin temperatures following from the simulation, respectively. Errorbars denote the standard deviation of the measurements.

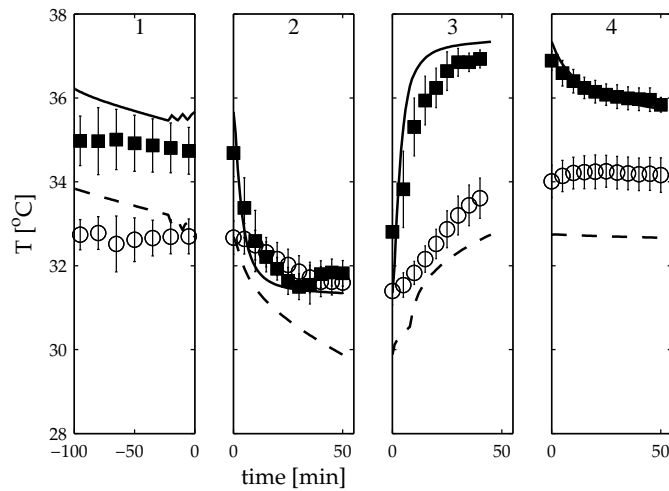


Figure 4.8: Coronary surgery. Simulations consist of four stages: 1. anesthesia stage 2. cooling with heart lung machine 3. warming with help of heart lung machine 4. post-bypass stage. ■ and ○ represent experimentally assessed core and mean skin temperature, respectively. — and - - represent the core and mean skin temperatures following from the simulation, respectively. Errorbars denote the standard deviation of the measurements.

nately, we did not possess information that could explain the low initial core temperature as found in the experiments of Rajek et al. (2000). However, the initial low core temperature, in combination with the relatively high initial skin temperature, suggests the administration of some premedication, with a vasoactive effect, prior to the start of the measurements. In the rewarming stage (stage 3), the model predictions lie outside the standard deviation of measurements. As not all details of the used warming protocol are known, this might explain the observed deviation.

Regarding the larger deviations between modelled and measured skin temperature, it must be noted that the measured value is actually averaged over values found over various locations on the body. The deviation between those values is much larger than the standard deviation on interindividual values that are shown in figures 4.7 and 4.8.

Aortic valve surgery at 30°C with forced-air heating

For testing the validity of the model for predicting core temperature afterdrop when using different temperature protocols, simulations with forced-air heating are compared to measurement data in which forced-air heating is used (see chapter 3). The protocol was the same as the aortic valve surgery described earlier, with the addition of a forced-air heater in the rewarming and postbypass stage. The studied group involved 8 patients with a mean weight of 78.6 kg, a height of 169 cm and a fat percentage of 36%. In figure 4.9 the results of the

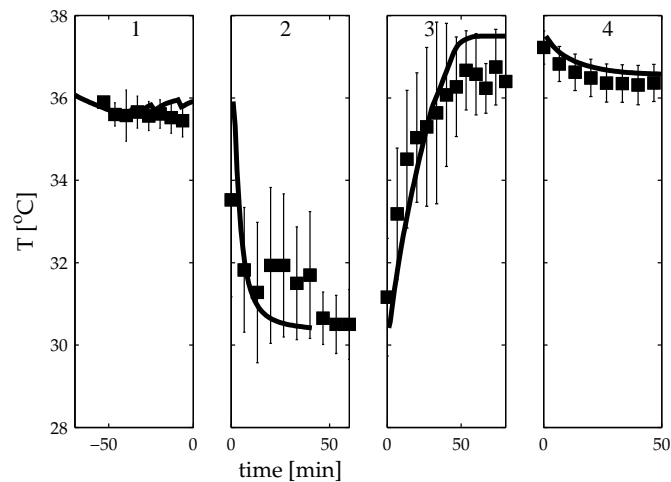


Figure 4.9: Validation study: an aortic valve surgery, in which a forced-air warmer is used. Simulations consist of four stages: 1. anesthesia stage 2. cooling with heart lung machine 3. warming with help of heart lung machine and forced-air blanket 4. postbypass stage with forced-air blanket. ■ represents the experimentally assessed core temperature. — represents the core temperature following from the simulation. Errorbars denote the standard deviation of the measurements.

simulation are shown. Core temperature predictions agreed again well with measurement data. The higher standard deviations observed in the measurements are thought to be caused by inter-patient differences in the used cooling and warming protocols during surgery.

Model sensitivity for reduction of metabolic heat production

According to Sessler (2000), metabolic heat production during anesthesia is reduced by 15% to 40%. In an experiment involving anesthetized volunteers, Matsukawa et al. (1995b, 1997) found a metabolic rate decrease of $33\pm 8\%$. In equation (4.2), a value of 30% was employed. In order to check the effect of using the lower and upper limit values mentioned by Sessler, simulations were run using the aortic valve protocol with 15% and 40% reductions of metabolic rate. Results of both cases and the value of 30% are given in figure 4.10. When a metabolic rate reduction of 15% is used, it appears that in the anesthesia stage and postbypass stage, core temperature is about 0.3°C higher than for the standard used value of 30%. A 40% reduction of metabolic rate results initially in the anesthesia stage in a 0.2°C lower core temperature, but vasoconstriction starts earlier. This results in a higher core temperature at the end of the anesthesia stage than for the standard value. In the postbypass stage, core temperature is 0.2°C lower than for the standard case.

From this, it follows that the upper and lower limit values of anesthesia induced metabolic rate reported in literature give core temperature predictions with a variation of maximum 0.3°C in the anesthesia stage and postbypass stage of a cardiac surgery, when comparing to the standard value.

In the remainder of the thesis, 30% reduction of metabolic rate is taken as the standard value.

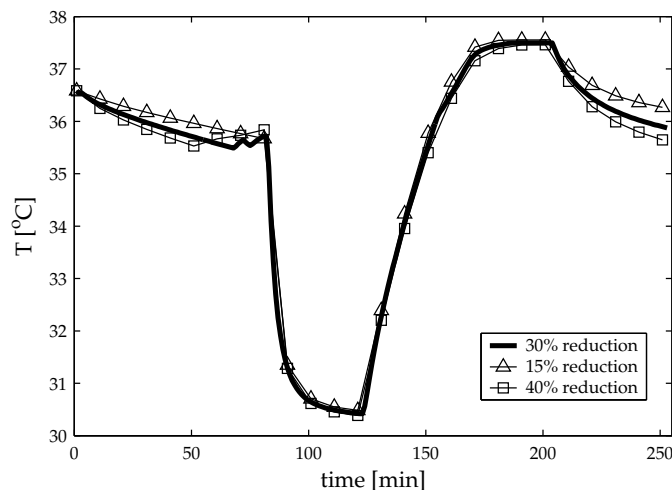


Figure 4.10: Simulation results of core temperature when using an anesthesia induced metabolic rate reduction of 15%, 30% (standard used value) and 40%. In the simulations the temperature protocol of the aortic valve surgery was used.

4.8 Discussion

For developing the thermoregulatory part of the model, a pharmacological anesthesia model was used. With help of this model, the drug concentration in the blood can be calculated. A relation was formulated between the drug concentration in the blood and the vasoconstriction threshold. If body temperature is lower than the threshold for vasoconstriction, vasoconstriction is triggered. As a first approach a stepwise model was employed for modelling the gain and intensity of the vasoconstriction tone.

For the development of the pharmacological model, it was assumed that the overall drug concentration was represented by the momentary propofol concentration. Propofol was the main drug in the measurement series described in chapter 3. In reality, a mixture of drugs is administered to the patient. This might lead to some drug-drug interaction. Nonetheless, according to Sessler (1997), the typical concentrations of anesthetics used during cardiac surgery roughly increase the interthreshold range in the same way. Therefore, the reduced propofol model will suffice as a first approach.

The propofol model was based on the compartmental physiological model for calculating propofol concentration in sheep developed by Upton and Ludbrook (1997). As Ludbrook and Upton (1997) found close agreement between human and sheep data, no large errors are expected when using this model for calculating drug concentration. This was also found by comparing results obtained with the sheep model, as used in this thesis, with results presented by Levitt and Schnider (2005) (PBPK model) and Schnider et al. (1998) (NONMEM). For the current application, the sheep model is therefore considered to be appropriate.

In a validation study, it was shown that good agreement exists between simulation results obtained with the computational model and experimental results. Measurement data from chapter 3 and measurement data from Rajek et al. (2000) were compared to simulation results. Errors between simulation and measurement results for core and skin temperature were smaller than two times the standard deviation of the measurement values for the measurement data of chapter 3. For the independent data set, core temperature error stayed within two times the standard deviation of the measurements, but skin temperature errors were sometimes bigger. The largest deviations between simulation and experiments in all cases occurred in the early stage of the surgery. This can be attributed to the uncertainties in initial conditions. The starting point in all simulations was that patients were in a thermoneutral condition before surgery. The thermoneutral temperature distribution was determined by calculating the equilibrium temperature distribution of a naked person at an environmental temperature of 30°C. In reality, patients have a history of (unknown) non-thermoneutral conditions. Hence, initial temperatures predicted by the model can deviate a lot from measured temperature values. Moreover, the initial temperatures also affect the predicted temperatures at later time points.

Mean skin temperature predictions seemed to be not as good as core temperature predictions. Temperature varies across the surface of the skin. Mean skin temperature is therefore obtained by taking the mean of local temperatures weighted according to the relative surface area, they are supposed to characterize. However, local skin temperatures often do not represent regional skin sites very well. Concurrently, interindividual variations can be large. Core

temperature is only represented by the nasopharyngeal temperature, and therefore regional differences do not play a role in this quantity. On top, the calculated skin temperature by the model is quite sensitive to the imposed boundary conditions (an increase in environmental temperature of 2°C lets skin temperature during surgery increase by typically 0.6°C). It is expected that more knowledge of the boundary conditions will reduce the error in measured and calculated skin temperatures. In addition, for obtaining a correct description of heat distribution in the periphery, when using forced-air heaters, a more complex heat transfer model is required, as follows from the perfusion data in chapter 3.

Anesthetics induce a decrease in metabolic heat production. The exact causes of the metabolic rate reduction are not well-established yet, but decreased brain activity contributes, as does mechanical ventilation, which spares the diaphragm and chest muscles (Sessler, 2000). Uncertainty of the anesthesia induced reduction of metabolic rate, using the upper and lower values that are reported by Sessler (2000), gives a typical variation of 0.3°C in the anesthesia and postbypass stage of a cardiac surgery. The values found in literature are based on indirect calorimetry measurements of volunteers before and under general anesthesia (with artificial respiration). No literature was found that discusses metabolic rate decrease during cardiopulmonary bypass surgeries, which take place without artificial respiration. During un-pump interventions, indirect calorimetry measurements can not be used. Other (metabolic) measurements techniques are needed to determine the metabolic rate reductions during cardiac surgery. A suggestion is to measure flow together with oxygen and carbon dioxide levels in the arterial and venous blood. However, in the cooling and rewarming stage it is seen that the uncertainty in the decrease of metabolic rate is of little importance for the predicted core temperature in these stages (figure 4.10). Hence, the error, that is induced by the uncertainty in metabolism during un-pump stages, is small.

At this moment, there is an abrupt transition between vasoconstriction and no vasoconstriction. For cardiac surgery, the stepwise approach does not introduce larger errors except in the anesthesia stage where a sawtooth profile is observed in the temperatures. In the other stages the errors are much smaller as the start and end points of the onset of vasoconstriction were close to the starting point and end point of active cooling and heating with the heart lung machine. In the on-pump periods, temperature changes in the body are very large which induces a vasoconstriction tone signal that is almost similar to a stepfunction. Nonetheless, for other applications, like under normal circumstances or other types of surgery, a smoother vasoconstriction model is needed in order to avoid sawtooth profiles. Hence, the next chapter focusses on the derivation and improvement of a smooth physiological vasoconstriction model.

Measurement of model coefficients of sympathetic vasoconstriction

5.1 Introduction

In the previous chapter, a drug-dose-dependent vasoconstriction model was formulated. A relation was derived that coupled the blood concentration propofol to the threshold temperature for vasoconstriction. For modelling the intensity and gain of the vasoconstriction response, a stepwise model was assumed. This approach leads to non-smooth temperature predictions (sawtooth profiles), which especially induces errors under conditions with slowly changing temperature gradients around the threshold temperature for vasoconstriction. Accordingly, this chapter concentrates on the derivation of a physiologically-based vasoconstriction model.

5.1.1 Physiology of the autonomous control of vasomotion

Under normothermic conditions, the smooth muscle cells of the cutaneous arterioles are at a basal tone. During cold stress, a thermoregulatory reflex is initiated by increased noradrenergic vasoconstrictor tone acting on arterioles. Both neural and local mechanisms are involved in this process (see figure 5.1).

Sympathetic neural activity activates vasoconstriction by noradrenergic mechanisms. Norepinephrine, which is secreted by the adrenal medullae, excites primarily α_1 and α_2 -receptors, and β -receptors to a less extent. These receptors are located in the vascular smooth muscle of cutaneous arterioles. Also cotransmitters, like neuropeptide Y, are thought to participate in noradrenergic vasoconstriction. By the excitation of the α and β receptors a vasoconstriction response is initiated (Kellogg, 2006).

Local cooling of the skin causes local, temperature-dependent vasoconstriction. Local temperature reductions are sensed by cold sensitive afferent nerves. Those nerves effect the release of norepinephrine from sympathetic active cutaneous vasoconstrictor nerves. In this way, local cooling leads to a progressive reduction in perfusion with falling local temperature.

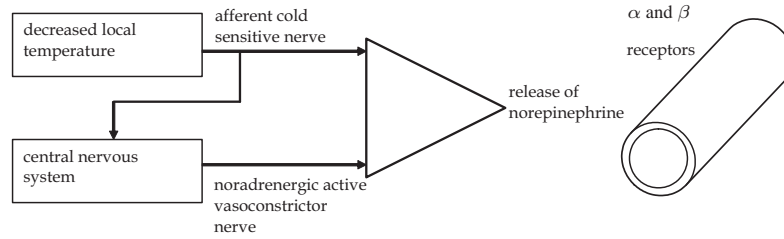


Figure 5.1: Local and neural mechanisms of vasoconstriction.

5.1.2 Control concept

For modelling thermoregulatory responses diverse feedback systems are suggested in literature. Consequently also a lot of controversies exist, see appendix A. In this thesis, the most important goal is to design a functional model, with which reliable predictions can be attained for diverse surgeries performed under hypothermic conditions. The choice of the used control concept is, in this case, of minor importance as long as the predictive power of the developed model is good. As no experimental or theoretical evidence exists that can point one as the best strategy, it was decided to use the most simple and straightforward concept: the basic engineering control strategy that compares and controls body temperature by comparing the temperature of the body to a reference signal (the setpoint).

5.1.3 Modelling the cutaneous sympathetic vasoconstrictor tone and amplification coefficients

Several researchers have already focussed on obtaining gains and intensities of vasoconstriction responses. Researchers like Gordon (1974), Fiala et al. (2001) and Tanabe et al. (2002) used models that were based on the work of Stolwijk (1971). The tentative expression that was used in the Stolwijk model, for describing skin blood flow yields:

$$w_b = \frac{w_{b,0} + a_{dl}DI}{1 + a_{cs}Cs} Q_{10}^{\frac{T-T_0}{10^\circ C}} \quad (5.1)$$

with w_b representing perfusion and a_{dl} and a_{cs} representing the amplification coefficients for vasodilation and vasoconstriction, respectively. T is the local temperature and DI and Cs denote the sympathetic vasodilation and vasoconstrictor tone, respectively. The magnitude of DI and Cs depend on a temperature error signal which represents the difference between the

actual temperature state and the temperature setpoint: $T - T_0$. Subscript 0 denotes the base line value. The value of Q_{10} equals 2.

In equation (5.1), it can be seen that also in the mathematical representation of blood flow, a division is made between the changes in perfusion induced by central sympathetic neural activity (the Cs and DI-terms) and by local temperature changes (the $Q_{10}^{\frac{T-T_0}{10^\circ C}}$ -term).

In the absence of clear measurement data, Stolwijk estimated the values for a_{cs} and Cs, that he used in his model. However, it is not clear where he based the estimations on. Later, Gordon (1974), Fiala et al. (2001) and Tanabe et al. (2002) reported also values for a_{cs} and Cs. In the work of Tanabe et al. (2002), no justification is given for the values that were used. Gordon (1974) and Fiala et al. (2001) explained the methods they employed for determining a_{cs} and Cs, but the methods that were used, seem to be very prone to errors. The basic idea of the methods of Gordon (1974) and Fiala et al. (2001) was that a_{cs} and Cs were determined by using their own passive models and measured temperature data. They assumed that the difference in temperature between the model predictions and the measurement data could be fully attributed to active thermoregulation. By fitting the model to the measurements, they derived values for a_{cs} and Cs. An enormous drawback of this method is, that when the passive model contains either programming or physiological errors, the active part will also be contaminated. When using those values in other thermal models, the correctness is questionable.

Another objection to the existing work is that they all used equation (5.1). In this equation vasodilation and vasoconstriction are treated differently although the essence of the manifestations is the same: widening or narrowing of blood vessels. Therefore, the physiological basis to put vasodilation linearly in the numerator while writing vasoconstriction in the denominator is odd. Hence, an alternative relation is proposed in this chapter, in which vasoconstriction and vasodilation are treated similarly.

The present chapter provides a method to determine physiological values for the vasoconstriction amplification factors and vasoconstrictor tone. Vasoconstriction values are derived for Stolwijk's relation and for the newly proposed relation by simultaneously performing measurements of perfusion and temperature distribution in volunteers under uniform environmental conditions. These experimentally determined parameters provide a physiological basis for a vasoconstriction model and can be implemented in the human thermal model.

5.2 Materials and methods

5.2.1 Subjects

Ten healthy male Caucasian volunteers participated in this study. The study protocol was approved by the Maastricht University Medical Ethical Committee. Before participating in the study, all subjects signed an informed consent. Subject characteristics are shown in table 5.1. Body fat percentage was determined by skinfold measurements at the m. biceps brachii, m. triceps brachii, subscapular and suprailiacal (Durnin and Womersley, 1974).

Table 5.1: Subject characteristics ($n=10$). Values are given as mean \pm standard deviation.

Subject characteristics	Mean \pm SD	Range
Weight [kg]	77.7 \pm 11.0	62–98
Height [cm]	186 \pm 8	176–198
Age [y]	28.1 \pm 4.9	20–34
BMI [kg m ⁻²]	22.5 \pm 2.6	18.5–25.5
Fat [%]	17.3 \pm 5.9	9.6–24.2
BSA [m ²]	2.0 \pm 0.2	1.7–2.3

5.2.2 Protocol

Subjects refrained from alcohol the day prior to the measurements. At the testing day, the subjects took a light breakfast at 8.00 AM. They did not drink coffee or tea at the morning before the test. From the moment the test began until the end of the test, the subjects were fasting. They arrived at the laboratory at 10:30 AM.

Subjects performed a light exercise at a stepping platform. The exercise was ended when the fingertip-forearm gradient was 0°C. In this way, a standardized situation was created prior to the start of the test, as the fingertip-forearm gradient is an indicator for thermoregulatory peripheral vasoconstriction (Rubinstein and Sessler, 1990). Thereafter, all sensors were attached as described in sections 5.2.3 to 5.2.6. Subsequently, the subjects entered a climate chamber (Schoffelen et al., 1997). They were in a semisupine position for 3.5 hours, lying on a stretcher. Subjects were given an option to watch television during the test. An overview of the experimental time schedule is shown in figure 5.2.

During 1.5 hour the room temperature was set to 27°C, which is in the thermoneutral zone

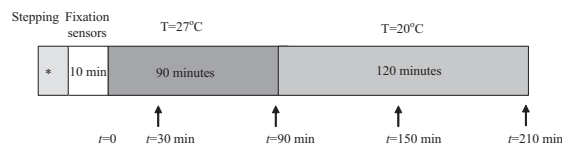


Figure 5.2: Time schedule of the experiment. * The volunteers used the stepping platform till the lower arm-fingertip gradient has become 0°C. \uparrow denote the time points where forearm blood flow was measured.

(Hardy and Stolwijk, 1966). In this period, the temperature of the subject stabilized. After this period, the room temperature was changed to 20°C. Under these conditions, no shivering response was expected on the basis of experiments performed by Hardy and Stolwijk (1966), which excludes disturbances in the measurements due to shivering effects. Moreover, the typical decrease in mean skin temperature ($\sim 3^\circ\text{C}$) agrees with the mean skin temperature decrease observed during aortic valve procedures performed at 30°C (Severens et al., 2007b).

Relative humidity was 55%.

Subjects were wearing standard clothing consisting of underwear (0.04 clo), a pair of short trousers (0.06 clo) and a t-shirt (0.09 clo). The face, lower arms, lower legs, hands and feet were directly exposed to the environment.

5.2.3 Temperature measurements

Skin temperatures were measured continuously at 1 minute intervals by sensors (iButton type DS192H, Maxim/Dallas Semiconductor Corp., USA) placed at the head, lower arm, upper arm, hand, fingertip, foot, toe, lower leg (anterior and posterior), thigh (anterior and posterior), chest, abdomen, scapula and lumbar. This type of sensors has recently been evaluated for studies in humans (Van Marken Lichtenbelt et al., 2006). They reported a mean precision of 0.09°C, with a maximum error of 0.4°C.

The mean skin temperature is calculated by using the 12-point-weighted formula of Hardy and Dubois (Mitchell and Wyndham, 1969), which in general has a good agreement over a large range of ambient temperatures, especially under cold conditions:

$$\begin{aligned}
 T_{\text{skin}} = & 0.07T_{\text{head}} + 0.0875T_{\text{chest}} + 0.0875T_{\text{abdomen}} + 0.0875T_{\text{scapula}} & (5.2) \\
 & + 0.0875T_{\text{lumbar}} + 0.14T_{\text{lower arm}} + 0.05T_{\text{hand}} + 0.095T_{\text{thigh anterior}} \\
 & + 0.095T_{\text{thigh posterior}} + 0.065T_{\text{calf anterior}} + 0.065T_{\text{calf posterior}} + 0.07T_{\text{foot}}
 \end{aligned}$$

The rectal temperature was measured continuously by a thermistor-probe (YSI probes, tip diameter 3.3 mm, series 402, Yellow Springs Instruments, Ohio, USA) inserted for at least 10 cm.

The fingertip-forearm gradient, which is used as an index of thermoregulatory peripheral vasoconstriction (Rubinstein and Sessler, 1990), was measured with an infrared thermometer (Infrared Tympanic Thermometer, First Temp Genius. Sherwood-Davis & Geck, UK) prior to entering the respiration chamber and by means of iButtons from the start to the end of the experiment.

5.2.4 Skin perfusion

Cutaneous blood flows under the big toe, at the ventral side of the lower leg (at the extensor digitorum longus muscle) and at the middle of the forearm (at the palmaris longus) were recorded using laser Doppler flowmetry (LDF). A two-channel laser Doppler flowmeter and a one-channel laser Doppler flowmeter were used (both Perimed 4001, with a 780 nm laser diode, 0.25mm fibre separation). The probes were calibrated with PF 1000 calibration equipment (Perimed AB). Sample rate was set to 8 Hz using a time constant of 0.2 s. Before starting the measurement the device was left for at least 30 minutes to warm up. All measurements were performed with a standard probe (Probe 408, Perimed AB). Probes were placed in a probe holder (PH 08-1, Perimed AB) and mounted with double-sided adhesive tape.

Temperature sensors were placed within 1 cm distance from the laser Doppler probes. Laser Doppler flowmetry does not provide absolute measurements of flow. Differences in base line values are therefore likely. However, by normalizing individual perfusion responses by individual base line values, perfusion indexes are obtained that are comparable within subjects (Kellogg et al., 1998).

5.2.5 Forearm blood flow

Forearm blood flow was measured by venous occlusion plethysmography (EC5R Strain Gauge and Photo Plethysmograph, Hokanson, Washington, USA) using mercury-in-silastic strain gauges applied to the widest part of the forearm. During measurement periods, the hand circulation was occluded by rapid inflation of a pediatric sphygmomanometer cuff, placed around the wrist, to a pressure of 200-220 mm Hg. In this way, forearm blood flow was assessed without interference of the hand circulation. The proximate cuff placed around the upper arm, was automatically inflated (and deflated) to 45 mmHg to achieve venous occlusion (E20 Rapid Cuff Inflator, Hokanson, Washington, USA) and obtain plethysmographic recordings. A complete set of forearm strain gauges was available, ranging from 16 to 30 cm in 2 cm increments. Measurements took place at 4 time points with an interval of one hour (figure 5.2). A measurement period lasted about 1.5 min, where the cuff was inflated every 4 seconds. The chart recorder range gain was set to 0.1%/cm. The flow rate after analyzing the slope of the plethysmograph readings is reported in percentage volume change per minute, which equals ml blood/(100ml tissue · min). Varying conditions of ambient temperatures were compensated by the electrical circuit in the device. In the analysis of the plethysmography output, no further adjustments for thermal compensation were therefore required.

5.2.6 ECG

Heart rate variability was calculated from ECG-data recorded using an ambulatory Holter ECG-monitor (GE Health Care, Freiburg, Germany). Heart rate variability directly quantifies the sympathetic contribution to heart rate and can be considered to be a measure for sympathetic activity. The very low frequency component (VLF<0.04 Hz) of the R-R interval spectrum is thought to be associated with sympathetic thermoregulation (Brenner et al., 1997; Matsumoto et al., 2001). Digital data obtained from the ECG was analyzed using fast Fourier transformations as described by Oida et al. (1997).

The skin surface at the electrode side was lightly rubbed and cleansed thoroughly with alcohol. 7 electrodes are attached to the skin and connected according to the AVF leads. The measurement data were analyzed for three time intervals: 1) 60-90 min 2) 120-150 min 3) 180-210 min.

5.2.7 Data analysis

Laser Doppler results were analyzed as a running average of 60 seconds epochs, to filter out motion artifacts. The temperature and perfusion values at $t=30$ minutes were used as base line value T_0 and $w_{b,0}$, respectively. Then, the temperature difference ($\Delta T_i = T_i - T_{i,0}$) and the relative perfusion ($\frac{w_{b,i}}{w_{b,i,0}}$) for a body part i were related, using the following equation:

$$\frac{w_{b,i}}{w_{b,i,0}} = Q_{\text{fit},i}^{\frac{\Delta T_i}{10^\circ\text{C}}} \quad (5.3)$$

$Q_{\text{fit},i}$ was determined with help of the perfusion and temperature data and equation (5.3). Subscript i represents the toe, lower leg and arm.

Method A

In method A, the structure of the established relation formulated by Stolwijk (1971) was kept:

$$w_{b,i} = \frac{w_{b,i,0} + a_{\text{dl},i} \text{Dl}}{1 + a_{\text{cs},i} \text{Cs}} Q_{10}^{\frac{\Delta T_i}{10^\circ\text{C}}} \quad (5.4)$$

When vasodilation is absent, equation (5.4) reduces to:

$$\frac{w_{b,i}}{w_{b,i,0}} = \frac{1}{1 + a_{\text{cs},i} \text{Cs}} Q_{10}^{\frac{\Delta T_i}{10^\circ\text{C}}} \quad (5.5)$$

Equation (5.3) should be identical to equation (5.5) for each body part i . This leads to the following relation for sympathetic vasoconstriction tone (Cs):

$$\text{Cs}^{\text{A}} = \frac{1}{a_{\text{cs},i}^{\text{A}}} \left(\frac{Q_{\text{fit},i}^{\frac{-\Delta T_i}{10^\circ\text{C}}}}{Q_{10}} - 1 \right) \quad (5.6)$$

with $a_{\text{cs},i}$ representing the amplification factor for vasoconstriction. Superscript A represents values obtained with method A. Local perfusion and temperature were measured at the toe, leg and arm.

Now, we have 4 unknowns, viz. the amplification factors $a_{\text{cs,toe}}$, $a_{\text{cs,leg}}$, $a_{\text{cs,forearm}}$ and the sympathetic vasoconstrictor tone Cs. The following set of equations was then solved at each time point:

$$\text{Cs}^{\text{A}} a_{\text{cs,toe}}^{\text{A}} = \frac{Q_{\text{fit,toe}}^{\frac{-\Delta T_{\text{toe}}}{10^\circ\text{C}}}}{Q_{10}} - 1 \quad (5.7)$$

$$\text{Cs}^{\text{A}} a_{\text{cs,leg}}^{\text{A}} = \frac{Q_{\text{fit,leg}}^{\frac{-\Delta T_{\text{leg}}}{10^\circ\text{C}}}}{Q_{10}} - 1 \quad (5.8)$$

$$\text{Cs}^{\text{A}} a_{\text{cs,arm}}^{\text{A}} = \frac{Q_{\text{fit,arm}}^{\frac{-\Delta T_{\text{arm}}}{10^\circ\text{C}}}}{Q_{10}} - 1 \quad (5.9)$$

C_s^A is the central vasoconstrictor tone, and therefore independent of the location. Eventually, this led to physiologically based values for the products of $C_s^A a_{cs,toe}^A$, $C_s^A a_{cs,leg}^A$ and $C_s^A a_{cs,arm}^A$ as function of time. It is chosen to bound the value for C_s^A to a maximum value of 1 at the point where vasoconstriction is highest and skin temperature is lowest. Note that this choice differs from the choices made by Stolwijk (1971), Fiala et al. (2001) (as was used in chapter 4 of this thesis) and Tanabe et al. (2002). Those authors chose the sum of the amplification coefficients of all body parts equal to 1: $\sum_{i=1}^n a_{cs,i} = 1$. As this makes the model less flexible for changing the number of body parts, this strategy was not followed here. In addition, as only three body parts were measured, it was not logical to normalize the sum of those three amplification coefficients to 1.

Method B

As an alternative to the Stolwijk model, we propose the perfusion-temperature relation in the following format:

$$\frac{w_b}{w_{b,0}} = (1 - a_{cs}^B C_s^B + a_{dl} D_l) Q_{10}^{\frac{T-T_0}{10^\circ C}} \quad (5.10)$$

where superscript B refers to method B. Vasoconstriction and vasodilation are now implemented in the same way. Vasoconstriction as well as vasodilation are incorporated in a linear way, while in equation (5.1) vasodilation is linearly implemented and vasoconstriction is implemented in the divisor. Again, vasodilation was omitted, which reduces equation (5.10) to:

$$\frac{w_b}{w_{b,0}} = (1 - a_{cs}^B C_s^B) Q_{10}^{\frac{T-T_0}{10^\circ C}} \quad (5.11)$$

The following set of equations is solved:

$$C_s^B a_{cs,toe}^B = 1 - \frac{Q_{fit,toe}^{\frac{\Delta T_{toe}}{10^\circ C}}}{Q_{10}} \quad (5.12)$$

$$C_s^B a_{cs,leg}^B = 1 - \frac{Q_{fit,leg}^{\frac{\Delta T_{leg}}{10^\circ C}}}{Q_{10}} \quad (5.13)$$

$$C_s^B a_{cs,arm}^B = 1 - \frac{Q_{fit,arm}^{\frac{\Delta T_{arm}}{10^\circ C}}}{Q_{10}} \quad (5.14)$$

The products $C_s^B a_{cs,toe}^B$, $C_s^B a_{cs,leg}^B$ and $C_s^B a_{cs,arm}^B$ were calculated according to method B, as function of time. Similar to method A, the value for C_s^B is bounded to a maximum value of 1 at the point where vasoconstriction is highest and skin temperature is lowest. As under current test circumstances the skin temperature and the perfusion level off, this approach is reasonable.

5.2.8 Statistics

Results are expressed throughout as means with standard deviation. Plethysmography readings, heart rate variability and temperature measurements were analyzed with a paired t-test.

Results are considered statistically significant when $P < 0.05$.

Values for $Q_{\text{fit},i}$ were derived using temperature and perfusion data, equation (5.3) and linear regression analysis after log-transformation. Control equations for vasoconstriction tone as function of an error signal were derived using nonlinear regression analysis. The statistical analyses were made with help of Statgraphics Plus 5.1.

5.3 Results

5.3.1 Temperature

Temperature fluctuations in the climate chamber stayed within 1°C , when the temperature was set to 27°C . When switching to the cool stage at $t=90$ min, it took about 40 minutes before a temperature of 20°C was reached. Then, temperature stayed within a 1.5°C range.

Rectal temperature fluctuations due to changes in environmental temperature conditions were about 0.1°C (see figure 5.3(a)). At the beginning of the measurement period, rectal temperature decreased by about 0.3°C , which is probably caused by the transition from standing position during exercise to semisupine position. Temperature differences at the end of the warm stage ($t=90$ min, the base line value), at $t=150$ min and at the end of the cold stage ($t=210$ min) were analyzed with a paired t-test, see table 5.2. No statistical difference in mean rectal temperature was observed during the experiment.

Table 5.2: Summarized temperature and perfusion data: mean (SD).

	$t = 90$ min (base line)	$t = 150$ min	P_{90-150}	$t = 210$ min	P_{90-210}
$T_{\text{core}} [^\circ\text{C}]$	36.92 (0.41)	36.92 (0.42)	0.91	36.86 (0.44)	0.53
$T_{\text{skin}} [^\circ\text{C}]$	33.7 (0.6)	31.2 (0.9)	$<0.001^*$	30.6 (1.0)	$<0.001^*$
$T_{\text{fingertip}} - T_{\text{lowerarm}} [^\circ\text{C}]$	0.6 (1.7)	-6.2 (1.9)	$<0.001^*$	-7.1 (1.6)	$<0.001^*$
Forearm blood flow $[\frac{\text{ml}}{100\text{ml} \cdot \text{min}}]$	4.2 (1.8)	2.7 (1.4)	0.006^*	2.2 (1.3)	0.001^*
VLF power [ms^2]	2198 (1231)	3719 (2458)	0.036^*	3568 (1313)	0.011^*

* Statistical significant result ($P < 0.05$).

VLF is the very low frequency component of the heart rate variability.

At $t=90$ min, mean skin temperature immediately decreased (figure 5.3(b)). Paired t-test results revealed that mean skin temperature at $t=150$ and $t=210$ min was significantly lower than mean skin temperature at $t=90$ min.

Fingertip-lower arm gradient is shown in figure 5.3(c). A 4°C gradient identifies significant vasoconstriction (Rubinstein and Sessler, 1990). Also, a significant change in the very low frequency (VLF) components of the heart rate variability is found between the warm and cold periods (see table 5.2). Accordingly, it is concluded that in the experiment an evident vasoconstriction response was present that can be used to derive the required parameters.

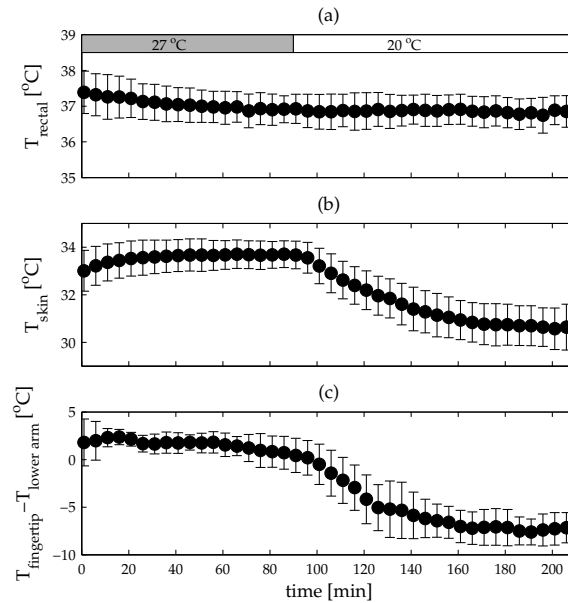


Figure 5.3: (a) Core temperature during the experiment (b) Mean skin temperature (c) Fingertip-forearm temperature gradient. Results are mean values (SD).

5.3.2 Perfusion

Plethysmography results

For the analysis only pulses were used that looked acceptable, i.e. with a clear ascending slope, after visual inspection (instructions were followed according to the Hokansson-NIVP3 software manual). The cuff artifact, the abrupt rise in limb volume that sometimes occurred due to reflux of blood when the cuff is inflated, was always excluded from the analysis. Paired t-tests reveal that forearm blood flow was significantly different at $t=150$ min ($P=0.006$) and $t=210$ min ($P=0.001$) from the base line blood flow (at $t=90$ min), see table 5.2.

Skin perfusion

Typical time traces for local skin perfusion and skin temperature at the measured spots are shown in figure 5.4. It is seen that when local temperature decreased, local skin perfusion decreased simultaneously.

In the perfusion signal sometimes peaks occur, as is seen in the arm signal in figure 5.4. One explanation is that those peaks are caused by movement artifacts. Another explanation is that the processing bandwidths of the laser Doppler flowmeters, that were used, are not tailored to adaptively detect the most important frequency range. Ideally, the lower cutoff frequency should be chosen in such a way that low-frequency artifacts due to tissue motion are filtered

out and that the higher cutoff frequency filters out the high-frequent noise (cf. Obeid et al. (1990) and Chen et al. (2004)). However, since in the remaining periods the signal seems to be quite stable and the periods with peaks are short, it is decided to include the signals in further analyses.

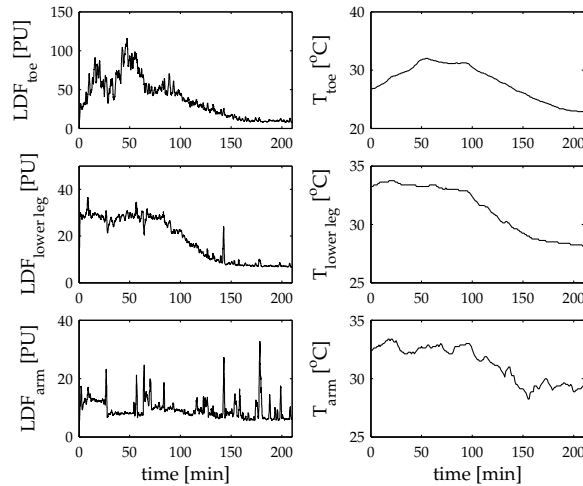


Figure 5.4: Example of time traces for skin perfusion measured with LDF (presented in dimensionless Perfusion Units [PU]) and skin temperature for toe, lower leg and arm, respectively.

5.3.3 Relation perfusion/temperature

Relation (5.3) was analyzed with help of perfusion and temperature data taken from $t=30$ to 210 minutes. First 30 minutes were not taken into account, as the temperature and perfusion during that period were stabilizing.

For each individual subject, temperature and perfusion data of the toe, lower leg and arm were fitted to equation (5.3). A linear fitting procedure was used after log-transformation. Also, the averaged data of all 10 subjects were used to fit equation (5.3). Best fits and fitting statistics of all individuals and the mean value of all subjects are detailed in table 5.3. In figure 5.5 the mean perfusion-temperature curves are shown for the 3 locations. Large intersubject variability was observed. To some extent, the high variation of relative perfusion might be related to the peaks in the laser Doppler signal. Toe temperature drop varied between 8 and 12°C, lower leg temperature decreased between 4 and 6°C and the decrease in arm temperature was between 3 and 6°C.

Table 5.3: Results of individual fits to equation 5.3. The results are normalized at 1. A linear fitting procedure is used after log-transformation.

Subject	$Q_{\text{fit,toe}}$	R^2	$Q_{\text{fit,leg}}$	R^2	$Q_{\text{fit,arm}}$	R^2
1	14.9	0.91	9.7	0.91	44.3	0.50
2	15.7	0.92	18.2	0.96	1.3	0.05
3	10.6	0.84	2.8	0.82	7.7	0.45
4	15.6	0.96	3.3	0.90	88.2	0.73
5	9.9	0.85	10.8	0.94	1.4	0.11
6	10.6	0.86	3.1	0.77	0.04	0.00
7	15.4	0.92	6.5	0.68	2.5	0.12
8	28.5	0.91	5.3	0.78	1.5	0.16
9	16.6	0.87	3.8	0.89	3.7	0.61
10	6.68	0.84	210.6	0.85	2.5	0.57
all	14.2 ± 0.1	0.87	5.9 ± 0.07 †	0.69 †	3.9 ± 0.11	0.20

† Data from subject 10 was not taken into account in the average fit, because it deviated a lot from the other subjects.

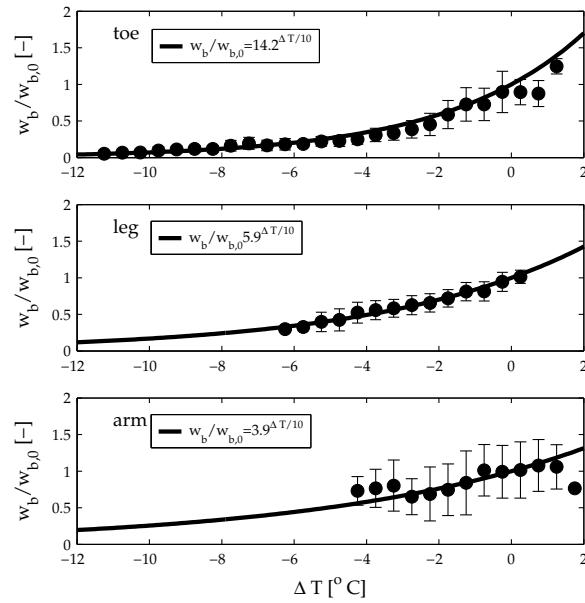


Figure 5.5: Mean perfusion-temperature curves (SD) of all volunteers. From top to bottom: toe, lower leg and arm.

5.3.4 Experimentally determined amplification coefficients and sympathetic vasoconstriction tone

Amplification coefficients

From the fingertip-lower arm gradient, shown in figure 5.3(c), it is seen that vasoconstriction started around $t=90$ minutes and lasted till the end of the measurement ($t=210$ min). It is observed that skin temperatures stabilized towards the end of the cold period. As mentioned in section 5.2.7, the maximum value of C_s was chosen to be 1. Therefore C_s was set to 1 at the end of the cold period because vasoconstrictor tone is expected to be largest at the time that skin temperatures were lowest. Then, the amplification coefficients $a_{cs,toe}^A$, $a_{cs,leg}^A$ and $a_{cs,arm}^A$ were calculated.

- Method A

With help of equation (5.7)-(5.9) and the assumption that $C_s=1$ at $t=210$ min, the amplification coefficient for the toe, leg and arm were determined for all subjects. This resulted in: $a_{cs,toe}^A = 7.42 \pm 3.24$, $a_{cs,leg}^A = 1.00 \pm 0.64$ and $a_{cs,arm}^A = 0.46 \pm 0.67$, see table 5.4.

Table 5.4: Mean values obtained of vasoconstriction amplification coefficients in the current study using method A. The relative values are also given to make comparison easier.

A	Severens: Method A range C_s : 0-1	
	absolute	relative
$a_{cs,toe}^A$	7.42 ± 3.24	$84\% \pm 36\%$
$a_{cs,leg}^A$	1.00 ± 0.64	$11\% \pm 7\%$
$a_{cs,arm}^A$	0.46 ± 0.67	$5\% \pm 7\%$

The a_{cs} results obtained with method A can be compared to the values used in other models (Stolwijk, 1971; Gordon, 1974; Fiala et al., 2001; Tanabe et al., 2002) by expressing them as percentages, see table 5.5. This is necessary as not all authors use the same sum of relative values of the three body parts: the sum of the amplification coefficients for all body parts ($\sum_{i=1}^n a_{cs,i}$) of Stolwijk (1971), Fiala et al. (2001) and Tanabe et al. (2002) was always equal to 1, while the sum of our amplification factors is not necessarily 1. Also Gordon (1974) did not normalize his amplification coefficients to 1. With the help of method A, relative values of 84%, 11% and 5% for the toe, leg and arm, respectively were found. It is seen that the feet in our experiment contribute more, while the arm contributes less to the vasoconstriction response than other models suggest (see tables 5.4 and 5.5).

The range of C_s obtained in current study can not be compared to that of other studies.

For instance, the range in the model of Fiala et al. (2001) under these conditions for Cs is between 0 and 110. The Cs values of the model of Stolwijk (1971) was between 0 and 18. The range of Tanabe et al. and Gordon could not be calculated as not all required temperatures were available for calculating Cs with their models (viz. pelvis, shoulder, head, face, neck data). However, it is possible to compare the products of the maximum value for $a_{cs,i}$ Cs of method A to the products of Stolwijk and Fiala et al.. The products of $a_{cs,i}^A Cs^A$ are 7.42 ± 3.24 , 1.00 ± 0.64 and 0.46 ± 0.67 for the toe, leg and arm, respectively. The products $a_{cs,i}$ Cs of Stolwijk are about 6.3, 0.9 and 0.9, respectively. According to Fiala et al., the products are 41, 22 and 21, respectively.

It is seen that current measured values (both the normalized values for $a_{cs,i}$ and the product $a_{cs,i}^A Cs^A$) are very close (within the intersubject variability) to the tentative values proposed by Stolwijk, but deviate considerably from the values used by Fiala et al. and Gordon. The normalized values for a_{cs} of current measurements are also within the range of Tanabe et al.'s values.

Table 5.5: Vasoconstriction amplification coefficients used by Stolwijk (1971), Fiala et al. (2001), Tanabe et al. (2002) and Gordon (1974). The relative values are also given to make comparison with current study easier.

A	Stolwijk (1971) range Cs: 0-18		Fiala et al. (2001) range Cs: 0-110		Tanabe et al. (2002) range Cs: unknown		Gordon (1974) range Cs: unknown	
	absolute	relative	absolute	relative	absolute	relative	absolute	relative
$a_{cs,toe}$	0.35 †	78%	0.3765 †	48%	0.152 †	78%	0.2961 †	38%
$a_{cs,leg}$	0.05	11%	0.20	26%	0.022	11%	0.2104	27%
$a_{cs,arm}$	0.05	11%	0.1945	25%	0.022	11%	0.2700	35%

† This value refers to the amplification coefficient of the whole foot.

- Method B

With the help of method B, the following amplification coefficients were found: $a_{cs,toe}^B = 0.87 \pm 0.05$, $a_{cs,leg}^B = 0.45 \pm 0.18$ and $a_{cs,arm}^B = 0.19 \pm 0.28$. After conversion to normalized percentages, this results in relative values of 58%, 30% and 13% for the toe, leg and arm, respectively. Again the sum of contributions of all amplification factors $\sum_{i=1}^n a_{cs,i}$ is not necessarily equal to 1.

No values in literature are available to compare the values found with help of method B, as no other study used this type of relation.

Comparison of the inter-subject variability of the values for $a_{cs,toe}$, $a_{cs,leg}$ and $a_{cs,arm}$ showed that overall method B shows a smaller variability than method A for the same dataset (table 5.7), especially for the toe value. Although it must be said that intersubject variability for the arm is also quite large for method B.

Table 5.6: Mean values of vasoconstriction amplification coefficients obtained in the current study using method B.

B	Severens: Method B range Cs: 0-1	
	absolute	relative
$a_{cs,toe}^B$	0.87 ± 0.05	$58\% \pm 3\%$
$a_{cs,leg}^B$	0.45 ± 0.18	$30\% \pm 12\%$
$a_{cs,arm}^B$	0.19 ± 0.28	$13\% \pm 19\%$

Table 5.7: Inter-subject variability of amplification coefficients (standard deviation/mean value · 100%) as percentage of the mean value for method A and B at $t=210$ minutes.

	A	B
$a_{cs,toe}^{A,B}$	44%	6%
$a_{cs,leg}^{A,B}$	64%	40%
$a_{cs,arm}^{A,B}$	146%	147%

Vasoconstrictor tone: Cs

The transient vasoconstrictor tone was determined for method A and B for all subjects. Results are given in figure 5.6(a) and figure 5.6(b). For both methods, a distinct increase in vasoconstrictor tone is visible starting from $t=90$ min. The responses of Cs determined with method A and B are quite similar.

Evolution of a vasoconstriction tone relation

The vasoconstrictor tone showed a clear rise for both methods, see figure 5.6. According to the basic engineering control concept, the vasoconstrictor tone is initiated by a so-called error signal. Although there is no general consensus if such regulation of physiological systems exists in reality or if core temperature is maintained within an interthreshold zone, this classical approach is a good tool for developing predictive models (Mekjavic and Eiken, 2006). An error signal is defined as the difference between the actual state of a variable x and its setpoint x_0 : $\Delta x = x - x_0$. It is known that mean skin temperature responds reflexly on cutaneous vasoconstrictor tone (Wissler, 2008) and can thus act as innervating error signal. Lopez et al. (1994) showed that vasoconstriction is also modulated by core temperature. For vasomotion, the core temperature to skin temperature contribution ratio is $3(\pm 2.5):1$, according to Frank et al. (1999). Cheng et al. (1995) reported that the cutaneous contribution of mean skin temperature to vasoconstriction is linear with a core temperature to skin temperature contribution

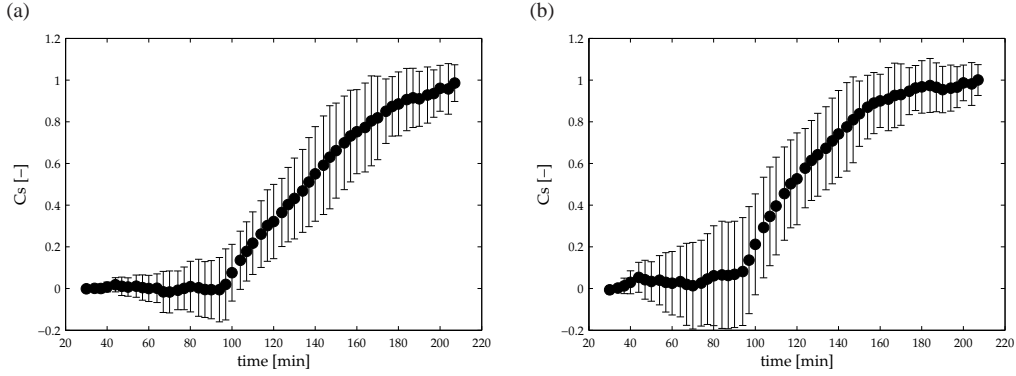


Figure 5.6: Mean C_s value of all subjects as function of time (SD) calculated with (a) method A, (b) method B.

ratio of $4(\pm 1.23):1$. Therefore, it is possible to use the measured skin and core temperatures at each threshold to calculate a core-temperature threshold that would have been observed if the skin was at a standardized temperature (Matsukawa et al., 1995a):

$$T_{\text{core,stand}} = T_{\text{core,obs}} + \left(\frac{\beta}{1 - \beta} \right) (T_{\text{skin,obs}} - T_{\text{skin,stand}}) \quad (5.15)$$

Subscripts stand and obs denote standardized and observed (measured) temperature, respectively. Relation (5.15) was used for calculating the standardized core temperature at which vasoconstriction was triggered in the measurements. Here, we use $\beta = 0.2$ and $T_{\text{skin,stand}} = 35.7^\circ\text{C}$ for vasoconstriction (values according to Matsukawa et al. (1995a) who based relation (5.15) on Cheng et al. (1995)). The start of vasoconstriction was defined as the moment in time when $T_{\text{finger}} - T_{\text{forearm}}$ started to show a sustained decrease (see for an example figure 4.5). At that time point, $T_{\text{core,obs}}$ was $36.9 \pm 0.4^\circ\text{C}$ and $T_{\text{skin,obs}}$ was $33.7 \pm 0.6^\circ\text{C}$, respectively. Accordingly, $T_{\text{core,stand},0}$ was: $36.4 \pm 0.4^\circ\text{C}$. The advantage of using the standardized core temperature as an error signal is that this structure can also be used during cardiac surgery, in which the threshold of vasoconstriction ($T_{\text{core,stand},0}$) changes in a drug-dose dependent way (see chapter 4).

Vasoconstrictor tone as function of the error signal of the standardized core temperature is depicted in figure 5.7 for both methods. From non-linear regression analysis, the following relations were defined for the effect of the error in standardized core temperature ($\Delta T_{\text{core,stand}} = T_{\text{core,stand}} - T_{\text{core,stand},0}$) on vasoconstriction tone (C_s):

- Method A

$$C_s^A = 0.5(1 + \tanh(-1.71(\Delta T_{\text{core,stand}} + 0.65))) \quad (5.16)$$

with $R^2=0.91$. The typical hyperbolic tangent shape was also used by Fiala et al. (2001) and Wissler (2008) to describe cutaneous vasoconstriction, as the signal levels off. As can be seen in equation (5.16), the C_s values are bounded between 0 and 1.

- Method B:

$$Cs^B = 0.5(1 + \tanh(-2.76(\Delta T_{\text{core,stand}} + 0.47))) \quad (5.17)$$

with $R^2=0.96$.

The R^2 -value is larger when using method B compared to method A.

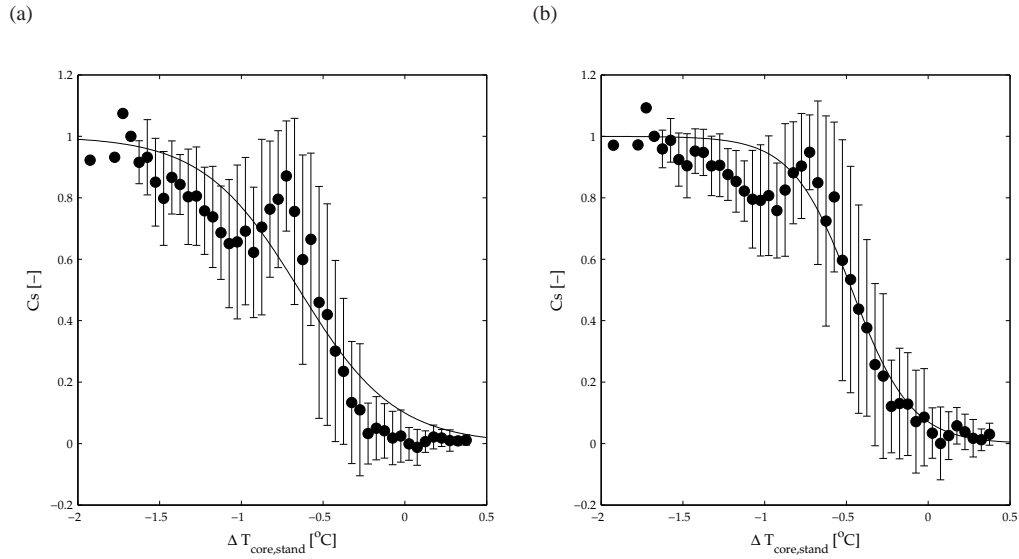


Figure 5.7: Mean C_s (SD) value as function of the error of the standardized core temperature, calculated with (a) method A, (b) method B. The setpoint of the error signal was: $T_{\text{core,stand},0} = 36.4^\circ\text{C}$.

5.3.5 Discussion of results

An experimental study was conducted to determine physiological values for vasoconstriction amplification coefficients and vasoconstrictor tone. Earlier published models, either based these parameters on estimations (Stolwijk, 1971) or by fitting their models to global body temperature data (Gordon, 1974; Fiala et al., 2001). Those methods are very sensitive to errors and have a restricted physiological basis. A measurement protocol was developed with which it was possible to determine vasoconstriction amplification coefficients and the transient vasoconstriction tone by directly measuring local perfusion and temperature.

When using method A, the contributions to the normalized amplification coefficient from toe, leg and arm were found to be 84%, 11% and 5%, respectively. In method B normalized contributions of 58%, 30% and 13% for toe, leg and arm were observed. Comparing the normalized amplification values found with method A to the values from literature, displayed that the values of Stolwijk (1971) and Tanabe et al. (2002) were within the standard deviation

range of our experimentally determined values. The amplification coefficients employed by Fiala et al. (2001) and Gordon (1974) deviate more from current measured values.

Vasoconstriction thresholds are a linear function of skin and core temperature (Matsukawa et al., 1995a). Therefore, the error signal of the standardized core temperature was used as an input variable for deriving the vasoconstrictor tone relation. For calculating the standardized core temperature, the core to skin temperatures contribution suggested by Cheng et al. (1995) was used. In current study a base line value for the standardized core temperature was found of $\Delta T_{\text{core,stand},0} = 36.6 \pm 0.4^\circ\text{C}$. This agrees well with the vasoconstriction threshold temperature observed by Matsukawa et al. (1995a), who found a value of $36.4 \pm 0.3^\circ\text{C}$. With help of non-linear regression analysis, a relation was formulated between the error signal of the standardized core temperature ($\Delta T_{\text{core,stand}}$) and vasoconstrictor tone (Cs) for both methods. The advantage of using the standardized core temperature as an error signal is that this format can also be used during cardiac surgery, in which the threshold of vasoconstriction changes in a drug-dose-dependent way. Another value will then be chosen as setpoint for $T_{\text{core,stand},0}$. Equation (5.16) or (5.17) can still be used during anesthesia as only the setpoint changes.

A suggestion for further research is to study in depth the validity of equation (5.15) when the core to skin temperature contribution ratio is chosen slightly different, for instance when using the values of Frank et al. (1999) instead of the values mentioned by Matsukawa et al. (1995a).

Method B gave results with smaller intersubject variability than method A (see table 5.7), although especially arm intersubject variability was high. The fit for developing control equations for vasoconstrictor tone also gave higher R^2 -values for method B. Overall, the newly proposed method B seems more suitable for describing the relation between skin perfusion and temperature than relation A.

The temperature range that was employed in the experiment resulted in reductions of mean skin temperature that are comparable to the skin temperature reductions that were observed during aortic valve procedures, performed at 30°C (chapter 3 and Severens et al. (2007b)). Accordingly, the acquired values for amplification factors and vasoconstrictor tone are expected to be applicable to our current model for predicting temperatures during cardiac surgery.

A restriction of the current investigation is that skin perfusion was measured at only three locations. Hence, a pilot experiment was designed in which also values for a_{cs} for the other body parts were assessed using the proposed method.

5.4 Determination of proportionality constants of other body parts

In the follow up short experiment, the protocol as described in section 5.2.2 was extended to more body locations. Experiments were performed on two male healthy subjects after obtaining informed consent (subject 1: age 34, 1.96m, 98 kg, 23.5% fat and subject 2: age 35, 1.93m, 85 kg, 24.2% fat). Both subjects were also involved in the previous study protocol.

Subjects stayed on two different days again 3.5 hours in the climate chamber, where the temperature protocol of section 5.2.2 was exploited. On both days, mean skin temperature and rectal temperature were measured according to the old protocol. But now, three laser Doppler devices were used at the same time with a total of 5 measurement channels: a two-channel Perimed 4001 with standard probes (Probe 408), a one-channel Perimed 4001 with standard probe (probe 408) and a two-channel Perimed 5010 laser Doppler flowmeter with 415-311 probes. According to the manufacturer, the measurement volumes of the used probe types inside the skin are equal (about 1 mm³) and therefore probes are considered to be interchangeable.

On the first measurement day skin perfusion and local skin temperature were measured at the head, shoulder, thorax, hand and lower leg. On the second test day, perfusion and local skin temperature measurements were performed on the neck, abdomen, face, hand and lower leg.

Data was analyzed in the same manner as described in section 5.2.7. The results for the proportional distribution coefficients of the two subjects and the average value per body part are given for methods A and B, see table 5.8.

The value of a_{cs} is an indicator of the amount and affinity of receptors that respond to sympathetic stimulation. Body parts with a higher a_{cs} -value give a stronger vasoconstrictive response than body parts with a lower a_{cs} -value.

Table 5.8: Values for $a_{cs}^{A,B}$ for methods A and B as found in the test with two healthy male subjects.

	Method A: a_{cs}^A			Method B: a_{cs}^B		
	subject 1	subject 2	average	subject 1	subject 2	average
head	0.67	0.28	0.48	0.40	0.22	0.31
face	0.81	1.26	1.04	0.45	0.56	0.51
neck	0.57	0.44	0.51	0.36	0.30	0.33
shoulder	0.58	0.98	0.78	0.37	0.50	0.44
thorax	0.58	0.08	0.33	0.37	0.07	0.22
abdomen	0.34	1.75	1.05	0.26	0.64	0.45
hand, day 1	4.52	2.62		0.82	0.72	
hand, day 2	1.04	1.68	2.47	0.51	0.63	0.67
leg, day 1	0.57	0.79		0.36	0.44	
leg, day 2	1.77	0.95	1.02	0.64	0.49	0.48

As in this short experiment only two volunteers were involved, it is hard to evaluate the reliability of the measurement results. However, the leg amplification coefficients were assessed in all three measurement sessions (the experiment described in section 5.2.2 and the two sessions described in this section). It was observed that the found average amplification

value for the leg of these volunteers is in good agreement with the group average of the ten volunteers (method A: 1.00 versus 1.02, method B: 0.45 versus 0.48). This gives some confidence that the average values of those two volunteers for the other body parts can be considered to be representative for using in the model.

5.5 Validity of the new model for healthy subjects

The vasoconstriction relation as defined by equation (5.17) was implemented in the active model. In table 5.9 a complete overview is given of the values for a_{cs}^B that are used during the simulations in the remainder of the thesis. The values for the foot, leg and arm are based on 10 subjects (see section 5.3.4) and for the head, shoulder, thorax, neck, abdomen, face and hand, the values based on 2 subjects were taken.

Table 5.9: Values for a_{cs}^B as will be used in the new model.

Body part	method B
head	0.31
face	0.51
neck	0.33
shoulder	0.44
thorax	0.22
abdomen	0.57
hand	0.67
arm †	0.19
leg †	0.45
foot †	0.78

† Value based on $n = 10$, see table 5.6.

First, the sensitivity of the model for inaccuracy and intersubject variability of the vasoconstriction amplification coefficients is examined by a sensitivity analysis. Then, the experimental and model results are compared for four different experiments involving healthy volunteers: the (partly) dependent experiments as described in section 5.2.2, two independent cooling experiments performed by Van Ooijen et al. (2004, 2005) and the protocol described by Kurz et al. (1995a) (see also section 2.4). All validation simulations use method B. As $a_{cs,i}^A$, Cs^A , $a_{cs,i}^B$ and Cs^B are fitted to the same data, models A and B give approximately the same predictions.

5.5.1 Sensitivity analysis of model coefficients

The sensitivity of method B for inaccuracies and intersubject variability of a_{cs}^B was tested by assigning random values for a_{cs}^B with $\mu_i \pm SD_i$ to a person with the standard anatomy characteristics (height 1.71m, weight 73.5 kg and a fat percentage of 14%). The average

value μ_i for each body part was based on table 5.9. The standard deviations for the foot, leg and arm were taken from table 5.7. For the other body parts the average percentage deviation with respect to the mean value per body part was used (calculated with the help of table 5.8), because due to the limited data no well-founded argument exists to assume that standard deviation divided by the mean value of a_{cs}^B of the body parts differ from each other. This led to $SD_i=0.2\mu_i$ for the other body parts. This procedure was repeated 100 times, resulting in 100 different body property input files. For each input file, a situation was simulated where initially body temperature was completely stabilized under thermoneutral conditions (30°C) and then room temperature was changed to 20°C for 60 minutes. It was assumed that the person wore underwear, t-shirt, short trousers and lay down on a stretcher. Mean results and standard deviation of core and mean skin temperatures are given in figure 5.8. From this, it

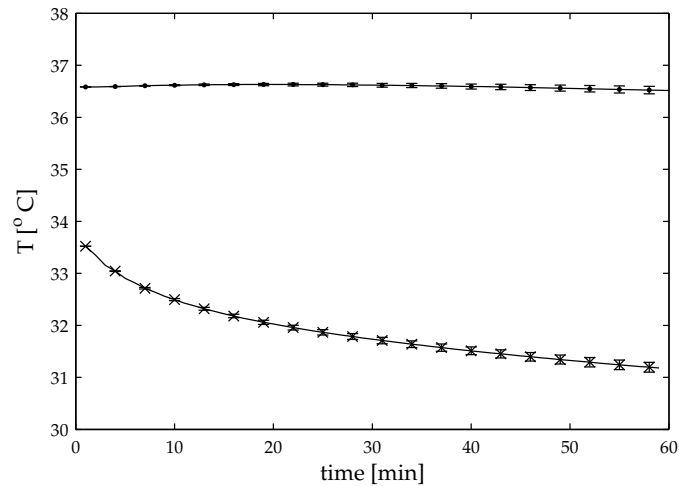


Figure 5.8: Sensitivity of core temperature and mean skin temperature to inaccuracies and intersubject variability in a_{cs}^B . Average (SD) results are shown for 100 persons with standard anatomy, exposed for 60 minutes to a temperature of 20°C , and with randomly assigned values for $a_{cs,i}^B$ using a normal distribution. ● represents core temperature and × represents mean skin temperature.

emerges that interindividual variations and inaccuracies in a_{cs}^B led under these circumstances to a typical standard deviation of 0.1°C in core temperature and a standard deviation of 0.2°C in mean skin temperature. As these variations are of the same order as the accuracy of the used modelling method (see section 2.2.3) and of the temperature sensors, the found variations are considered to be acceptable.

5.5.2 Dependent experiment

Cooling from 27°C to 20°C

The protocol as described in section 5.2.2 was simulated with the model. Summarized: 10 subjects lay in semisupine position for 90 minutes in a room of 27°C, followed by a period of 120 minutes at an ambient temperature of 20°C. Subjects wore underwear (0.04 clo), a pair of short trousers (0.06 clo) and a t-shirt (0.09 clo). Average body characteristics: length 186 ± 8 cm, weight 77.7 ± 11 kg and fat percentage $17.3 \pm 5.9\%$. Results of simulation and experiments are given in figure 5.9(a). In order to see the influence of the active system, also a simulation was run for the same case with only the passive model, see figure 5.9(b).

It can be seen that core and mean skin temperature results of the simulation in figure 5.9(a) lie within the standard deviation interval of the mean temperature measurements, except for the core temperature in the last 10 minutes. Here simulated core temperature is 0.05-0.10°C out of the standard deviation range of the measurements.

In figure 5.9(b), it is seen that core temperature errors are very large when only the passive model is used. Core temperature errors in the last 5 minutes are around 1.8°C. Mostly, skin temperature is within the standard deviation range of the measurements, but is not as good as skin temperature predicted with using the active model. Because of the lack of vasoconstriction, skin temperature in the cold predicted with the passive model is higher than in the model with the active part.

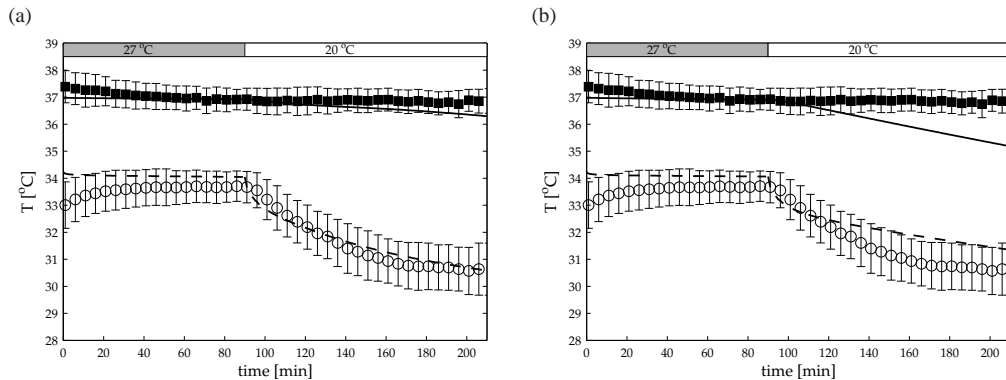


Figure 5.9: Warming-cooling cycle as described by the protocol in section 5.2.2 as calculated with (a) method B and with (b) the passive model. ■ and ○ represent experimentally assessed core and mean skin temperature, respectively. — and — — represent the core and mean skin temperatures following from the simulation, respectively.

5.5.3 Independent experiments

Three independent data sets were used for validating the model. Data were based on experiments from Van Ooijen et al. (2004, 2005) and Kurz et al. (1995a). Because relation (5.16) was based on skin temperature ranges between roughly 30-34°C, we mainly considered temperature data in that range.

Cooling from 21.5 °C to 15°C

In the first experiment of Van Ooijen et al. 11 subjects were exposed to a temperature of 21.5°C for 60 minutes, while lying on a bed, wearing a sweater (0.37 clo), trousers (0.28 clo), underwear (0.04 clo) and socks (0.02 clo). Hereafter the temperature was decreased to a value of 15.0°C, while the subjects stayed in the same position with the same garments for an additional 180 minutes (Van Ooijen et al., 2005). The average length of the 11 subjects was 1.82 ± 0.11 m with a mean body mass of 76.3 ± 8.2 kg and a fat percentage of 22.9 ± 9.7 %. Results are shown in figure 5.10.

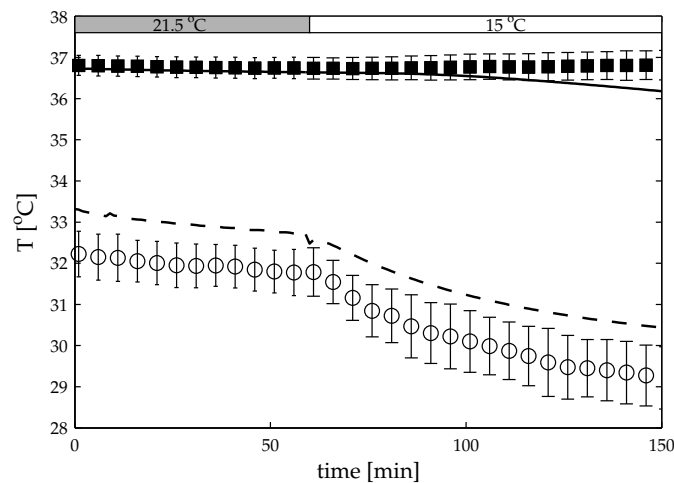


Figure 5.10: Cooling cycle as described by the protocol in Van Ooijen et al. (2005). ■ and ○ represent experimentally assessed core and mean skin temperature, respectively. — and — — represent the core and mean skin temperatures following from the simulation, respectively.

Initially, core temperature predicted by the model is within the standard deviation range of the measurements. However, from $t=120$ min core temperature in the model is decreasing while the measured core temperature stays at the same level. As equation (5.16) was based on mean skin temperature between 30-34°C and in this experiment the mean skin temperature decreases till lower values than 30°C, it is unknown if equation (5.16) holds. Plausibly, the C_s values are higher than the maximum value 1 that can be obtained with equation (5.16).

Lying in the cold with and without blanket

In the second independent experiment, 11 subjects were exposed to a temperature of 15.0°C while lying on a bed covered by a blanket for 30 minutes. After that period, the blanket was removed and the subjects had to remain on the bed wearing only underwear for a final 60 minutes (Van Ooijen et al., 2004). The average length of the ten subjects was 1.81 ± 0.09 m with a mean body mass of 67.8 ± 9.6 kg and a fat percentage of $17.9 \pm 8.6\%$. The blanket is modelled with the help of clothing parameters given in appendix B.3, using the values for the cotton drape. Results are given in figure 5.11.

Core temperature error over the whole period was about 0.6°C. No explanation exists for this, but it is remarkable that the core temperature of the volunteers is around 37.4°C in the measurement series, while in the other two data series core temperature was around 36.9°C. The simulated skin temperature is at the upper and lower value of the standard deviation of the measured mean skin temperature. Partly, this could be due to differences in temperature regulation, but possibly, better knowledge of used blanket types and accompanying clothing model values and environmental conditions can lead to considerable improvements of the mean skin temperature results.

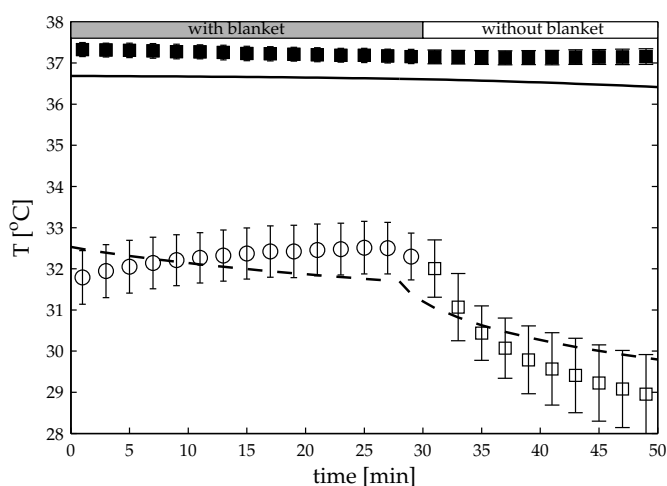


Figure 5.11: Cooling cycle as described by the protocol in Van Ooijen et al. (2004). ■ and ○ represent experimentally assessed core and mean skin temperature, respectively. — and — — represent the core and mean skin temperatures following from the simulation, respectively.

General anesthesia

With help of the complete model the protocol of Kurz et al. (1995a), see section 2.4, is resimulated. In short: nine healthy males (1.75 ± 0.04 m, 74 ± 11 kg and $18 \pm 4\%$ fat) were

administered general anesthetic drugs and exposed to a room temperature of 22°C for six hours. In the first two hours the propofol induction was 150 $\mu\text{gkg}^{-1}\text{h}^{-1}$. According to Kurz et al. (1995a) this dose was reduced after 2 hours. No value was mentioned in literature, but in the simulation an arbitrarily chosen dose of 75 $\mu\text{gkg}^{-1}\text{h}^{-1}$ was used. In figure 5.12 it is seen that the new results, including the vasoconstriction model, much more resemble the measurement results of Kurz et al. (1995a) (see figure 2.7(a)) than the simulation results with only the passive model. After six hours, the core temperature decrease was 3.5°C, which was also found in the measurements. In the last hours of the simulation, core temperature is still decreasing while in the measurements of Kurz et al. a plateau occurs after four hours. This can on the one hand be explained by the assumptions that were made regarding the administered dose of drugs in the second stage. On the other hand, it was seen that mean skin temperature in the simulation in the last four hours was between 28 and 30°C, which is lower than the specified working range (30-34°C) of the vasoconstriction model. The small increase in core temperature after two hours is caused by the decrease in blood drugs concentration, which allows the activation of vasoconstriction.

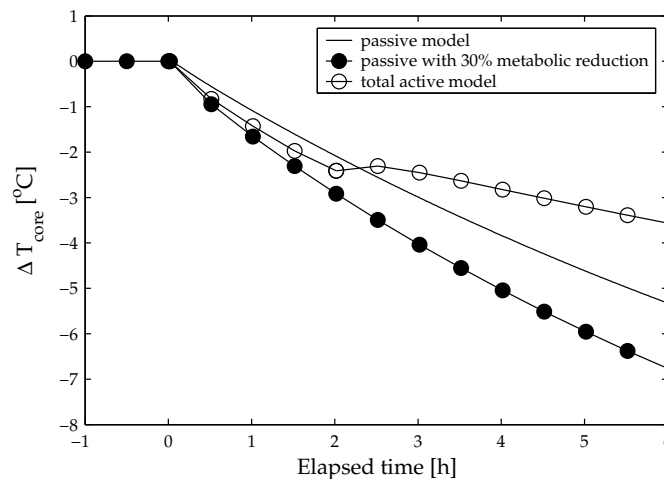


Figure 5.12: Simulation of the protocol as performed by Kurz et al. (1995a), see also section 2.4.

5.6 Validity of the model for cardiac surgery under moderate hypothermic conditions

With help of the newly developed vasoconstriction model, the protocols of aortic valve replacement and coronary bypass surgery, as described in section 4.7 are repeated. The vasoconstriction tone relation as given by equation (5.17) was used with the standardized core

temperature as error signal. At each time point the momentary standardized core temperature was calculated with equation (5.15) and compared to the momentary setpoint value. This setpoint value, that represents the momentary threshold of vasoconstriction ($T_{\text{core,stand},0}$) is calculated with help of the pharmacological model as described in chapter 4. The vasoconstriction threshold that follows from equation (4.30) is used for the standardized vasoconstriction threshold $T_{\text{core,stand},0}$ at that time step.

5.6.1 Aortic valve surgery

The protocol of the aortic valve surgery was simulated again using the simulation values as outlined in section 4.7 but using the new vasoconstriction relations as derived in this chapter. Core temperature and mean skin temperature results of the stepwise model of chapter 4 and new model are visible in figure 5.13. Local skin temperatures of the head, lower leg, foot and lower arm are shown in figure 5.14.

In figure 5.13, it is seen that the sawtooth profile at the end of stage 1, that occurred when using the stepwise model, does not occur for method B. The mean skin temperature in stage 3 is also somewhat smoother for method B than for the stepwise model. In figure 5.14 only subtle differences in local skin temperatures of the leg, foot and arm are observed between method B and the stepwise model. However, the skin temperature of the head considerably improved in stages 1, 2 and 3 when using method B instead of the stepwise model.

5.6.2 Coronary surgery

The simulation was run again for the coronary surgery (for details, see section 4.7) and using method B as vasoconstriction model. Core and mean skin temperatures predicted by the new and old model are shown together with the measurement data in figure 5.15.

Again, the biggest difference between method B and the stepwise model is that the sawtooth profile in stage 1 has disappeared.

5.7 Discussion of model achievements

Core temperature and mean skin temperature of the partly dependent data set were better predicted by the model than the independent datasets of Van Ooijen et al. (2004, 2005). Core temperature of the dependent data set and of the first independent experiment were underestimated by the model in the last minutes, while in the second independent experiment core temperature predicted by the model was lower during the whole cycle.

Skin temperature of the dependent dataset agreed very well (within 0.5°C), while in the independent experiments a larger deviation (typically 1°C) between simulation and experimental results was found. The larger initial deviation in the independent experiments (1.5°C at the begin situation and maximal 1°C in the remaining period) than in the dependent experiment might be explained by the fact that in the dependent dataset efforts were made to precondition

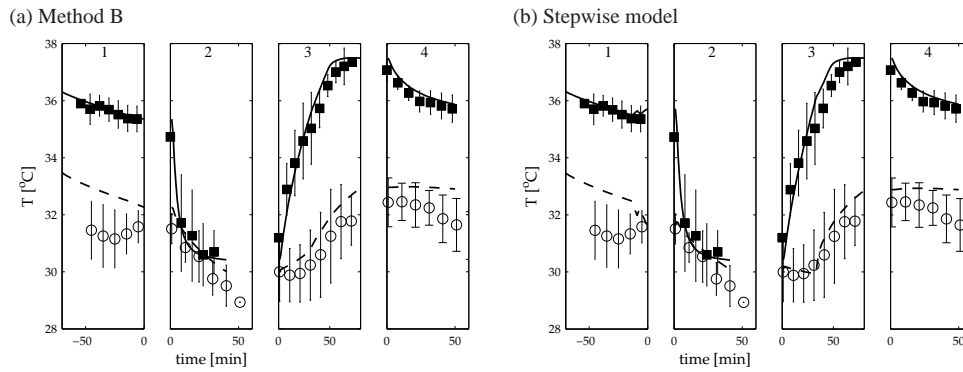


Figure 5.13: Aortic valve surgery obtained with (a) model of chapter 5, method B, (b) stepwise model (chapter 4). ■ and ○ represent experimentally assessed core and mean skin temperatures, respectively. — and - - represent the core and mean skin temperatures following from the simulation, respectively.

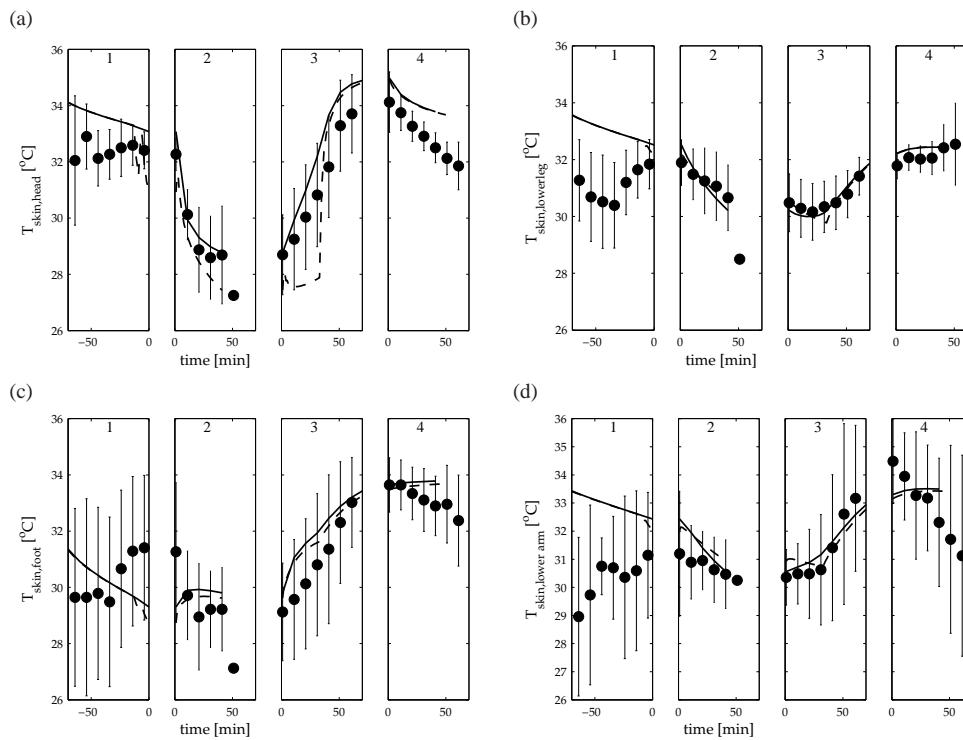


Figure 5.14: Predictions of local skin temperatures of the (a) head, (b) lower leg, (c) foot (d) lower arm. —, - - and • represent skin temperatures obtained with method B, the stepwise model of chapter 4 and the measurements, respectively.

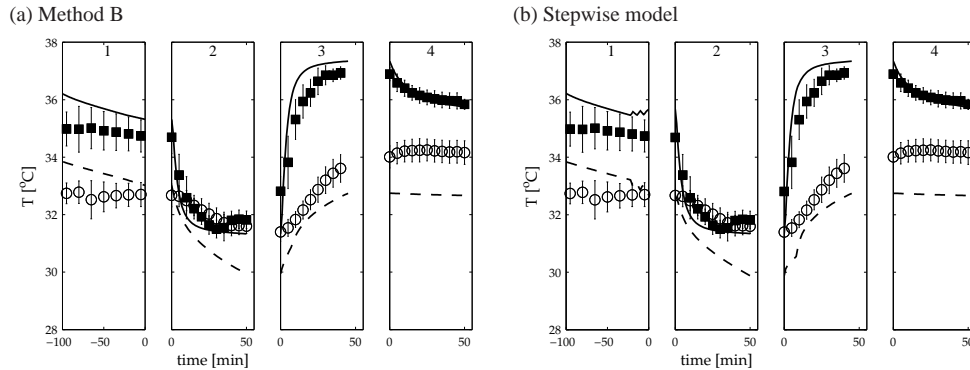


Figure 5.15: Coronary surgery obtained with (a) model of chapter 5: method B, (b) the stepwise model (chapter 4). ■ and ○ represent experimentally assessed core and mean skin temperatures, respectively. — and — — represent the core and mean skin temperatures following from the simulation, respectively.

the subjects to a thermoneutral condition by a light exercise before the start of the measurement. In the independent data sets no preconditioning efforts were made. When simulating the protocols of the independent data sets, it was assumed that at time $t=0$ the subjects already were at 21.5°C and 15°C for 15 minutes before the measurements started, respectively. However, it can not be verified if this actually was the case during the experiment. This could be a reason for the somewhat higher discrepancy in the independent experiments. When comparing model predictions to experiments, it is therefore strongly recommended to conduct the experiments under controlled laboratory conditions and to let the subjects acclimatize in a thermoneutral environment.

Especially, the core temperature calculated by the model for the first independent experiment has a tendency to decrease more than the experimentally assessed core temperature at the end of the studied period. The fact that relation (5.16) was based on mean skin temperatures between $30\text{--}34^{\circ}\text{C}$ while in experiment of Van Ooijen et al. skin temperatures decrease till lower temperatures might have contributed to this discrepancy. When using the model for colder temperature ranges, more efforts are needed to elaborate the Cs-relation to other temperature ranges, and if necessary also develop and implement control equations for cold-induced thermogenesis and shivering which might play a role in lower temperature ranges.

With the help of the complete model, including the drug-dose dependent active model, the protocol of Kurz et al. (1995a) has been resimulated. It was shown that the results obtained with the complete model much more resembled the measured values than simulation results obtained with only the passive model.

In figures 5.13 and 5.15, it was observed that using the newly developed vasoconstriction model did not lead to big differences in absolute temperature in comparison to the stepwise model when simulating a cardiac surgery. Only when body temperature was around the

threshold temperature for vasoconstriction (end of stage 1), the new model with method B responded much better. While the stepwise model showed a sawtooth profile in calculated temperature, the new model gave smooth results. From figure 5.14, it was seen that skin temperature of the head was predicted much better with the new model, but other skin temperatures did not change much. The better response of the head might be explained by the higher perfusion of the skin of the head and the higher arterial arrival temperature of the blood in the same, because of the absence of counter-current heat exchange.

By comparing the passive model, the passive model with the 30% reduction in metabolic rate (results discussed in chapter 3), the stepwise model (chapter 4) and the refined model with 30% reduction in metabolism (chapter 5: method B), it can be seen that results of last three models give core temperature results that differ less than 0.2°C from each other and skin temperature predictions that differ less than 0.6°C, when simulating cardiac surgery at moderate hypothermic conditions. The difference between the passive model without the metabolic rate reduction and the other models is much bigger (up to 1.0 °C difference in core temperature). The refined model (with method B) gives smoother results without sawtooth profiles than the stepwise model and gives also better predictions for the skin temperature of the head. The flexible methods that are used for developing the vasoconstriction model make it also possible to use model B for healthy people with a normal thermoregulatory system. This can not be accomplished without an active model. However, it must be stressed that this model is only derived and mainly tested for mean skin temperatures in the range from 30 to 34°C and that outside this temperature range, the validity is not verified.

Overall, it is thought that the model is suitable to give temperature predictions of healthy persons and patients undergoing surgery at temperatures between moderate hypothermia and normothermia, with skin temperatures ranging between 30 and 34°C, regardless of the surgical trauma.

Additional applications of the computer model

6.1 Introduction

Mathematical whole body temperature models are useful tools to quickly estimate the temperature response of the body due to changes in environmental conditions. In contrast to most other thermal models, that can only describe thermal responses of humans with an intact thermoregulatory system, the current model can also be used for patients with an impaired thermoregulatory system caused by anesthesia. The model, as it is, offers possibilities to use it also for a broad spectrum of other applications involving vasoconstriction response. The model can be utilized for both healthy volunteers and anesthetized patients under circumstances in the range from thermoneutral conditions to vasoconstriction, where no shivering or non-shivering thermogenesis occurs. In this chapter, some model applications are demonstrated. The following situations are considered:

- deep-cooled (17°C) cardiac surgery patients
- orthopedic back surgeries with large surgical wounds.
- the effect of changing temperature protocols
 1. cooling the head during deep hypothermic cardiac arrest
 2. comparison of old and new cardiac surgical procedures: moderate versus mild hypothermia
 3. affect of changing temperature protocols on afterdrop after cardiac surgery under moderate hypothermic conditions

Simulation results are compared to experimental data, whenever possible. For the deep-cooled patients, simulation data are compared to experimental data available in literature. The simulations of patients undergoing orthopedic surgery are compared to data that were collected in the academic hospital in Maastricht (AZM) during a short experiment involving 3 patients.

6.2 Cardiopulmonary bypass at 17°C

The computational model was used to mimic a deep-cooled cardiac surgery involving circulatory arrest. The use of deep hypothermic circulatory arrest as a method of cerebral protection was first described by Griep et al. (1975). This technique allows the surgeon to work in a quiet, bloodless field uncluttered by proximal clamps and perfusion cannulae (Chong et al., 2004). Deep hypothermia reduces the metabolic rate of the central nervous system and lengthens the period of tolerated ischemia, mainly of the brain, during the circulatory arrest period. This type of surgery consists of five stages: 1) the anesthesia stage 2) the cooling stage with the heart lung machine 3) the circulatory arrest period, without blood circulation 4) rewarming with help of the heart lung machine 5) the postbypass stage. In figure 6.1 the risk for brain damage as function of brain temperature and duration of cerebral ischemia is depicted (figure taken from Prêtre and Turina (2003)). It can be seen that reduction of brain temperature and swift surgery help to prevent brain damage.

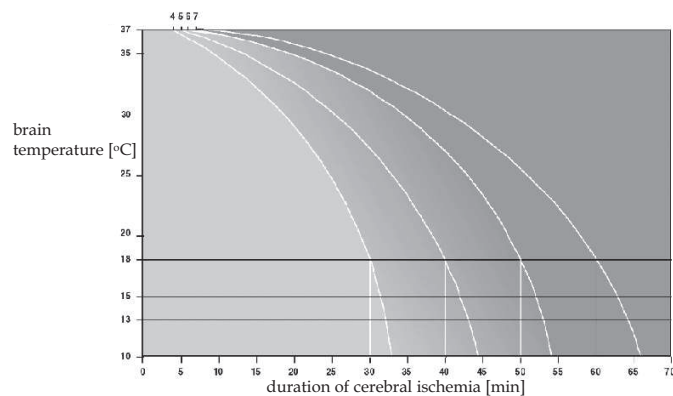


Figure 6.1: Consequences of circulatory arrest in relation to temperature and duration of cerebral ischemia. The light color depicts the periods of safe circulatory arrest. The dark color depicts the periods of obligatory harmful circulatory arrest. The transitional area depicts the periods where the risk and extent of brain damage are dependent on the conduct of surgery and pharmacological intervention. The light gray area is compatible with reversible deficits, while the dark gray area is associated with irreversible injuries. Figure taken from Prêtre and Turina (2003).

In the simulation the temperature protocol as described by Rajek et al. (1999) was employed, as outlined below. Since additional impairing thermoregulatory effects occur during deep cooling, the thermoregulatory part of the model was extended to make it suitable for simulating extreme cold.

6.2.1 Protocol

Rajek et al. (1999) collected temperature data of eight patients undergoing thoracic aorta graft procedures. The patients (mean body characteristics: weight 83.6 kg, height 172 cm, fat percentage 35.6%) were cooled during cardiopulmonary bypass to a minimal nasopharyngeal temperature of $16.8 \pm 1.1^\circ\text{C}$. Bypass flow was set to $2.5 \text{ l min}^{-1} \text{ m}^{-2}$. Towards the end of the surgery, patients were rewarmed to a nasopharyngeal temperature of 36.5°C . The fluid-blood gradient was kept around 8°C . Patients were covered by standard surgical draping; no active surface warming was used during the study period. No information was available about the temperature in the operating room, but for the model simulation we made the assumption that the surrounding temperature was 21°C (this was the approximate room temperature in other experiments of Rajek et al. (2000)).

During the thoracic aorta graft procedure, deep hypothermic circulatory arrest is applied in all patients with an average duration of 28 ± 7 min. The activity and oxygen need in the brains should then be completely abolished. By depressing the cell metabolism, the body's cells can survive 30 minutes to more than one hour without blood flow during the surgical procedure.

6.2.2 Model adjustments for extreme cold

Once the body core temperature has fallen below 28°C , the ability of the body to regulate temperature is lost (Guyton and Hall, 1996). The body is not longer capable to react to the cold by adjusting the thermoregulatory tone or by shivering. This process is also known as 'cold paralysis' (Ivanov and Arokina, 1998). At a low temperature, activity of ATP-synthesizing enzymes sharply decreases. This suppresses Ca^{2+} transport from the cytosol into the extracellular space. In this way, calcium ions accumulate in the cytosol. This impairs cell metabolism and paralyzes cell function. Unfortunately, no literature was found that reports on the re-establishment of the vasoconstriction response after cold paralysis. Therefore, the assumption was made that when core temperature is higher than 28°C , the vasoconstriction recuperates back to normal.

Hence, the thermoregulatory part of the model as described in chapter 4 and 5 is extended with an extra condition:

- If $T_{\text{core,stand}}(t) < T_{\text{core,stand},0}(t)$ and $T_{\text{abdomen,core}}(t) > 28^\circ\text{C}$ then the vasoconstrictor tone is given by:

$$Cs(t) = 0.5(1 + \tanh(-2.76(\Delta T_{\text{core,stand}}(t) + 0.47)) \quad (6.1)$$

with $\Delta T_{\text{core,stand}}(t) = T_{\text{core,stand}}(t) - T_{\text{core,stand},0}(t)$, see equations (4.28) and (4.30).

- If $T_{\text{core,stand}}(t) < T_{\text{core,stand},0}(t)$ and $T_{\text{abdomen,core}}(t) < 28^\circ\text{C}$ then the vasoconstrictor tone is absent: $Cs(t) = 0$.
- If $T_{\text{core,stand}}(t) > T_{\text{core,stand},0}(t)$ then $Cs(t) = 0$.

Deep hypothermic cardiac arrest is arbitrarily modelled by decreasing $\beta_i = \rho_b c_b w_{b,i}$ to 1/100% of the base line value, since some Brownian fluid motion will still take place.

6.2.3 Results

The core and mean skin temperature results of the simulation are compared to the experimental observations of Rajek et al. (1999) (see figure 6.2). Simulation results are based on average body characteristics of the patient group.

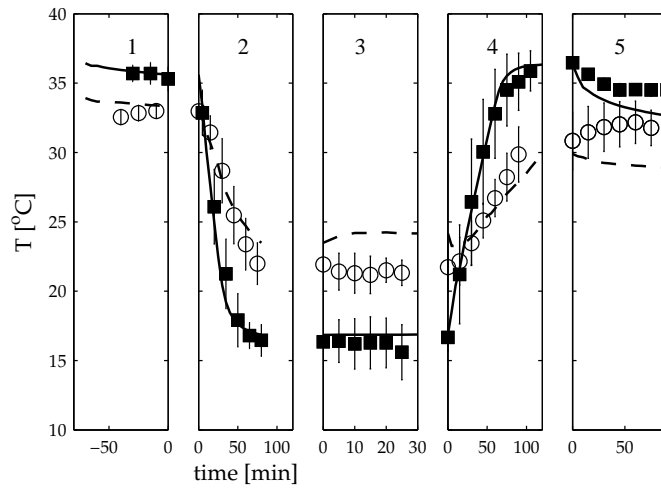


Figure 6.2: Simulation and experimental data of thoracic aorta graft procedures. Simulations consist of four stages: 1. anesthesia stage 2. cooling with heart lung machine 3. deep hypothermic cardiac arrest 4. warming with help of heart lung machine 5. postbypass stage. ■ and ○ represent experimentally assessed core and mean skin temperature, respectively. — and - - represent the core and mean skin temperatures following from the simulation, respectively. Errorbars denote the standard deviation of the experimental results. In the simulation, it was assumed that vasoconstriction after cold paralysis re-establishes completely when core temperature is higher than 28°C .

In the anesthesia stage (1), the cooling stage (2), during cardiac arrest (3) and the rewarming stage (4) good agreement was found between core temperature predicted by the model and found in experiments. In the postbypass stage (5), it is seen that core temperature after-drop is overestimated by the model (approximately 1.5°C).

The modelled skin temperatures initially follows the pattern of the measured skin temperature

quite well, but in the cardiac arrest stage, the rewarming stage and the postbypass stage the deviation between model and experimental results increases to about 3°C. In the rewarming stage the deviation becomes smaller, but in the postbypass stage the deviation again increases to approximately 2°C.

Reasons for the deviation between model and experimental results are the large uncertainty of the experimental boundary conditions as data was collected by other researchers and the assumptions that were made about the elimination and re-establishment of the vasoconstriction response during cold paralysis. Moreover, the active model that was derived in chapter 5 was based on skin temperatures in the range from 30 to 34°C, while the skin temperature in current case decreased even till 15 °C.

Additionally, a simulation was run in which it is assumed that the re-establishment of the vasoconstriction response after cold paralysis takes place at a higher temperature than the start temperature of cold paralysis. This temperature was arbitrarily chosen to be 36°C. This means that in stages 3 and 4 cold paralysis takes place, but that in stage 5 vasoconstriction again works. Results of this simulation are shown in figure 6.3. As can be seen in the figure, core temperature and mean skin temperature are now in much closer agreement with the measurement results compared to the previous assumption. This example demonstrates the possibilities of the model to use it for examining unknown processes. Obviously, more research is needed on this topic, but the model shows that it is more likely that vasoconstriction after cold paralysis re-establishes at a core temperature of 36°C than at 28°C.

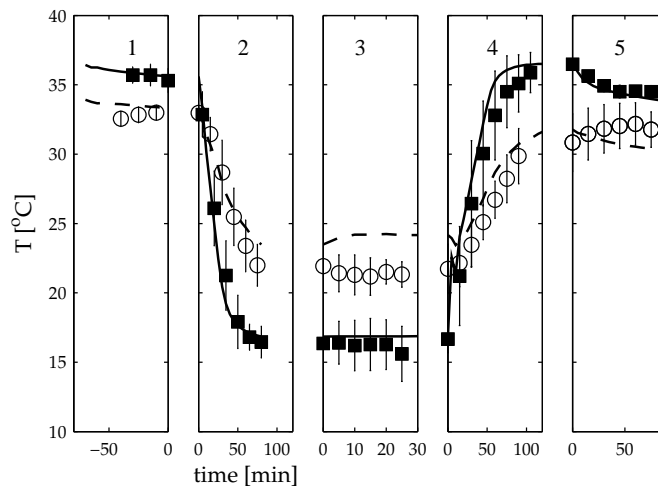


Figure 6.3: Simulation and experimental data of thoracic aorta graft procedures. In the simulation, it was assumed that vasoconstriction after cold paralysis did not take place before core temperature has reached 36°C.

6.3 Heat transfer during orthopedic back surgery

It is postulated that the developed model can also be used to predict transient temperatures of patients undergoing hypothermic surgery without active cooling by a cardiopulmonary bypass pump. Therefore, the model is used to simulate a regular type of surgery. In chapter 4, it was seen that the model offers possibilities to mimic surgical heat loss through the surgical wound. Here, the model was used to simulate a surgery involving large wounds. It was chosen to mimic orthopedic back surgery, as this type of surgery comprehends large wounds and takes place without active on-pump cooling.

A measurement protocol was developed to obtain transient temperature data of the skin, core and wound surface during orthopedic back surgery.

6.3.1 Experimental protocol

Three patients were followed during orthopedic back surgery. The study protocol was approved by the Maastricht University Medical Ethical Committee. All studied patients signed an informed consent.

Prior to the surgery, the body fat percentage of the patients was determined with the help of skinfold measurements at the m. biceps brachii, m. triceps brachii, subscapular and suprailiacal (Durnin and Womersley, 1974). Also weight and height of the patient were assessed. Skin temperatures were collected at 1 minute intervals with the help of iButtons (Van Marken Lichtenbelt et al., 2006) at: forehead, chest, abdomen, scapula, lumbar, forearm, hand, thigh (anterior and posterior), calf (anterior and posterior), foot, toe and finger. Average skin temperature was calculated according to the 12 point weighted formula of Hardy/Dubois (Mitchell and Wyndham, 1969):

$$\begin{aligned}
 T_{\text{skin}} = & 0.07T_{\text{head}} + 0.0875T_{\text{chest}} + 0.0875T_{\text{abdomen}} + 0.0875T_{\text{scapula}} + 0.0875T_{\text{lumbar}} \\
 & + 0.14T_{\text{lower arm}} + 0.05T_{\text{hand}} + 0.095T_{\text{thigh anterior}} + 0.095T_{\text{thigh posterior}} \quad (6.2) \\
 & + 0.065T_{\text{calf anterior}} + 0.065T_{\text{calf posterior}} + 0.07T_{\text{foot}}
 \end{aligned}$$

Finger temperature and toe temperature are measured because forearm-fingertip gradients and lowerleg-toe gradients are indicators of vasoconstriction (Rubinstein and Sessler, 1990). Rectal temperature data were collected every 15 minutes with help of a rectal temperature probe (HP21075A) with an accuracy of 0.1°C. An ambulant infrared camera (Thermacam PM575) was used to make pictures of the surgical wound. Emissivity was taken equal to skin emissivity: $\varepsilon = 0.99$. The pictures were taken for at least 4 times per hour, whenever possible. Pictures were made from the head of the operating table (this is a non sterile area) from a distance of approximately 1 meter and an angle of approximately 30° with the horizontal. In a short laboratory experiment, the temperature values of infrared images were compared to iButton temperatures. Skin temperature of wetted skin was measured simultaneously with the infrared camera and iButtons, while the camera was placed at an angle of 30° with the horizontal. Under these conditions, the infrared camera had a typical accuracy of 0.3°C.

During the surgery, surgeons and anesthetists were free to follow their normal (temperature) procedures. For active surface warming, forced-air heaters were used (Bair Hugger, model 522 Upper Body Blanket, Arizant Healthcare Inc.).

6.3.2 Simulation protocol

Surgery times and surgery protocols were all different and no designated time points could be appointed for changes in external boundary conditions. Hence, for each individual patient a separate simulation was run. The following assumptions were made:

- The pharmacological propofol model, as described in chapter 4 was used, regardless of the drugs that were used in reality. It is assumed that all general anesthesia have similar effect on the thermoregulatory responses.
- The incision length equals the length of the abdomen segment.
- Heat loss only takes place in radial direction.
- The model was run with 20 segments, as it is very complex to change the number of segments back and forth (from 19 to 20 and then again back to 19). The initial state is represented by an open back element with a very small angle (1°). The 20th element is the open back element, see figure 6.4.

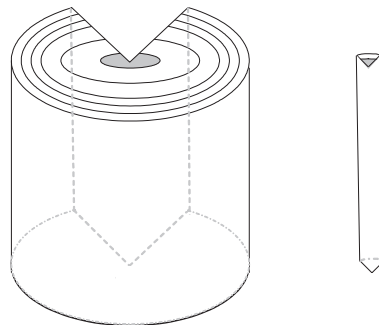


Figure 6.4: Left: model of the abdomen element during the actual surgery consisting of a core, bone, muscle, fat, inner and outer skin layer. Right: model of the wound element (element 20) consisting of core tissue and a blood layer.

- The back of the abdomen segment is opened/closed stepwise in approximately 5 minutes to a maximum of 75° : opening/closing rate is 15°min^{-1} .
- To keep the surgery field surveyable, the shed blood is frequently removed from the surface. In the model, it is assumed that the thickness of the blood layer is constant. It is assumed that the time that it takes to remove the blood is much smaller than the

clotting reaction time (6-10 minutes (Guyton and Hall, 1996)). The amount of shed blood that is removed is based on the blood loss during surgery 1: a total of 0.8l blood was removed in 350 minutes, which is $3.83 \cdot 10^{-5} \text{ l s}^{-1}$ in a volume of $1.7 \cdot 10^{-5} \text{ m}^3$ (calculated volume of blood layer in the model). This leads to a w_b of $2.25 \text{ l m}^{-3} \text{ s}^{-1}$.

- The blood layer of the wound element has a thickness of 0.5 mm. In the evaporation model, the blood properties are chosen to be equal to water. In reality, blood contains 55% plasma and 45% cells. Blood plasma consists of 90% water and 10% dry matter.
- The convective, radiative and evaporative heat loss from the wound surface are given by the relations as described in section 2.3.5.
- The temperature of the surgery light is approximately 50°C . This value was determined with help of the infrared camera (Thermacam PM575). In the model, this is accounted for by setting the local wall temperature above the wound to 50°C . This affects the radiative heat loss.

6.3.3 Results

For all surgeries, the main temperature characteristics of the surgery are detailed. Patient characteristics are given in table 6.1. In case a forced-air warmer was used, the simulation was run with the submodel of the forced-air heater where the neck, arms, hands, shoulders, upper and lower back were covered.

A typical temperature image of the wound is depicted in figure 6.5. Results of simulation and experiments of surgery 1-3 are given in figures 6.6 to 6.8.

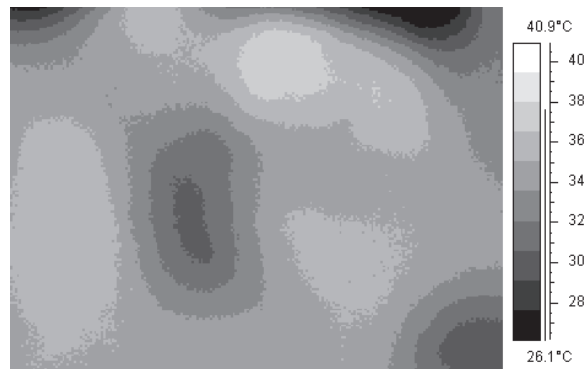


Figure 6.5: Infrared image of the wound. The dark oval spot in the middle is the surgical wound. The length of the shown incision is about 20 cm. The warm spots are thought to be caused by reflection of the surgery light.

• Surgery 1

The first surgery was a decompression and backside spondylodesis L4-5-S1 surgery. At

Table 6.1: Subject characteristics of the orthopedic back surgery ($n=3$).

	Patient 1	Patient 2	Patient 3
Gender (m/f)	f	m	f
Weight (kg)	60	84	62
Height (cm)	168	172	167
Age (y)	46	40	41
BMI (kg m^{-2})	21.3	28.4	22.2
Fat%	32.1	18.5	33.8
BSA (m^2)	1.68	1.97	1.70

$t=0$ min, anesthesia was induced, at $t=35$ min the incision was made. Simultaneously, forced-air heating was used with an air temperature of 43°C . At $t=195$ min the forced-air heater temperature was changed to 32°C and at $t=340$ min the surgery was ended. Halfway of the surgery, the patient's core temperature increased and it was the expert's opinion that it could be due to fever. Results are given in figure 6.6.

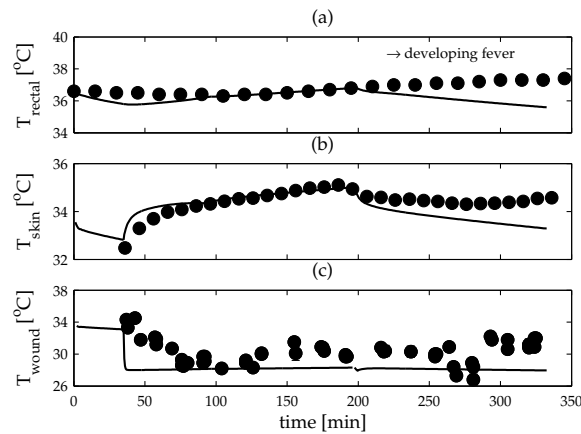


Figure 6.6: Patient 1: temperature results of (a) core (typical measurement accuracy of 0.1°C) (b) mean skin (c) wound surface (standard deviation in measurement was typically $<0.5^\circ\text{C}$ and therefore hardly visible in the figure). $t=0$ min: induction anesthesia, $t=35$ min: incision and switching on forced-air heater with air temperature of 43°C , $t=195$ min: forced-air heater switched to 32°C , $t=340$ min: end of surgery. • and – give the measurement and simulation results, respectively.

• Surgery 2

The second surgery was a flexible spondylosis L5-S1 surgery. At $t=0$ min, anesthesia was administered, at $t=50$ min the incision was made and a forced-air heater was used with an air temperature of 43°C . At $t=160$ min the surgery was finished. Results are

shown in figure 6.7.

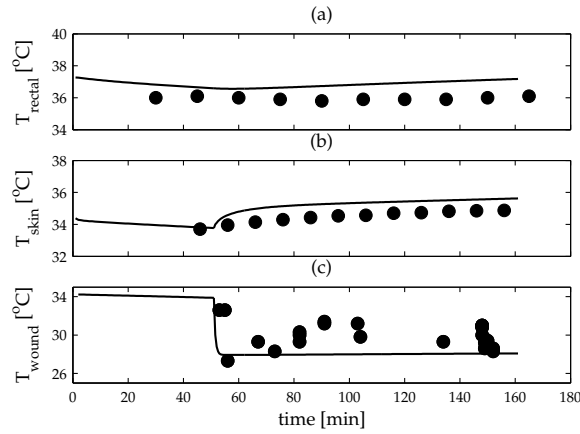


Figure 6.7: Patient 2: temperature results of (a) core (typical measurement accuracy of 0.1°C) (b) mean skin (c) wound surface (standard deviation in measurement was typically $<0.5^{\circ}\text{C}$ and therefore hardly visible in the figure). $t=0$ min.: induction anesthesia, $t=50$ min: incision and switching on forced-air heater with air temperature of 43°C $t=160$ min: end of surgery. • and – give the measurement and simulation results, respectively.

• Surgery 3

The third surgery involved an inspection spondylodesis surgery. At $t=0$ min induction of anesthesia took place, at $t=35$ min the incision was made and a forced-air heater was used with an air temperature of 43°C . At $t=165$ min the surgery was ended. Results are visible in figure 6.8.

In general, the temperatures predicted by the model and the measured temperatures were in good agreement. Larger deviations were observed at the end of surgery 1, where core temperature was underestimated by the model. In this period, the experts thought that the patient developed fever. Fever and hyperthermic responses are not included in the model. In this way the large deviation in the rectal temperature in the final stage is explained. The deviations in wound temperature can to a large part be contributed to the high temperature variation across the wound surface, that was observed in the experiments. At some points in time, temperature variations of 4°C were observed between (blood-covered) tissue and spine. In the model simulation, it was assumed that the wound surface was a homogeneous tissue layer covered with a homogeneous blood layer. This can explain the differences between model results and measurement results and also the high standard deviation that is sometimes seen in the experimental wound surface data.

Till now, no studie has assessed wound temperatures in humans during surgical interventions because of technical difficulties (Sessler, 2000). Here it was shown, by means of on the one hand infrared images and on the other hand model calculations, that it is possible to

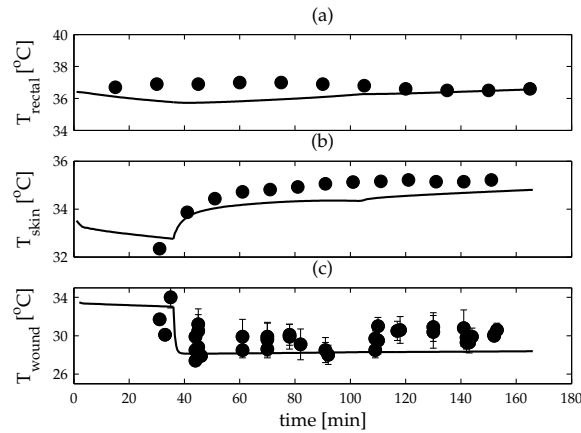


Figure 6.8: Patient 3: temperature results of (a) core (typical measurement accuracy of 0.1°C) (b) mean skin (c) wound surface. $t=0$ min: induction anesthesia, $t=35$ min: incision and switching on forced-air heater with air temperature of 43°C $t=165$ min: end of surgery. • and – give the measurement and simulation results, respectively.

acquire information about wound temperature and heat loss. Model calculations show that the typical heat loss from the wound (sum of evaporative, radiative, convective heat losses in the open back element) is around 5 W. With a typical metabolic rate of 80 W, it can be seen that the heat loss from the wound contributes to about 6% of the total heat balance.

6.4 Effect of changing temperature protocols

Mathematical human models are strong tools to investigate the effect of changing conditions on body temperature. Before exposing patients to a different protocol, the utility of the new protocol can already be verified by simulations. Here, three application examples are considered.

6.4.1 Cooling the head during deep hypothermic cardiac arrest

In figure 6.1, it was seen that brain temperature during cardiac circulatory arrest is a major factor for preventing the occurrence of brain damage. To keep the brain temperature as low as possible, sometimes ice-packs are put on the head of patients during the period of circulatory arrest. However, it is questioned if those ice-packs are able to change temperature in the brain and if they are really effective. With help of the computer model, the effect of ice-packs on brain temperature is studied. Additionally, the effect of using a higher ambient temperature on brain temperature, without ice-pack cooling is investigated.

In the simulation, the temperature protocol as described in section 6.2 was exploited. In

addition three simulations were run with an ice-pack covering the head during the period of circulatory arrest. The temperature of the ice-pack was set to 0, -10°C and -15°C. Heat transfer between the ice-pack and the skin of the head was modelled by:

$$q_i'' = h_{\text{icepack}}(T_{\text{skin},i} - T_{\text{icepack}}) \quad (6.3)$$

with the heat transfer coefficient h_{icepack} assumed to be equal to the heat transfer coefficient of a circulating water mattress ($120 \text{ Wm}^{-2}\text{K}^{-1}$, see section 2.3.4). Perfect contact was assumed between the ice-pack and the head.

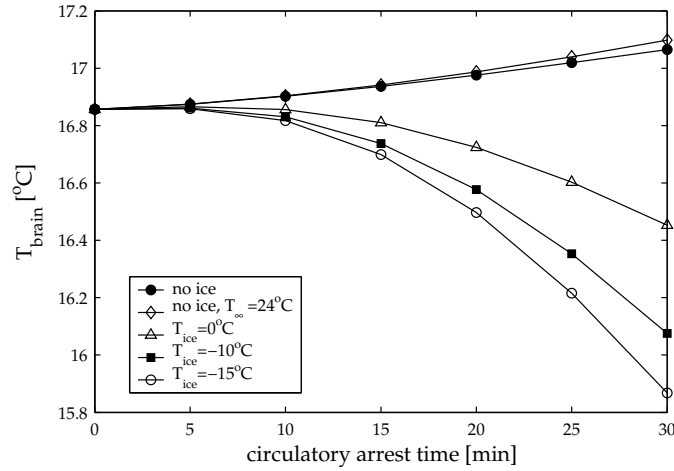


Figure 6.9: Brain temperature (5 cm below the skin) versus circulatory arrest duration. Results are shown of simulation without ice-pack (at $T_\infty=21$ and 24°C) and with ice-pack temperatures of 0, -10 and -15°C (at $T_\infty=21^\circ\text{C}$).

In figure 6.9 calculated brain temperatures (5 cm below the skin) as function of the time without blood circulation are depicted for a surgery where no ice-pack was used and where ice-packs with different temperatures were used. It was seen that ice-packs of 0, -10 and -15°C reduce brain temperature after 30 minutes without circulation by 0.6, 1.0 and 1.2°C , respectively in comparison to no ice-pack cooling. When no ice-pack is used the passive body warms up because of the warmer environmental temperature. This leads to higher temperatures and consequently also to higher metabolic rates in the tissues, see equation (4.1). As a result, brain temperature increases by 0.2°C (also visible in figure 6.9). Increasing the ambient temperature to 24°C instead of 21°C , when no ice-pack is used, only leads to a brain temperature increase of 0.03°C .

According to these findings, ice-packs are found to be effective. Even small reduction in brain temperature can give surgeons a few minutes more for their surgical actions without introducing risk for brain damage, see figure 6.1. However, the influence of ice-packs in comparison to the pump cooling effect prior to the circulatory arrest stage, is of course relatively small.

6.4.2 Comparison of old and new cardiac surgical procedures: moderate versus mild hypothermia

Over the decades, there have been a variety of changes in the standpoints regarding temperature management during surgery. Traditionally, moderate to deep hypothermia has been thought of and used perioperatively as a strategy to reduce risk of cerebral and myocardial ischemia. Nowadays, however, it is often believed that keeping patients close to normothermia leads to improved outcomes in patients undergoing all types of surgery, even cardiac surgery (Insler and Sessler, 2006; Cook, 1999).

In the time period of this research, also shifts towards higher peri-operative temperatures were observed in the hospitals where this research took place (AMC and AZM, The Netherlands). While previously perioperative moderate hypothermia (28-32°C) was the established treatment for many cardiac surgeries, nowadays often only mild hypothermia (32-35°C) is applied. With the improvements of heart lung machines and hemodilution techniques, blood circulation is almost equal as seen during intact circulation, which reduces the risk for ischemia and makes the application of higher bypass temperatures possible. The clinical impression with using mild hypothermia is that postoperative hypothermia is less common and less severe. In order to test if this effect is also seen in the model, a simulation was run for a patient that is cooled to 33°C. The surgery characteristics and patient morphology of the standard situation are taken equal to the surgery described in section 4.7. Results of the simulation using the new (33°C) and old protocol (30°C) are shown in figure 6.10.

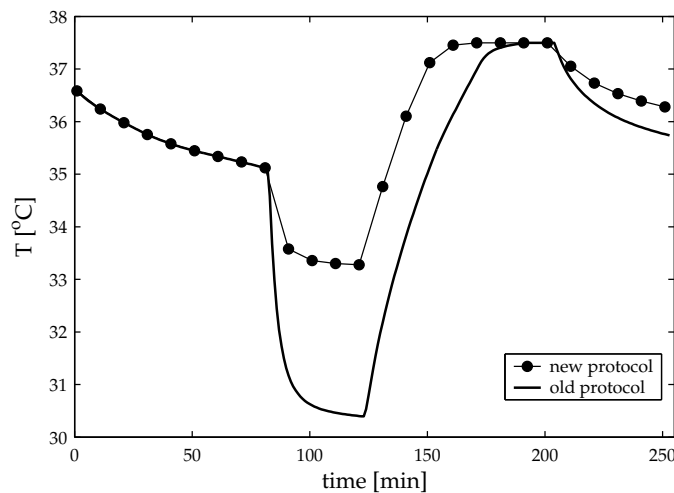


Figure 6.10: Transient core temperature as function of surgery time: comparison of the new and old protocol.

The model simulations show that afterdrop can be reduced by approximately 0.5°C when using a mild hypothermia protocol instead of a moderate hypothermia protocol during cardiac

surgery.

6.4.3 Influence of changing temperature protocols on afterdrop under moderate hypothermic conditions

The model was used to study the effect of adjusting external temperature influences on afterdrop. The standard surgery characteristics and patient morphology are chosen according to the surgery described in section 4.7.

Three situations were studied to examine the effect of different temperature protocols on the amount of afterdrop: 1) adding a forced-air warmer with an air temperature of 43°C in the rewarming and postbypass stage, 2) perform the surgery at an environmental temperature of 25°C, and 3) using a heating mattress with a temperature of 40°C during the whole surgery.

Using a forced-air heater considerably improved core temperature at the end of the surgery, as shown in table 6.2 and figure 6.11. Increasing the temperature of the surrounding also led to a higher core temperature, but was not as effective as forced-air heating. Using a heating mattress resulted in a higher core temperature too. The latter method was more effective than increasing the environmental temperature, but not as effective as the use of a forced-air warmer.

Table 6.2: Parameter study: effect of changes in external model parameters.

Parameter	When	$T_{\text{core}}(t = 250 \text{ min})$
standard condition	whole surgery	35.7
forced-air heater at 43°C	rewarming/postbypass	36.5
$T_{\infty} = 25^{\circ}\text{C}$	whole surgery	36.2
$T_{\text{mattress}} = 40^{\circ}\text{C}$	whole surgery	36.3

6.5 Discussion

In this chapter, some possible application areas are demonstrated of the whole body thermal model that was developed. It was shown that the model is not only capable to predict temperatures during cardiac surgery performed at moderate hypothermia, but also gives good predictions during deep-cooled cardiac interventions with circulatory arrest and for surgeries where no heart lung machines are used, like orthopedic surgeries. Furthermore, it was shown that wound temperatures predicted with the model are in good agreement with measured wound temperatures. In the past wound temperature and heat flux have never been assessed experimentally in humans, because of technical difficulties (Sessler, 2000). Here, it was shown, by both experiments and model simulations, that it is possible to obtain relevant information about wound temperature. Wound temperature during orthopedic surgery was found to be typically 30°C and by model calculations a heat loss from the surgical wound

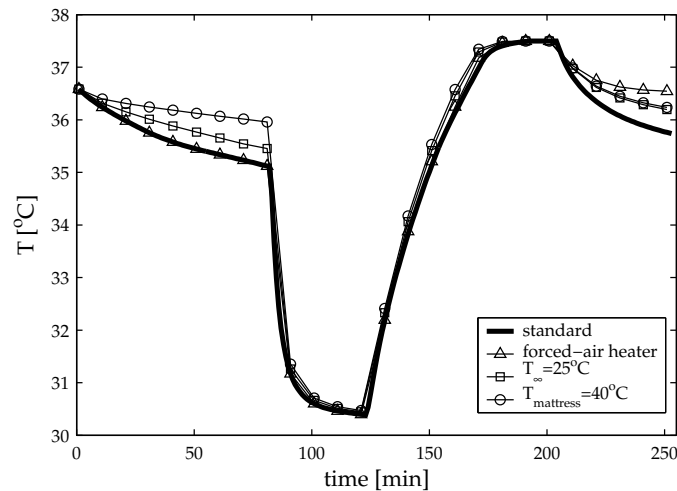


Figure 6.11: Effect of external temperature protocol on core temperature during moderate hypothermic conditions.

of about 5 W was found. The variation in experimentally determined wound temperature is explained by the large spatial differences across the wound surface. The obtained knowledge might help in the study of heat balance during surgery and may in the future be helpful for preventing wound infection and disturbed coagulation function, which depend on local wound temperature.

The model is also a useful tool to study the effects of different, and sometimes adjustable, external parameters on the patient's temperature distribution. For instance, with the help of the model the effectiveness of using ice-packs to cool the brain during deep hypothermic circulatory arrest was demonstrated. It was observed that using an ice-pack with a temperature of -15°C reduces brain temperature by 1.2°C compared to circulatory arrest without using ice-packs.

Another use of the model is to study the effects of alternative temperature procedures during surgery. Nowadays, there is a tendency to perform cardiac surgery at higher temperatures than in the past. The model predicted that using mild hypothermia instead of moderate hypothermia during a typical aortic valve replacement reduces afterdrop by 0.5°C .

The influence of changing external boundary conditions was assessed with the model. A parameter study showed that using a forced-air heater, with a temperature of 43°C , increases core temperature at the end of the surgery by 0.8°C , compared to a standard aortic valve procedure with only passive insulation. Usage of a forced-air heater prevailed over the effect of a 5°C increase in environmental temperature, and also prevailed over the use of a 40°C circulating water mattress. This shows the abilities of the model to use it as a study tool.

The ultimate application of the model is to use it in such a way that it helps clinicians to

choose for each individual patient the temperature protocol that gives the optimal temperature response. This can help to reduce postoperative thermal discomfort for the patient and leads to faster recovery times.

Conclusions and recommendations for further research

7.1 Conclusions

Patients often become hypothermic during and after surgery under general anesthesia. In some surgical interventions, like cardiac surgery, peri-operative hypothermia is desirable, but mostly it is an unwanted side effect of anesthetics. For preventing unwanted hypothermia, more insight is needed in heat transfer in anesthetized humans and the effect that different temperature protocols have on temperature in the body. Especially, the undesirable afterdrop effect following cardiac surgery needs to be addressed. The goal of this thesis was to develop a mathematical whole body temperature model that can predict the temperature of a patient during and after surgery.

A heat transfer model for humans during surgery with general anesthesia has been developed. This model consists of three main parts: the passive part, flexible submodels and an active part.

The passive part describes the geometry of the human body, the passive heat processes in the body and the heat interaction between the body and the environment. Flexible submodels account for the patient's body characteristics and for different thermal influences, like the use of heart lung machine, forced-air heaters, a circulating water mattress and heat loss through the surgical wound. Model simulations with the passive part showed that the contribution of heat losses through the surgical wound to the total heat balance is small during cardiac surgery (about 3% of the total heat loss). During open heart surgeries, surgical wound heat losses are therefore of minor importance. Furthermore, it was observed that with a model that only incorporates passive heat processes the core temperature response that occurs during normal surgeries can not be mimicked. From this, it was concluded that an active model, which takes

into account thermoregulation and metabolic rate changes during anesthesia, is inevitable.

For the development of the active part of the model, patient data was collected. Two patient groups were followed during aortic valve surgery. One group was rewarmed with forced-air heating and the other group was covered with only passive insulation. From the measurement data, it was concluded that forced-air heaters are effective in reducing post-operative afterdrop. However, using forced-air heaters did not lead to clinically relevant improvements in deep peripheral temperature. The temperature and perfusion results suggest that the majority of the extra heat from forced-air heaters is directly transported from the skin capillaries to the heart and from there mainly redistributed to the core organs and not so much to the periphery.

Comparison of the passive model simulation to the gathered patient temperature data showed that the passive model can predict the general behaviour of core and mean skin temperature trends during an aortic valve surgery, but the quantitative behaviour is somewhat different. Results considerably improve (error in core temperature decreases by about 1°C in the anesthesia stage and postbypass stage) when the anesthesia induced reduction of metabolism of typically 30%, which is reported in literature, is taken into account.

Vasoconstriction is the prime thermoregulatory response in hypothermic anesthetized patients. The threshold at which vasoconstriction is triggered depends on the concentration of drugs in the blood. With help of a pharmacological model and the measurement data of the aortic valve patients, a relation was derived that described the connection between drug concentration in the blood and the body's threshold temperature for vasoconstriction. As a first approach the gain and intensity of the vasoconstriction response were approximated by a step function. This drug-dose-dependent vasoconstriction model and the reduced metabolic rate, caused by anesthetics, were added in the human body model. With this model, simulation results were obtained that typically predicted core and mean skin temperature within two times the value of the standard deviation observed in the measurements. The amount of afterdrop was predicted within 0.2°C. However, the stepwise model resulted in sawtooth-shaped temperature solutions.

Perfusion and temperature data collected from healthy volunteers were used to quantify the local amplification coefficients for vasoconstriction for different body parts and the magnitude of the centrally mediated vasoconstrictor tone. The experiment was designed in such a way that the skin temperature decrease was in the same range as during surgeries performed in the temperature range from normothermia until moderate hypothermia. A general applicable relation was formulated that described the vasoconstriction tone as a function of standardized core temperature. Simulations performed with the human thermal model, including the newly developed vasoconstriction relations, were compared to different data sets of healthy volunteers and patients undergoing cardiac surgery at moderate hypothermic conditions. With this model, smooth (i.e. no sawtooth) solutions were obtained. In the validation cases, it was observed that predicted core temperature deviated typically less than 0.5°C from measured values, while mean skin temperature deviated typically less than 1°C.

The developed model offers a wide range of possibilities to predict human body tem-

perature under cold conditions, during which only vasoconstriction response is triggered. It was demonstrated that the model can be used to simulate patient temperature during deep hypothermia with circulatory arrest and during orthopedic back surgery. Mostly, simulation results were in good agreement with measured core and skin temperatures. The largest error was the overestimation of the afterdrop after deep hypothermia by 1.5°C. The probable reason for this is that the thermoregulatory model, used in the analysis, is not suitable for deep hypothermia and recovery after cold paralysis. Predicted temperatures of orthopedic surgical wounds agreed well with experimentally assessed wound temperatures (commonly around 30°C). A typical error between experiments and simulated wound temperature was found of 1°C. The heat flux through the surgical wound predicted by the model was found to be 5 W, which is small compared to the whole body heat balance.

Finally, the model was used to study the influence of changing temperature protocols. It has been shown that using ice-packs during circulatory arrest helps to cool the brain and is an effective remedy for reducing the risk on brain damage. It was found that using mild hypothermia instead of moderate hypothermia during cardiac surgery reduced afterdrop by approximately 0.5°C. Numerical calculations showed that using a forced-air heater considerably reduces afterdrop and is more effective than using a heating mattress or increasing the temperature in the surgery room.

7.2 Recommendations for further research

The model that has been developed is very extensive and it was found to be applicable to various surgery types and for healthy persons under specific circumstances. Nevertheless, the model can be improved. In this section, some research proposals on model improvements and suggestions for measurements and application fields for future research are given.

The human body is represented by assuming that body parts are cylindrical or spherical shaped. In reality, the elements are more elliptical shaped, which might effect the heat interaction in the body and between the body and the environment. Ferreira and Yanagihara (2001) described a method to account for non-perfect circular element shapes and applied coordinate transformation methods to turn elliptical cylinders to rectangular parallelepipeds. It would be interesting to compare results using this approach to the current approach.

The body parts between themselves are only connected via the central blood pool. Under predominantly homogeneous condition, this approach will suffice. However, under non-homogeneous conditions like frontal heating or local cooling or heating, methods need to be found to link body parts together in the model. For this, experiments are required that focus on heat exchange of blood vessels that connect body parts. In the model, a more detailed vasculature system should be implemented, probably in a similar way as recently proposed by Salloum et al. (2007).

The thermoregulatory model does not depend on the rates at which core and skin temperature change. The drug-dependent vasoconstriction thresholds were determined using data taken during aortic valve surgery, while the gains and intensity of the vasoconstriction per

body part were determined using data obtained by exposing volunteers to a cooling cycle experiment. The extent to which time-dependent influences might have contributed to the before mentioned obtained threshold and gain formulation, and to what extent they play a role when using the model for simulating other situations remain unclear (see also Sessler (1993)) and should be investigated.

Another suggestion is to study the anesthesia induced decrease of metabolism during cardiopulmonary bypass surgery. In literature (limited) information is available of metabolic reduction during general anesthesia. This information was based on indirect calorimetry measurements of anesthetized volunteers that were treated with artificial breathing. Indirect calorimetry measurements can not be used during on-pump periods because the respirator is switched off. An alternative could be to measure pump flow together with oxygen and carbon dioxide levels of the arterial and venous blood and use this information to derive the metabolic rate.

At this moment, impaired thermoregulation is coupled to the drug concentration of propofol in the blood. It is assumed that the administered drugs can be represented by propofol. In reality, often a mixture of drugs is used, which can lead to drug-drug interaction. Nonetheless, the typical venously injected anesthetics mixtures during surgery roughly increase the interthreshold range in a comparable and linear way. On the other hand, commonly used volatile anesthetics, such as isoflurane and desflurane, decrease the threshold temperatures for cold responses in a nonlinear fashion. Currently, this non-linearity is not implemented in the model. In future, efforts are needed to elaborate the pharmacological model for this non-linear behaviour.

Some surgical procedures are not taken into account in the model, like the application of iodine to the skin, which causes evaporative heat losses before surgery, or the fact that frequently vasoactive medication is used to control blood pressure. More insight should be gained if including such information in the model is relevant. A practical issue when adding this information in the model is that those quantities are very patient and also surgeon dependent. Detailed information of the followed surgery protocol is required when incorporating that kind of information in the model.

Differences between experimental and simulation responses are caused both by modelling limitations and by experimental flaws. Modelling errors include not only uncertainties and assumptions that are made during the model formulation stage but also unaccounted parameter variations between human subjects (inter-subject variations), which can be high, and effects influencing the same individual at different times (intra-subject variations). Experimental flaws involve limited accuracy of the measurement equipment and differences in used protocols, like using different cooling and warming rates with the heart lung machine or not using standardized temperature protocols prior to measurements. Therefore, attention should be paid to standardize as much as possible.

Parameter and tissue values in the model are mainly based on existing and sometimes old literature. Many of these variables, both in the passive model and active model, were not actually measured *in vivo* and their values were often deduced from indirect measurements. As

measurement techniques are improving, there are probably possibilities to re-assess a number of parameters and empirically determined relations using modern measurement techniques (like MRI/MRA, laser Doppler imaging etc.) or manikins.

Not much information is available about cold paralysis. It is known that cold paralysis occurs when body temperature is lower than approximately 28°C, but in literature no information is found about the recovery of thermoregulatory responses after cold paralysis. More information is needed about thermoregulation during and after cold paralysis.

Before the model can be implemented in, for instance, an advisory or monitoring decision system for using in a surgery room, the response and limitations of the human thermoregulatory model must be characterized in more detail. Methods should be developed to use the model in such a way that only minimal and recent data input is required, but that it is able to predict the temperature response for the next period of time. This information can be used to alter the temperature protocol or compare the current protocol to alternative protocols. Moreover, decisions should be made what the minimal desired accuracy of such a monitoring tool must be for different application fields and if the developed model satisfies the requirements or needs further research.

The model's application field can be extended much more by developing active models for vasodilation, sweating, shivering and non-shivering thermogenesis. In addition, the thermal model can be coupled to thermal sensation and thermal comfort models. In future, such models can be very useful tools for the design of climate systems and new energy-efficient buildings.

References

- Aarons, L. (2005). Physiologically based pharmacokinetic modelling: a sound mechanistic basis is needed. *Br J Clin Pharmacol*, 60(6):581–583.
- Abbot, N. and Beck, J. (1993). Biological zero in laser Doppler measurements in normal, ischaemic and inflamed human skin. *Int J Microcirc Clin Exp*, 12(1):89–98.
- Arkin, H., Xu, L., and Holmes, K. (1994). Recent development in modeling heat transfer in blood perfused tissue. *IEEE Trans Biomed Eng*, 41(2):97–107.
- Bejan, A. (1993). *Heat Transfer*. New York: John Wiley & Sons Inc.
- Belani, K., Sessler, D., Sessler, A., Schroeder, M., McGuire, J., Merrifield, B., Washington, D., and Moayeri, A. (1993). Leg heat content continues to decrease during the core temperature plateau in humans anesthetized with isoflurane. *Anesthesiology*, 78(5):856–863.
- Bertens, E., Stam, T., Verberne, C., and Visser, B. (2006). *Lokaal thermisch comfort*. Internal report TU/e.
- Binzoni, T., Leung, T., Seghier, M., and Delpy, D. (2004). Translational and Brownian motion in laser-Doppler flowmetry of large tissue volumes. *Phys Med Biol*, 49(24):5445–5458.
- Bonner, R. and Nossal, R. (1981). Model for laser doppler measurements of blood flow in tissue. *Appl Optics*, 20(12):2097–2107.
- Bräuer, A., Pacholik, L., Perl, T., English, M., Weyland, W., and Braun, U. (2004a). Conductive heat exchange with a gel-coated circulating water mattress. *Anesth Analg*, 99(6):1742–1746.

- Bräuer, A., Perl, T., Uyanik, Z., English, M., Weyland, W., and Braun, U. (2004b). Perioperative thermal insulation: minimal clinically important differences? *Br J Anaesth*, 92(6):836–840.
- Bräuer, A., Weyland, W., Kazmaier, S., Trostdorf, U., Textor, Z., Hellige, G., and Braun, U. (2004). Efficacy of postoperative rewarming after cardiac surgery. *Ann Thorac Cardiovasc Surg*, 10(3):171–177.
- Brenner, I., Thomas, S., and Shephard, R. (1997). Spectral analysis of heart rate variability during heat exposure and repeated exercise. *Eur J Appl Physiol Occup Physiol*, 76(2):145–156.
- Cereda, M. and Maccioli, G. (2004). Intraoperative temperature monitoring. *Int Anesth Clin*, 42(2):41–54.
- Cezeaux, J. and Van Grondelle, A. (1997). Accuracy of the inverse Womersley method for the calculation of hemodynamic variables. *Ann Biomed Eng*, 25(3):536–546.
- Chen, Y., Lin, Y., Jan, I., Liu, R., Chou, N., and Jan, G. (2004). Adaptive processing bandwidth adjustment for laser Doppler flowmetry. *Med Biol Eng Comput*, 42(3):277–281.
- Cheng, C., Matsukawa, T., Sessler, D., Ozaki, M., Kurz, A., Merrifield, B., Lin, H., and Olofsson, P. (1995). Increasing mean skin temperature linearly reduces the core-temperature thresholds for vasoconstriction and shivering in humans. *Anesthesiology*, 82(5):1160–1168.
- Choi, J., Miki, K., Sagawa, S., and Shiraki, K. (1997). Evaluation of mean skin temperature formulas by infrared thermography. *Int J Biometeorol*, 41(2):68–75.
- Chong, S., Chow, M., Kang, D., Sin, Y., Sim, E., and Ti, L. (2004). Deep hypothermic circulatory arrest in adults undergoing aortic surgery: local experience. *Ann Acad Med Singap*, 33(3):289–293.
- Cook, D. (1999). Changing temperature management for cardiopulmonary bypass. *Anesth Analg*, 88(6):1254–1271.
- Cooper, K. (2002). Some historical perspectives on thermoregulation. *J Appl Physiol*, 92:1717–1724.
- Daanen, H. (1997). *Central and peripheral control of finger blood flow in the cold*. PhD thesis. Vrije Universiteit Amsterdam, Amsterdam.
- Dennis, B., Eberhart, R., Dulikravich, G., and Radons, S. (2003). Finite-element simulation of cooling of realistic 3-D human head and neck. *J Biomech Eng*, 125(6):832–840.
- Drummond, J. and Shapiro, H. (1994). *Cerebral physiology*. In: Anesthesia, edited by R.D. Miller. New York: Churchill Livingstone.

- Dubois, D. and Dubois, E. (1916). A formula to estimate the approximate surface area if height and weight be known. *Arch Intern Med*, 17:863–871.
- Durnin, J. and Womersley, J. (1974). Body fat assessed from total body density and its estimation from skinfold thickness: measurements on 481 men and women aged from 16 to 72 years. *Br J Nutr*, 32(1):77–97.
- Fanger, P. (1973). *Thermal comfort- Analysis and applications in environmental engineering*. McGraw-Hill, New York-London-Sydney-Toronto.
- Ferreira, M. and Yanagihara, J. (2001). Development of the passive system of a human thermal model. *ASME -publications- BED*, 50:757–758.
- Fiala, D., Lomas, K., and Stohrer, M. (1999). A computer model of human thermoregulation for a wide range of environmental conditions: the passive system. *J Appl Phys*, 87(5):1957–1972.
- Fiala, D., Lomas, K., and Stohrer, M. (2001). Computer prediction of human thermoregulatory and temperature responses to a wide range of environmental conditions. *Int J Biometeorol*, 45(3):143–159.
- Fournier, R. L. (1999). *Basic Transport Phenomena In Biomedical Engineering*. Taylor & Francis.
- Frank, S., Raja, S., Bulcao, C., and Goldstein, D. (1999). Relative contribution of core and cutaneous temperatures to thermal comfort and autonomic responses in humans. *J Appl Physiol*, 86(5):1588–1593.
- Gage, A. (1973). Rational temperature indices of man's thermal environment and their use with a 2-node model of his temperature regulation. *Fed Proc*, 32(5):1572–1582.
- Gordon, R. (1974). *The response of a human temperature regulatory system model in the cold*. PhD thesis. University of California, Santa Barbara.
- Gredell, J., Turnquist, P., Maciver, M., and Pearce, R. (2004). Determination of diffusion and partition coefficients of propofol in rat brain tissue: implications for studies of drug action in vitro. *Br J Anaesth*, 93(6):810–817.
- Griep, R., Stinson, E., Hollingsworth, J., and Buehler, D. (1975). Prosthetic replacement of the aortic arch. *J Thorac Cardiovasc Surg*, 70(6):1051–1063.
- Guyton, A. (1976). *Organ physiology, Structure and function of the nervous system*. Philadelphia-London-Toronto: W.B. Saunders Company.
- Guyton, A. and Hall, J. (1996). *Textbook of medical physiology*. Philadelphia-London-Toronto-Montreal-Sydney-Tokyo: W.B. Saunders Company.

- Hardy, J. and Dubois, E. (1938). The technic of measuring radiation and convection. *J Nutr*, 15:461–475.
- Hardy, J. and Stolwijk, J. (1966). Partitional calorimetric studies of man during exposures to thermal transients. *J Appl Physiol*, 21(6):1799–1806.
- Hohn, L., Schweizer, A., Kalangos, A., Morel, D., Bednarkiewicz, M., and Licker, M. (1998). Benefits of intraoperative skin surface warming in cardiac surgical patients. *Br J Anaesth*, 80(3):318–323.
- Huizenga, C., Hui, Z., and Arens, E. (2001). A model of human physiology and comfort for assessing complex thermal environments. *Energ Buildings*, 36:691–699.
- Incropera, F. and DeWitt, D. (2002). *Fundamentals of heat and mass transfer*. John Wiley & sons, New York-Chichester-Weinheim-Brisbane-Toronto-Singapore, 5th edition.
- Inslar, S. and Sessler, D. (2006). Perioperative thermoregulation and temperature monitoring. *Anesthesiol Clin*, 24(4):823–837.
- Ivanov, K. and Arokina, N. (1998). Cold induced paralysis of the thermoregulation center and restoration of its functions at the paralysis temperature. *Biull Eksp Biol Med*, 125(1):45–47.
- Janssen, F. (2007). *Modelling physiological and biochemical aspects of scalp cooling*. PhD thesis. Technische Universiteit Eindhoven, Eindhoven.
- Janssen, F., Rajan, V., Steenbergen, W., Van Leeuwen, G., and Van Steenhoven, A. (2007). The relationship between local scalp skin temperature and cutaneous perfusion during scalp cooling. *Physiol Meas*, 28(8):829–839.
- Janssen, F., Van Leeuwen, G., and Van Steenhoven, A. (2005). Modelling of temperature and perfusion during scalp cooling. *Phys Med Biol*, 50(17):4065–4073.
- Jones, B. (2002). Capabilities and limitations of thermal models for use in thermal comfort standards. *Energ Buildings*, 24(6):653–659.
- Kellogg, D. (2006). In vivo mechanisms of cutaneous vasodilation and vasoconstriction in humans during thermoregulatory challenges. *J Appl Physiol*, 100(5):1709–1718.
- Kellogg, D., Morris, S., Rodriguez, S., Liu, Y., Grossmann, M., Stagni, G., and Shepherd, A. (1998). Thermoregulatory reflexes and cutaneous active vasodilation during heat stress in hypertensive humans. *J Appl Physiol*, 85(1):175–180.
- Kernick, D., Tooke, J., and Shore, A. (1999). The biological zero signal in laser Doppler fluximetry - origins and practical implications. *Pflugers Arch*, 437(4):624–631.

- Kim, J., Shinn, H., Oh, Y., Hong, Y., Kwak, H., and Kwak, Y. (2006). The effect of skin surface warming during anesthesia preparation on preventing redistribution hypothermia in the early operative period of off-pump coronary artery bypass surgery. *Eur J Cardiothorac Surg*, 29(3):343–347.
- Knighton, D., Halliday, B., and Hunt, T. (1986). Oxygen as an antibiotic- a comparison of the effects of inspired oxygen concentration and antibiotic administration on in vivo bacterial clearance. *Arch Surg*, 121(2):191–195.
- Kotte, A., Van Leeuwen, G., De Bree, J., Van der Koijk, J., Crezee, H., and Lagendijk, J. (1996). A description of discrete vessel segments in thermal modelling of tissues. *Phys Med Biol*, 41(5):865–884.
- Kurz, A., Sessler, D., Christensen, R., and Dechert, M. (1995a). Heat balance and distribution during the core-temperature plateau in anesthetized humans. *Anesthesiology*, 83(3):491–499.
- Kurz, A., Xiong, J., Sessler, D., Dechert, M., Noyes, K., and Belani, K. (1995b). Desflurane reduces the gain of thermoregulatory arteriovenous shunt vasoconstriction in humans. *Anesthesiology*, 83(6):1212–1219.
- Leahy, M., de Mul, F., Nilsson, G., and Maniewski, R. (1999). Principles and practice of the laser-Doppler perfusion technique. *Technol Health Care*, 7(2-3):143–162.
- Lean, M., Han, T., and Morrison, C. (1995). Waist circumference as a measure for indicating need for weight management. *BMJ*, 311:158–161.
- Levitt, D. and Schnider, T. (2005). Human physiologically based pharmacokinetic model for propofol. *BMC Anesthesiol*, 5(1):4.
- Lopez, M., Sessler, D., Walter, K., Emerick, T., and Ozaki, M. (1994). Rate and gender dependence of the sweating, vasoconstriction, and shivering thresholds in humans. *Anesthesiology*, 80(4):780–788.
- Ludbrook, G. and Upton, R. (1997). A physiological model of induction of anaesthesia with propofol in sheep. 2. Model analysis and implications for dose requirements. *Br J Anaesth*, 79(4):505–513.
- Matsukawa, T., Hanagata, K., Ozaki, M., Iwashita, H., Koshimizu, M., and Kumazawa, T. (1997). I.m. midazolam as premedication produces a concentration-dependent decrease in core temperature in male volunteers. *Br J Anaesth*, 78(4):396–399.
- Matsukawa, T., Kurz, A., Sessler, D., Bjorksten, A., Merrifield, B., and Cheng, C. (1995a). Propofol linearly reduces the vasoconstriction and shivering thresholds. *Anesthesiology*, 82(5):1169–1180.

- Matsukawa, T., Sessler, D., Sessler, A., Schroeder, M., Ozaki, M., Kurz, A., and Cheng, C. (1995b). Heat flow and distribution during induction of general anesthesia. *Anesthesiology*, 82(3):662–673.
- Matsumoto, T., Miyawaki, C., Ue, H., Kanda, T., Yoshitake, Y., and Moritani, T. (2001). Comparison of thermogenic sympathetic response to food intake between obese and non-obese young women. *Obes Res*, 9(2):78–85.
- Matthews, J., Altman, D., Campbell, M., and Royston, P. (1990). Analysis of serial measurements in medical research. *BMJ*, 300(6719):230–235.
- McDonald, D. (1955). The relation of pulsatile pressure to flow in arteries. *J Physiol*, 127(3):533–552.
- McIntyre, D. (1980). *Indoor climate*. UK: Applied Science Publishers, London.
- Mekjavic, I. and Eiken, O. (2006). Contribution of thermal and nonthermal factors to the regulation of body temperature in humans. *J Appl Physiol*, 100:2065–2072.
- Merchant, R., Soar, J., Skrifvars, M., Silfvast, T., Edelson, D., Ahmad, F., Huang, K., Khan, M., Vanden Hoek, T., Becker, L., and Abella, B. (2006). Therapeutic hypothermia utilization among physicians after resuscitation from cardiac arrest. *Crit Care Med*, 34(7):1935–1940.
- Michaux, B., Vanhoutte, J., Jaffrin, M., and Fontenier, G. (1979). Calibration-free mercury strain-gauge plethysmograph. *Med Biol Eng Comput*, 17(4):539–542.
- Mitchell, D. and Wyndham, C. (1969). Comparison of weighting formulas for calculating mean skin temperature. *J Appl Physiol*, 26(5):616–622.
- Mort, T., Rintel, T., and Altman, F. (1996). The effects of forced-air warming on postbypass central and skin temperatures and shivering activity. *J Clin Anesth*, 8(5):361–370.
- Obeid, A., Barnett, N., Dougherty, G., and Ward, G. (1990). A critical review of laser Doppler flowmetry. *J Med Eng Technol*, 14(5):178–181.
- Oida, E., Moritani, T., and Yamori, Y. (1997). Tone-entropy analysis on cardiac recovery after dynamic exercise. *J Appl Physiol*, 82(6):1794–1801.
- Pennes, H. (1948). Analysis of tissue and arterial blood temperatures in the resting human forearm. *J Appl Physiol*, 1:93–122.
- Polderman, K. (2004). Application of therapeutic hypothermia in the intensive care unit: opportunities and pitfalls of a promising treatment modality-part 2: Practical aspects and side effects. *Intens Care Med*, 30(5):757–769.
- Prêtre, R. and Turina, M. (2003). *Deep hypothermic circulatory arrest*. In: Cardiac surgery in the adult, edited by L.H. Cohn and L.H. Edmunds. New York: McGraw-Hill.

- Rajek, A., Lenhardt, R., Sessler, D., Brunner, G., Haisjackl, M., Kastner, J., and Laufer, G. (2000). Efficacy of two methods for reducing postbypass afterdrop. *Anesthesiology*, 92(2):447–456.
- Rajek, A., Lenhardt, R., Sessler, D., Grabenwöger, M., Kastner, J., Mares, P., Jantsch, U., and Gruber, E. (1999). Tissue heat content and distribution during and after cardiopulmonary bypass at 17 degrees C. *Anesth Analg*, 88(6):1220–1225.
- Rajek, A., Lenhardt, R., Sessler, D., Kurz, A., Laufer, G., Christensen, R., Matsukawa, T., and Hiesmayr, M. (1998). Tissue heat content and distribution during and after cardiopulmonary bypass at 31 degrees C and 27 degrees C. *Anesthesiology*, 88(6):1511–1518.
- Richards, H., Czosnyka, M., Kirkpatrick, P., and Pickard, J. (1995). Estimation of laser-Doppler flux biological zero using basilar artery flow velocity in the rabbit. *Am J Physiol*, 268(1):H213–217.
- Roe, C. (1971). Effect of bowel exposure on body temperature during surgical operations. *Am J Surg*, 122(1):13–15.
- Rubinstein, E. and Sessler, D. (1990). Skin-surface temperature gradients correlate with fingertip blood flow in humans. *Anesthesiology*, 73(3):541–545.
- Rudy, L., Heymann, M., and Edmunds, L. (1973). Distribution of systemic blood flow during cardiopulmonary bypass. *J Appl Physiol*, 34(2):194–200.
- Salloum, M., Ghadar, N., and Ghali, K. (2007). A new transient bioheat model of the human body and its integration to clothing models. *Int J Therm Sci*, 46(4):371–384.
- Schmidt, R. and Thews, G. (1989). *Human Physiology*. Springer-Verlag Berlin Heidelberg New York London Paris Tokyo Hong Kong: second edition.
- Schnider, T., Minto, C., Gambus, P., Andresen, C., Goodale, D., Shafer, S., and Youngs, E. (1998). The influence of method of administration and covariates on the pharmacokinetics of propofol in adult volunteers. *Anesthesiology*, 88(5):1170–1182.
- Schoffelen, F., Westerterp, K., Saris, W., and Ten Hoor, F. (1997). A dual-respiration chamber system with automated calibration. *J Appl Physiol*, 83(6):2064–2072.
- Schuh, H. (1957). Differenzenverfahren zum Berechnen von Temperatur-Ausgleichsvorgängen bei Eindimensionaler Wärmeströmung in Einfachen und Zusammengesetzten Körpern. *VDI-Forschungsheft*, 459:1–37.
- Sessler, D. (1993). Perianesthetic thermoregulation and heat balance in humans. *FASEB J*, 7(8):638–644.
- Sessler, D. (1995). Deliberate mild hypothermia. *J Neurosurg Anesthesiol*, 7(1):38–46.

- Sessler, D. (1997). Mild perioperative hypothermia. *N Engl J Med*, 336(24):1730–1737.
- Sessler, D. (2000). Perioperative heat balance. *Anesthesiology*, 92(2):587–596.
- Severens, N., Van Marken Lichtenbelt, W., Frijns, A., Van Steenhoven, A., De Mol, B., and Sessler, D. (2007a). A model to predict patient temperature during cardiac surgery. *Phys Med Biol*, 52(17):5131–5145.
- Severens, N., Van Marken Lichtenbelt, W., Van Leeuwen, G., Frijns, A., Van Steenhoven, A., De Mol, B., Van Wezel, H., and Veldman, D. (2007b). Effect of forced-air heaters on perfusion and temperature distribution during and after open-heart surgery. *Eur J Cardiothorac Surg*, 32(6):888–895.
- Sherrington, C. (1906). *The integrative action of the nervous system*. New Haven, CT: Yale University Press.
- Sigdell, J. (1969). A critical review of the theory of the mercury strain gauge plethysmography. *Med Biol Eng*, 7(4):365–371.
- Stańczyk, M., Van Leeuwen, G., and Van Steenhoven, A. (2007). Discrete vessel heat transfer in perfused tissue—model comparison. *Phys Med Biol*, 52(9):2379–2391.
- Stolwijk, J. (1971). *A mathematical model of physiological temperature regulation in man*. NASA contractor report CR-1855, Washington DC: Aeronautics and space administration.
- Stolwijk, J. and Hardy, J. (1966). Temperature regulation in man—a theoretical study. *Pflugers Arch Gesamte Physiol Menschen Tiere*, 291(2):129–162.
- Storm, C., Steffen, I., Schefold, J., Krueger, A., Oppert, M., Jörres, A., and Hasper, D. (2008). Mild therapeutic hypothermia shortens intensive care unit stay of survivors after out-of-hospital cardiac arrest compared to historical controls. *Crit Care*, 12:R78.
- Taguchi, A. and Kurz, A. (2005). Thermal management of the patient: where does the patient lose and/or gain temperature? *Curr Opin Anaesthesiol*, 18(6):632–639.
- Taguchi, A., Ratnaraj, J., Kabon, B., Sharma, N., Lenhardt, R., Sessler, D., and Kurz, A. (2004). Effects of a circulating-water garment and forced-air warming on body heat content and core temperature. *Anesthesiology*, 100(5):1058–1064.
- Tanabe, S., Kobayashi, K., Nakano, J., Ozeki, Y., and Konishi, M. (2002). Evaluation of thermal comfort using combined multi-node thermoregulation (65mn) and radiation models and computational fluid dynamics (cfd). *Energ Buildings*, 34:637–646.
- Tarbell, J., Chang, L., and Hollis, T. (1982). A note on wall shear stress in the aorta. *J Biomech Eng*, 104(4):343–345.

- Tindall, M., Peletier, M., Severens, N., Veldman, D., and De Mol, B. (2008). Understanding post-operative temperature drop in cardiac surgery: a mathematical model. *Math Med Biol*, in press.
- Tsangaris, S. and Stergiopoulos, N. (1988). The inverse Womersley problem for pulsatile flow in straight rigid tubes. *J Biomech*, 21(3):263–266.
- Upton, R. and Ludbrook, G. (1997). A physiological model of induction of anaesthesia with propofol in sheep. 1. Structure and estimation of variables. *Br J Anaesth*, 79(4):497–504.
- Valeri, C., Feingold, H., Cassidy, G., Ragno, G., Khuri, S., and Altschule, M. (1987). Hypothermia-induced reversible platelet dysfunction. *Annals of surgery*, 205(2):175–181.
- Van De Graaff, K. (1995). *Human anatomy*. Oxford: Wm. C. Brown publishers, 4th ed.
- Van Leeuwen, G., Hand, J., Lagendijk, J., Azzopardi, D., and Edwards, A. (2000). Numerical modeling of temperature distributions within the neonatal head. *Pediatr Res*, 48(3):351–356.
- Van Marken Lichtenbelt, W., Daanen, H., Wouters, L., Fronczek, R., Raymann, R., Severens, N., and Van Someren, E. (2006). Evaluation of wireless determination of skin temperature using ibuttons. *Physiol Behav*, 88(4-5):489–497.
- Van Marken Lichtenbelt, W., Frijns, A., Van Ooijen, A., Fiala, D., Kester, A., and Van Steenhoven, A. (2007). Validation of an individualized model of human thermoregulation for predicting responses to cold air. *Int J Biometeorology*, 51(3):169–179.
- Van Ooijen, A., Van Marken Lichtenbelt, W., Van Steenhoven, A., and Westerterp, K. (2004). Seasonal changes in metabolic and temperature responses to cold air in humans. *Physiol Behav*, 82(2-3):545–553.
- Van Ooijen, A., Van Marken Lichtenbelt, W., Van Steenhoven, A., and Westerterp, K. (2005). Cold-induced heat production preceding shivering. *Br J Nutr*, 93:387–391.
- Verotta, D., Sheiner, L., Ebling, W., and Stanski, D. (1989). A semiparametric approach to physiological flow models. *J Pharmacokinet Biopharm*, 17(4):463–491.
- Wan, X. and Fan, J. (2008). A transient thermal model of the human body-clothing-environment system. *J Therm Biol*, 33:87–97.
- Washington, D., Sessler, D., Moayeri, A., Merrifield, B., McGuire, J., Prager, M., Belani, K., Hudson, S., and Schroeder, M. (1993). Thermoregulatory responses to hyperthermia during isoflurane anesthesia in humans. *J Appl Physiol*, 74(1):82–87.
- Webb, P. (1995). The physiology of heat regulation. *Am J Physiol*, 268(4):R838–850.
- Werner, J. (1980). The concept of regulation for human body temperature. *J Therm Biol*, 5(2):75–82.

- Wijers, S., Schrauwen, P., Saris, W., and Van Marken Lichtenbelt, W. (2008). Human skeletal muscle mitochondrial uncoupling is associated with cold induced adaptive thermogenesis. *PLoS ONE*, 3:e1777.
- Wissler, E. (1985). *Mathematical simulation of human thermal behaviour using whole body models*. In: Heat transfer in medicine and biology—Analysis and applications, edited by A. Shitzer and R.C. Eberhart. New York: Plenum, vol. 1, chapter 13, 325–373.
- Wissler, E. (1998). Pennes' 1948 paper revisited. *J Appl Physiol*, 85(1):35–41.
- Wissler, E. (2008). A quantitative assessment of skin blood flow in humans. *Eur J Appl Physiol*, 104(2):145–157.
- Womersley, J. (1957). *The mathematical analysis of the arterial circulation in a state of oscillatory motion*. Technical report wade-tr-56-614, Wright Air Development Center.
- Wyndham, C. and Atkins, A. (1968). A physiological scheme and mathematical model of temperature regulation in man. *Pflugers Arch*, 303:14–30.
- Xu, X. and Werner, J. (1997). A dynamic model of the human/clothing/environment-system. *Appl Human Sci*, 16(2):61–75.
- Zhong, J., Seifalian, A., Salerud, G., and Nilsson, G. (1998). A mathematical analysis on the biological zero problem in laser Doppler flowmetry. *IEEE Trans Biomed Eng*, 45(3):354–364.

APPENDIX A

Setpoint theory and its alternatives

A.1 Introduction

The temperature setpoint of a body can be defined as the integrated steady-state body temperature at which neither the mechanisms for heat elimination nor those for protection against cold are active (Schmidt and Thews, 1989). When using the term setpoint in this connection, it is as if it is pretended that a controlled variable exists that is intended to be maintained with the smallest possible variation. In case of the thermal system the exact intention can not be specified. One can only determine the constellation of temperatures at which the individual control processes come into operation. Such analysis provides the threshold curves, most of times expressed as combination of mean skin and core temperature, of the thermoregulatory processes .

In literature still a lot of controversies exist about the existence and use of temperature setpoints. Although Cooper (2002) states: 'it is generally accepted that the body temperatures is regulated about a physiological setpoint', still several researchers question the setpoint theory concept. This appendix tries to give an overview of the different points of view on body temperature control that are found in literature, starting with the distributed parameter control concept, the heat balance concept and the reciprocal cross-inhibition concept that do not need setpoints and finishing with the basic engineering concept that is based on setpoints.

A.2 Concepts

The distributed parameter control concept

According to Werner (1980), the regulated variable of human temperature regulation is certainly not a locally defined single temperature, it is probably not heat flow and not mean body temperature, but it seems to be a flexible and adaptable integrative temperature signal according to a distributed parameter control strategy. According to Werner, the regulator for such a distributed parameter control strategy does not need any explicit reference, neither in the form of a neuronal signal nor in the form of the indifferent zone. Negative feedback can simply be achieved by an odd number of negative input/output relations of the subsystems in the closed loop. The steady-state situation is then formed by a quadruple of compatible values for the affecter frequency, the effector frequency, the controlled variable (like blood flow, metabolism, evaporation and behaviour) and the temperature. In figure A.1 this steady state concept is illustrated. Here, temperature and affecter frequency are negatively related, while affecter-effector frequency, effector frequency-controlled variable (e.g. metabolism) and the controlled variable-temperature are positively related. This fulfills the condition that there should be an odd number of negative input/output relations. In the figure it is seen that arbitrary values (the dotted lines) do not yield a steady state (the solid lines). However, the crucial question that remains unanswered in this concept is the quantitative description of the local receptor, its controller and the local effector activity.

The heat balance concept

Another hypothesis of heat regulation is proposed by Webb (1995). According to him, heat regulation controls heat balance over a wide range of heat loads. So, instead of temperature control this concept is based on heat balance control. Heat flow to or from the body is sensed, and physiological responses defend the body heat content. Heat content varies over a range that is related to heat load. Changes in body heat content drive deep body temperatures.

For this concept, sensors should be available in the surface of the body that sense the transcutaneous temperature gradient. The physical arrangement would consist of temperature sensors just below the skin and one or more at deeper levels, but experimental evidence of this is not comprehensive. Also, the behaviour of such a heat loss controller is not understood. But it is thought that such a controller is a continuous controller, in contrast to a setpoint temperature controller.

The reciprocal cross-inhibition concept

By Mekjavic and Eiken (2006) distinction is made between the thermoneutral zone and the interthreshold zone. In the thermoneutral zone, defense of body temperature is solely achieved by changes in vasomotor tone. The thermoneutral zone will vary in width as a consequence of the influence of nonthermal factors (e.g. motion sickness, fever and anesthesia). Once

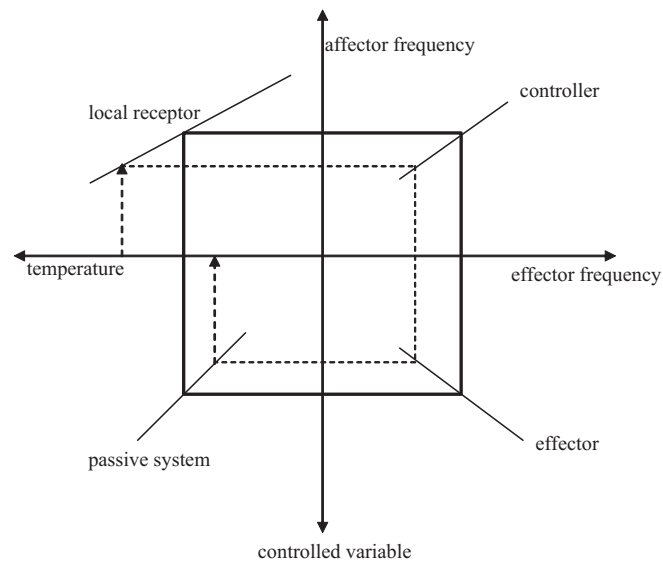


Figure A.1: Steady state concept of thermoregulation according to Werner (1980). The solid rectangular line determines the steady-state of the closed control loop. To carry out the control task, neither a reference signal nor a comparison of two or more controller inputs are necessary, as the steady state reached is the only one which is possible under assumed circumstances. The dotted line demonstrates that arbitrary values do not yield a closed-circuit, i.e. a steady-state (solid line).

the capacity of the vasomotor response to maintain core temperature is exceeded, sweating or shivering are activated. The core temperature, at which these effectors are initiated, is defined as the thermoeffector threshold. The gain and the interthreshold zone of these responses may also be influenced by nonthermal factors.

According to this concept there is no support for likelihood of body temperature being regulated at a precise level like in the setpoint concept.

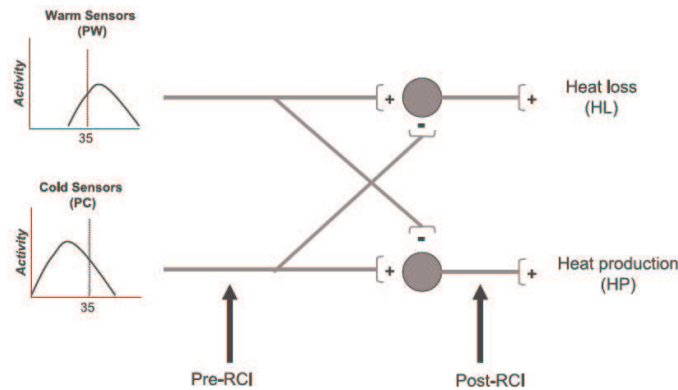


Figure A.2: Visualization of the reciprocal cross-inhibition (RCI) concept, taken from Mekjavic and Eiken (2006).

Sherrington (1906) introduced the concept of reciprocal cross-inhibition of sensor-to-effector pathways. Wyndham and Atkins (1968) were the first who incorporated this concept in their human thermoregulation model. The most important feature of this model is the absence of a reference signal. The temperature is established by the reciprocal inhibitions of the heat production and heat loss pathways, see figure A.2.

According to the reciprocal cross-inhibition theory, thermoafferent information from peripheral and core temperature sensors provide the neural drive for heat production and heat loss. The excitatory drive in the heat production sensor-to-effector pathways also provides an inhibitory drive in the heat loss sensor-to-effector pathway, and vice versa. In this way, the overlapping activity and temperatures of the cold and warm sensors can regulate the core temperature, and therefore provides an alternative to the setpoint theory (Mekjavic and Eiken, 2006). Although the theory is supported by some animal studies, its relevance in human thermoregulation needs to be elucidated.

The basic engineering concept

Temperature regulation in mammals is often treated in analogy with the classical control systems theory. Such engineering models assume that body temperature is somehow compared with a reference temperature, resulting in a temperature error signal, which then evokes appropriate effector responses, see figure A.3.

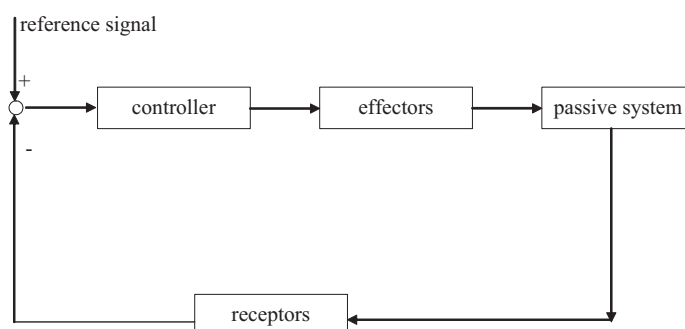


Figure A.3: The engineering control concept, that uses a reference signal.

The controlling system attempts to minimize the error signal, thereby ensuring that body temperature is regulated at a certain setpoint. Although it is questionable if this representation is physiologically correct, this type of control systems are good didactic tools and are a convenient approach for developing predictive models (Mekjavic and Eiken, 2006). Most existing thermo-physiological models, like the models of Stolwijk (1971); Gordon (1974); Xu and Werner (1997); Fiala et al. (1999, 2001); Tanabe et al. (2002); Severens et al. (2007a); Wan and Fan (2008); Wissler (2008) indeed use the basic engineering control strategy form for describing the active part in their models and those models give reasonable results.

A.3 Discussion

Till date, the phenomenon of thermoregulation has not been completely understood. In literature several different concepts are given about human thermoregulation, with different control strategies. Nevertheless, at this moment no experimental or theoretical evidence exists that can point one of them as the best strategy. Therefore, when one tries to incorporate an active (thermoregulatory) part in a human thermo-physiological model, it has to be decided what control concept will be used. In this thesis, it was decided to use the basic engineering control strategy with setpoints, as this is the simplest, clearest, most straightforward and most used and successful method for modelling thermoregulation till so far.

APPENDIX B

Properties of the passive part

B.1 Model properties of the different body parts

The model properties of the passive model, that are used for model development in chapter 2, are summarized in table B.1 and B.2.

Table B.1: Model properties of the passive system, based on Fiala et al. (1999): length of the cylinder L , counter current heat exchange coefficient h_x and heat exchange coefficients for mixed convection $h_{c,mix}$ with regression coefficients for natural convection a_{nat} , forced convection a_{fre} and mixed convection a_{mix} in equation (2.4).

Element	L	h_x	$h_{c,mix}$		
	$\times 10^{-2}$ [m]	[W/K]	a_{nat}	a_{fre}	a_{mix}
1. Head	*	0	3.0	113	-5.7
2. Face	9.84	0	3.0	113	-5.7
3. Neck	8.42	0	1.6	130	-6.5
4. Shoulders (2x)	16.0	0.4	5.9	216	-10.8
5. Thorax	30.6	0	0.5	180	-7.4
6. Abdomen	55.2	0	1.2	180	-9.0
7. Arms (4x)	31.85	1.0325	8.3	216	-10.8
8. Hands (2x)	31.0	0.285	8.3	216	-10.8
9. Legs (4x)	34.75	1.725	5.3	220	-11.0
10. Feet (2x)	24.0	1.7	6.8	210	-10.5

In table B.3 the number of nodes in each layer per sector n , outer radius of layer r , thermal conductivity k , density ρ , specific heat c , basal blood perfusion rate w_b and basal metabolic

Table B.2: Sector properties, based on Fiala et al. (1999): sector angle ϕ (see figure B.1), view factor between sector and surrounding ψ_{sr} , emission coefficient for radiation ε .

Element	Sector	ϕ	ψ_{sr}	ε
		[deg]	[-]	[-]
1. Head	forehead	10	1.0	0.99
	head	170	0.9	0.8
2. Face	all	210	0.9	0.99
3. Neck	anterior	180	0.7	0.99
	posterior	180	0.75	0.99
4. Shoulders	all	130	0.9	0.99
5. Thorax	anterior	150	0.8	0.99
	posterior	150	0.95	0.99
	superficialis	60	0.05	0.99
6. Abdomen	anterior	150	0.8	0.99
	posterior	150	0.95	0.99
	superficialis	60	0.20	0.99
7. Arms	anterior	135	0.75	0.99
	posterior	135	0.80	0.99
	medialis	90	0.10	0.99
8. Hands	dorsalis	180	0.80	0.99
	palmaris	180	0.10	0.99
9. Legs	anterior	150	0.85	0.99
	posterior	150	0.95	0.99
	tibialis	60	0.10	0.99
10. Feet	dorsalis	180	0.90	0.99
	plantaris	180	1.9	0.99

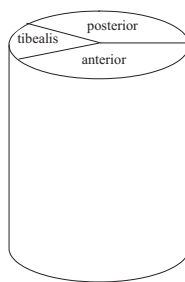


Figure B.1: Illustration of the sector angles (ϕ) of the leg.

rate \dot{q}_m are given.

B.2 Convective heat transfer coefficients

In current model, the convective heat transfer coefficients are defined according to the equation formulated by Fiala et al. (1999):

$$h_{c,\text{mix}} = \sqrt{a_{\text{nat}} \sqrt{T_{\text{skin}} - T_{\infty}} + a_{\text{frc}} \nu_{a,\text{eff}} + a_{\text{mix}}} \quad (\text{B.1})$$

where a_{nat} , a_{frc} and a_{mix} are regression coefficients, as given in table B.1 and $\nu_{a,\text{eff}}$ is the effective relative air speed. In the table, it is seen that the regression coefficients are segment specific.

In order to examine the results that are obtained with this equation, the results were compared to two other methods: the engineering approach for convection around cylinders and the model of Fanger (1973).

The fundamental nondimensional quantities describing mixed convection, where forced convection is involved as well as natural convection, are the Nusselt number (Nu), Prandtl number (Pr), Rayleigh number (Ra) and Reynolds number (Re). These are expressed as follows:

$$\text{Nu}_D = \frac{h_c D}{k} \quad (\text{B.2})$$

$$\text{Pr} = \frac{\nu}{\alpha} \quad (\text{B.3})$$

$$\text{Ra}_D = \frac{g \beta (T_{\text{skin}} - T_{\infty}) D^3}{\alpha \nu} \quad (\text{B.4})$$

$$\text{Re}_D = \frac{\nu_{a,\text{eff}} D}{\nu} \quad (\text{B.5})$$

where h_c is the convective heat transfer coefficient [$\text{W m}^{-2} \text{K}^{-1}$]; k is the thermal conductivity of the air [$\text{W m}^{-1} \text{K}^{-1}$]; D is the characteristic dimension of the body or the segment in question such as diameter of cylindrical segments [m]; ν is the kinematic viscosity [$\text{m}^2 \text{s}^{-1}$], α is the thermal diffusivity [$\text{m}^2 \text{s}^{-1}$], g the gravitational acceleration [ms^{-2}] and β is the coefficient of volumetric thermal expansion [K^{-1}]. The values of air properties are temperature dependent and were based on Bejan (1993).

For natural convection flow, generally confined to air speeds lower than 0.2 ms^{-1} , around a cylinder positioned horizontally in a fluid reservoir, the Nusselt number is calculated as (Bejan, 1993):

$$\overline{\text{Nu}}_{D,\text{hor}} = \left\{ 0.6 + \frac{0.387 \text{Ra}_D^{1/6}}{[1 + (0.559/\text{Pr})^{9/16}]^{8/27}} \right\}^2 \quad (\text{B.6})$$

for $10^{-5} < \text{Ra}_D < 10^{12}$. For natural convection of a vertically placed cylinder the Nusselt relation becomes:

$$\overline{\text{Nu}}_{D,\text{ver}} = \left\{ 0.825 + \frac{0.387 \text{Ra}_D^{1/6}}{[1 + (0.492/\text{Pr})^{9/16}]^{8/27}} \right\}^2 \quad (\text{B.7})$$

Table B.3: Material and spatial properties, based on Fiala et al. (1999).

Element	Material	n	r	k	ρ	c	w_b	\dot{q}_m
			$\times 10^{-2}$ [m]	[W/mK]	(kg/m ³)	[J/kgK]	[l/sm ³]	[W/m ³]
1. Head	Brain	3	8.60	0.49	1080	3850	10.132	13400
	Bone	1	10.05	1.16	1500	1591	0	0
	Fat	1	10.20	0.16	850	2300	0.0036	58
	Inner skin	1	10.30	0.47	1085	3680	5.48	743.21
	Outer skin	1	10.40	0.47	1085	3680	0	0
2. Face	Muscle	1	2.68	0.42	1085	3768	0.538	684
	Bone	1	5.42	1.16	1500	1591	0	0
	Muscle	1	6.80	0.42	1085	3768	0.538	684
	Fat	2	7.60	0.16	850	2300	0.0036	58
	Inner skin	1	7.70	0.47	1085	3680	11.17	740.82
	Outer skin	1	7.80	0.47	1085	3680	0	0
3. Neck	Bone	1	1.90	0.75	1357	1700	0	0
	Muscle	2	5.46	0.42	1085	3768	0.538	684
	Fat	1	5.56	0.16	850	2300	0.0036	58
	Inner skin	1	5.64	0.47	1085	3680	6.8	507.36
	Outer skin	1	5.67	0.47	1085	3680	0	0
4. Shoulders	Bone	1	3.70	0.75	1357	1700	0	0
	Muscle	1	3.90	0.42	1085	3768	0.538	684
	Fat	2	4.40	0.16	850	2300	0.0036	58
	Inner skin	1	4.50	0.47	1085	3680	1.01	744.28
	Outer skin	1	4.60	0.47	1085	3680	0	0
5. Thorax	Lung	1	7.73	0.28	550	3718	4.30	600
	Bone	1	8.91	0.75	1357	1700	0	0
	Muscle	1	12.34	0.42	1085	3768	0.538	684
	Fat	2	12.68	0.16	850	2300	0.0036	58
	Inner skin	1	12.8	0.47	1085	3680	1.58	677.3
	Outer skin	1	12.9	0.47	1085	3680	0	0
6. Abdomen	Core	1	7.85	0.53	1000	3697	4.31	4100
	Bone	1	8.34	0.75	1357	1700	0	0
	Muscle	1	10.90	0.42	1085	3768	0.538	684
	Fat	2	12.44	0.16	850	2300	0.0036	58
	Inner skin	1	12.54	0.47	1085	3680	1.44	590.2
	Outer skin	1	12.6	0.47	1085	3680	0	0
7. Arms	Bone	1	1.53	0.75	1357	1700	0	0
	Muscle	2	3.43	0.42	1085	3768	0.538	684
	Fat	1	4.01	0.16	850	2300	0.0036	58
	Inner skin	1	4.11	0.47	1085	3680	1.1	631
	Outer skin	1	4.18	0.47	1085	3680	0	0
8. Hands	Bone	1	0.70	0.75	1357	1700	0	0
	Muscle	1	1.74	0.42	1085	3768	0.538	684
	Fat	1	2.04	0.16	850	2300	0.0036	58
	Inner skin	1	2.16	0.47	1085	3680	4.54	744.43
	Outer skin	1	2.26	0.47	1085	3680	0	0
9. Legs	Bone	1	2.20	0.75	1357	1700	0	0
	Muscle	2	4.80	0.42	1085	3768	0.538	684
	Fat	2	5.33	0.16	850	2300	0.0036	58
	Inner skin	1	5.43	0.47	1085	3680	1.05	742.8
	Outer skin	1	5.53	0.47	1085	3680	0	0
10. Feet	Bone	1	2.00	0.75	1357	1700	0	0
	Muscle	1	2.50	0.42	1085	3768	0.538	684
	Fat	2	3.26	0.16	850	2300	0.0036	58
	Inner skin	1	3.40	0.47	1085	3680	1.5	640.3
	Outer skin	1	4.50	0.47	1085	3680	0	0

for $10^{-1} < Ra_D < 10^{12}$.

For forced-air convection around a cylinder oriented across a fluid flow, the Nusselt number is given by (Bejan, 1993):

$$\overline{Nu}_{D,\text{forced}} = 0.3 + \frac{0.62Re_D^{1/2}Pr^{1/3}}{[1 + (0.4/Pr)^{2/3}]^{1/4}} \left[1 + \frac{Re_D^{5/8}}{282000} \right]^{4/5} \quad (\text{B.8})$$

In a combined problem, in which natural and forced convection both contribute, the mixed Nusselt number can be approximated by:

$$\overline{Nu}_{D,\text{mixed}} \cong (Nu_{D,\text{forced}}^3 + Nu_{D,\text{natural}}^3)^{1/3} \quad (\text{B.9})$$

Implementing equation (B.6) and (B.8) in (B.9) for a horizontally placed cylinder and (B.7) and (B.8) in (B.9) for a vertical cylinder leads to the mixed Nusselt number for the two cylinder configurations. With help of equation (B.2) and using the obtained mixed Nusselt numbers, the convective heat transfer coefficient h_c can be calculated for the horizontal and vertical cylinder cases.

Fanger's PMV (1973) model supplies the following approximation for h_c for the human body under natural convection:

$$h_c = 2.38(T_{\text{skin}} - T_{\infty})^{1/4} \quad (\text{B.10})$$

The results of the three methods are compared for a wind speed of 0.05 ms^{-1} , at an environmental temperature of 20°C (typical wind speed and temperature in surgery theatre) for skin temperatures between 20 and 25°C . The values for a_{nat} , a_{frc} and a_{mix} were set to 3 , 200 and -7 , respectively (following from Fiala et al. (1999), see table B.1). A typical diameter was chosen of 0.20 m .

Results are shown in figure B.2. The three methods give results with the same trend and of the same order of magnitude. In addition, the order of magnitude calculated with the three methods showed good agreements with Stolwijk's (1970) assumed natural heat transfer coefficients that were in the range $0.66\text{-}6.05 \text{ Wm}^{-2}\text{K}^{-1}$. Equation (B.1) seems therefore a suitable method for calculating convective heat transfer coefficients.

B.3 Clothing parameters

The local heat transfer coefficient U_{cl} [$\text{Wm}^{-2}\text{K}^{-1}$] of a clothing (including draping) ensemble with m layers is computed in the model by the following relation proposed by Fiala et al. (1999):

$$U_{\text{cl}} = \frac{1}{\sum_{i=1}^m (I_{\text{cl}})_i + \frac{1}{f_{\text{cl}}(h_{c,\text{mix}} + h_r)}} \quad (\text{B.11})$$

with $I_{\text{cl},i}$ representing the local heat resistance of the i -th clothing layer, f_{cl} the local clothing area factor of the m -th clothing layer and $h_{c,\text{mix}}$ and h_r the local coefficients for convection

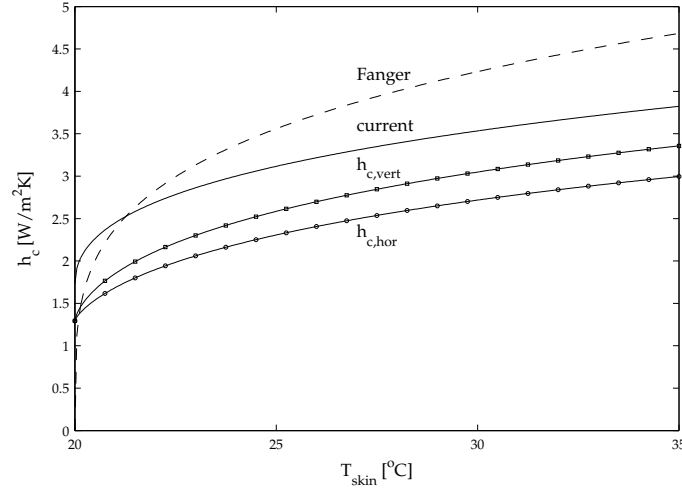


Figure B.2: Convective heat transfer coefficients as a function of skin temperature at $T_\infty=20^\circ\text{C}$. From top to bottom: results from Fanger (1973), current model (based on Fiala et al. (1999)), engineering prediction of vertical cylinder and engineering prediction of horizontal cylinder.

and radiation, respectively given by equation (2.4) and (2.8) and using local values. In case of a covered subject the convective and radiative heat losses are given by:

$$q''_{\text{convection+radiation}} = U_{\text{cl}}(T_{\text{skin}} - T_\infty) \quad (\text{B.12})$$

In accordance with Fiala et al. (1999), the evaporative coefficient of clothing U_E [$\text{Wm}^{-2}\text{Pa}^{-1}$] is obtained using the local moisture permeability index i_{cl} , the local clothing resistance I_{cl} , the clothing area factor of the m -th clothing layer, the local convection coefficient $h_{c,\text{mix}}$ and the Lewis constant for air ($\text{Le}=16.65^\circ\text{CkPa}^{-1}$, for more details see McIntyre (1980)):

$$U_E = \frac{\text{Le}}{\sum_{i=1}^m \left(\frac{I_{\text{cl}}}{i_{\text{cl}}} \right)_i + \frac{1}{f_{\text{cl}} h_{c,\text{mix}}}} \quad (\text{B.13})$$

Values for I_{cl} , f_{cl} and i_{cl} , as used in this research are given in table B.4.

B.4 Determination of the forced-air heat exchange coefficients

For determining the heat exchange coefficient h_{fa} in equation (2.19), experiments were performed using a forced-air heating blanket placed around an aluminium cylinder, with the characteristic dimensions of a leg ($L=0.35$ m, $D=0.15$ m), in the same way as during surgery.

Table B.4: Overview of relevant local parameters of used clothing/draping.

garment	I_{cl} [clo] †	f_{cl} [-]	i_{cl} [-]
bed	0.90	1.20	0.29
sterile cover	0.83	1.20	0.49
cotton drape	0.78	1.20	0.49
short trousers	0.76	1.35	0.39
briefs	0.13	1.03	0.45
T-shirt	0.26	1.08	0.54
socks	0.69	1.18	0.60

† 1 clo=0.155m²KW⁻¹. Note that the clo-values are local parameters, in contrast to the often used global clo-values.

In figure B.3 an overview is given of the measurement setup and the position of the thermocouples. The setup consisted of a tube-shaped forced-air heating blanket, the aluminium cylinder, a wooden block that helped to place the blanket in the same way as during surgery and insulation material at the symmetry axis of the setup, as it is expected that the right and left side react the same. The temperature of the unit was set to 43°C. It is assumed that at $t=0$

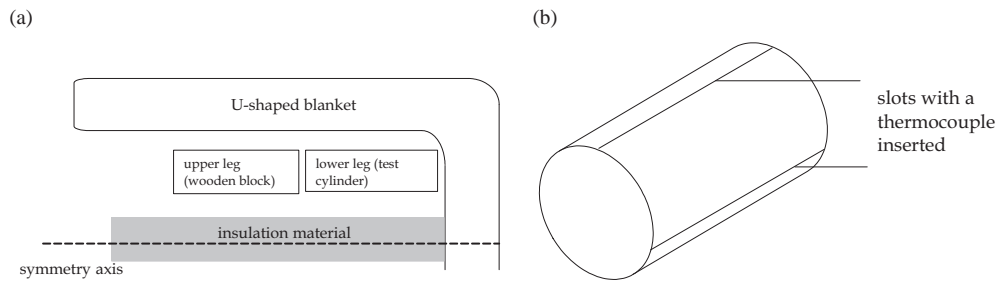


Figure B.3: (a) Measurement setup with aluminium cylinder representing the lower leg, (b) Measurement positions of temperature with help of thermocouples.

min the temperature of the cylinder is homogeneous ($T = T_0$), and that during warming the temperature of cylinder stays homogeneous (the calculated Biot-number: $\frac{hR}{k}$ was $\ll 1$). For a closed system that experiences zero work transfer, the first law of thermodynamics reduces to:

$$q = \frac{dE}{dt} = \rho c V \frac{dT}{dt} \quad (\text{B.14})$$

The net heat transfer into the cylinder is given by:

$$q = h_{fa} A (T_{\infty} - T) \quad (\text{B.15})$$

with h_{fa} the heat exchange coefficient. Substituting equation (B.15) in equation (B.14) leads to:

$$\frac{dT}{dt} = -\frac{h_{fa} A}{\rho c V} (T - T_{\infty}) \quad (\text{B.16})$$

By integrating (B.16) and implementing the starting conditions, the following relation is found:

$$\frac{T - T_\infty}{T_0 - T_\infty} = \exp\left(-\frac{h_{fa}A}{\rho cV}(t - t_0)\right) \quad (\text{B.17})$$

By taking the natural logarithm of (B.17), the equation is represented by:

$$\ln\left(\frac{T - T_\infty}{T_0 - T_\infty}\right) = -h_{fa}\frac{A}{\rho cV}(t - t_0) \quad (\text{B.18})$$

As can be seen, equation (B.18) is a linear equation in time, where steepness depends on h_{fa} . With help of a temperature warming curve as function of time of the aluminium cylinder (see a typical example in figure B.4), and using equation (B.18), a value of forced-air warmer heat exchange coefficients was found of $16.4 \pm 0.3 \text{ Wm}^{-2}\text{K}^{-1}$ (Bertens et al., 2006).

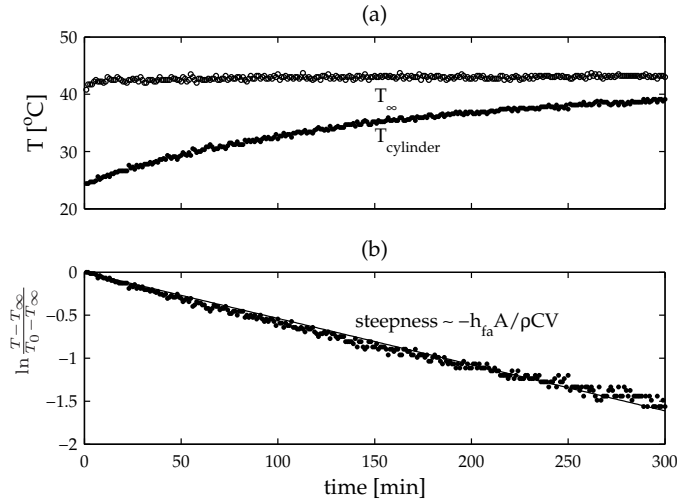


Figure B.4: (a) Typical warming curve of the cylinder and air temperature in forced-air blanket as function of time. (b) Left hand side of equation (B.18) as function of warming time. The steepness of the linearly fitted line is directly related to the heat exchange coefficient h_{fa} .

B.5 Evaporative heat losses from the wound surface

The mass flux of water that evaporates from the wound surface is given by (Bejan, 1993):

$$\dot{m}'' = \bar{h}_m(\rho_w - \rho_\infty) \quad (\text{B.19})$$

with \dot{m}'' denoting the mass flux in $[\text{kgm}^{-2}\text{s}^{-1}]$, \bar{h}_m the mass transfer coefficient $[\text{ms}^{-1}]$ and ρ the mass concentration of water vapor $[\text{kgm}^{-3}]$. The difference in water vapor density can

be written as:

$$\rho_w - \rho_\infty = 0.622\rho_{\text{air}} \left(\frac{p_{\text{sat,w}}}{p} - \frac{\phi p_{\text{sat},\infty}}{p} \right) \quad (\text{B.20})$$

in which p_{sat} is given by Antoine's equation, see equation (2.9) and ϕ is the relative humidity. The relevant properties of dry air at 20°C and atmospheric pressure are (Bejan, 1993): $\rho = 1.205 \text{ kgm}^{-3}$, $\nu = 1.5 \cdot 10^{-5} \text{ m}^2\text{s}^{-1}$, $D = 2.7 \cdot 10^{-5} \text{ m}^2\text{s}^{-1}$. The mass transfer coefficient \bar{h}_m is related to the Sherwood number, that is defined by:

$$\overline{\text{Sh}}_L = \frac{\bar{h}_m L}{D} \quad (\text{B.21})$$

where ν is the kinematic viscosity and L is the characteristic length of the plane surface:

$$L = \frac{A}{P} \quad (\text{B.22})$$

with A the area of the plane surface and P the perimeter. Typical length and width of the wound are 0.5 m and 0.08 m, which gives a typical L of 0.034 m.

It is assumed that air velocity in the wound cavity is negligible, and that only local variations of vapour concentration induce a concentration buoyancy effect.

For choosing the correct Sh-number, the mass transfer Rayleigh number (Ra) has to be calculated. This Ra-number yields:

$$\text{Ra}_m = \frac{g\beta_c(\rho_w - \rho_\infty)L^3}{\nu D} \quad (\text{B.23})$$

in which g is gravitational acceleration [ms^{-2}] and β_c is the composition expansion coefficient which equals $0.51 \text{ m}^3 \text{ kg}^{-1}$ for an air/water vapor mixture (Bejan, 1993). At a typical wound temperature of 30 °C, an environmental temperature of 20°C and a ϕ of 40%, $\rho_w - \rho_\infty = 0.0247 \text{ kgm}^{-3}$. From this follows that the Ra-number is $11.99 \cdot 10^3$, which is order of magnitude $O(1 \cdot 10^4)$. For hot surfaces facing upward, with a $10^4 < \text{Ra}_m < 10^7$ the appropriate Sherwood relation, in accordance with the heat and mass transfer analogy, is (Bejan, 1993):

$$\overline{\text{Sh}}_L = 0.54 \text{Ra}_m^{1/4} \quad (\text{B.24})$$

For the heat and mass transfer analogy to be valid, the following relation must be satisfied (Incropera and DeWitt, 2002):

$$\frac{\overline{\text{Nu}}}{\text{Pr}^n} = \frac{\overline{\text{Sh}}}{\text{Sc}^n} \quad (\text{B.25})$$

with Pr representing the Prandtl number given by $\frac{\nu}{\alpha}$ [-] and Sc the Schmidt number that is equal to $\frac{\nu}{D}$ [-]. According to (B.25) the Nusselt/Sherwood analogy holds in case the ratio $\frac{\text{Sc}}{\text{Pr}}$ is approximately 1. For a water vapor/air mixture, this ratio is 0.86 (Bejan, 1993), which is close to 1. Hence, it is decided that the analogy can be used for this case.

Combining equation (B.19), (B.21), (B.23) and (B.24) gives for the mass flux of water:

$$\dot{m}'' = 0.54 \frac{D}{L} \left(\frac{g\beta_c(\rho_w - \rho_\infty)L^3}{\nu D} \right)^{1/4} (\rho_w - \rho_\infty) \quad (\text{B.26})$$

The evaporative heat flux then yields:

$$q''_{\text{evaporation,water}} = \dot{m}'' \lambda_{\text{H}_2\text{O}} \quad (\text{B.27})$$

with $\lambda_{\text{H}_2\text{O}}$ the latent heat of vaporization of water.

APPENDIX C

Measurement techniques

C.1 Laser Doppler flowmetry

With the help of laser Doppler flowmetry, it is possible to assess skin blood flow in a non-invasive manner. A laser Doppler flowmetry instrument consists of a light emitting part and a detector. The light emitting part sends out coherent light to the tissue. When coherent light is scattered in tissue, a part of the light will be scattered by moving red blood cells. This causes a shift in frequency Δf , called Doppler shift, which is dependent on the velocity of the moving red blood cells (v):

$$\Delta f = \frac{2vn}{\lambda_0} \cos \theta \quad (\text{C.1})$$

Here, n is the refractive index of the medium, λ_0 is the wavelength of the incident light and θ is the angle between the direction of incidence and the direction of scattering.

The detector will receive a mix of both the frequency broadened light and the light scattered from static tissue. This mix will cause intensity fluctuations with Doppler frequencies. Since the light is scattered in many directions, there will be no single Doppler frequency. Instead, the detector will receive a whole spectrum. The spectral power density of the photocurrent, $S(\omega)$, can be used to relate photocurrent to blood flow. Here, the angular frequency ω is defined as $\omega = 2\pi f$. The moment M of order i of the power spectrum is defined as:

$$M_i = \int_a^b \omega^i S(\omega) d\omega \quad (\text{C.2})$$

in which a and b are the bandwidth frequencies. Bonner and Nossal (1981) showed that the first moment of the power spectrum $i=1$ is linearly proportional to the root mean square

velocity of moving red blood cells times the average concentration of red blood cells. The zero order moment ($i=0$) is proportional to the concentration of red blood cells. Hence, the weighted first moment of the spectral power density defined as:

$$M_{1,\omega} = \frac{M_1}{M_0} \quad (\text{C.3})$$

is proportional to the root-mean-square velocity of the red blood cells: $\sqrt{\langle v^2 \rangle} \sim M_{1,\omega}$. Since the Doppler device cannot present blood flow in absolute values (due to variation in local tissue area, the used set-up, interindividual variation, time variation in capillary density and absorbency), perfusion is expressed in terms of arbitrary perfusion units (PU).

C.2 Skin temperature *

In this research, human skin temperature was assessed with help of iButtons type DS1291H (Dallas Maxim), see chapter 3, chapter 5 and chapter 6. An iButton is a small (16x6 mm²), rugged self-sufficient system that measures temperature and records the results in a protected memory section. Afterwards, time and temperature data can be transferred to a computer for data analysis. Because of its small size and absence of wiring, iButtons are particularly valuable for long-term and ambulatory monitoring. According to the manufacturing company, the temperature range of this type of iButtons is between 15°C and 46°C with an accuracy of 1°C and a precision of 0.125°C. In a validation study, it was observed that iButtons performed better than the specifications provided by the manufacturer. An average accuracy of 0.09°C was found, with a maximum deviation of 0.4°C. A typical response time in water was found of 19 seconds. But it must be noted that response time on the skin is probably larger because the heat capacity and conductivity of water are higher than that of skin and only part of the iButton is in direct contact with the skin.

Mean skin temperature: measurements

True mean skin temperature can only be obtained by obtaining an infinite number of measuring sites of temperature on the skin. However, in practice it is impossible to determine skin temperatures over the entire surface of the body. Therefore, many formulas with various skin temperature sites have been proposed to estimate mean skin temperature. An overview can be found in for instance the papers of Mitchell and Wyndham (1969) and Choi et al. (1997). With help of those formulas, mean skin temperature can be calculated from a limited number of measurement sites.

In this thesis, the mean skin temperature, as presented in chapter 5 and 6, is calculated by

*This section is based on:

Van Marken Lichtenbelt W.D., Daanen H.A.M., Wouters L., Fronczek R., Raymann R.J.E.M., Severens N.M.W. and Van Someren E.J.W. (2006). Evaluation of wireless determination of skin temperature using iButtons. *Physiol Behav*, 88:489–497.

using the 12-point-weighted formula of Hardy and Dubois (Mitchell and Wyndham, 1969), which is given by:

$$\begin{aligned} T_{\text{skin}} = & 0.07T_{\text{head}} + 0.0875T_{\text{chest}} + 0.0875T_{\text{abdomen}} + 0.0875T_{\text{scapula}} \\ & + 0.0875T_{\text{lumbar}} + 0.14T_{\text{lower arm}} + 0.05T_{\text{hand}} + 0.095T_{\text{thigh anterior}} \\ & + 0.095T_{\text{thigh posterior}} + 0.065T_{\text{calf anterior}} + 0.065T_{\text{calf posterior}} + 0.07T_{\text{foot}} \end{aligned} \quad (\text{C.4})$$

Attachment points of the iButtons are given in figure C.1.

In the aortic valve patients in chapter 3, the seven-point system of Hardy and Dubois (1938)

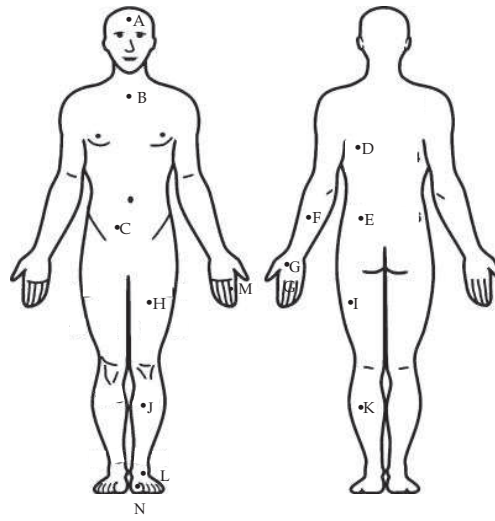


Figure C.1: Locations where thermistors were attached during orthopedic back surgery.

was used, adjusted to a six-point system according (leaving the contribution of the chest out, because of sterility reasons) to:

$$\begin{aligned} T_{\text{skin}}^* = & (0.07T_{\text{forehead}} + 0.14T_{\text{posterior forearm}} + 0.05T_{\text{hand}} + \\ & 0.19T_{\text{anterior thigh}} + 0.13T_{\text{anterior calf}} + 0.07T_{\text{foot}})/0.65 \end{aligned} \quad (\text{C.5})$$

Mean skin temperature: model

When comparing model results to experimental results always the same body sites and formula were used as during the experiment, given by equations (C.4) and (C.5). In case an isolated simulation was run, where no comparison with experimental data was performed, always equation (C.4) was used.

C.3 Ultrasound

Ultrasound imaging is a non-invasive measurement technique that can be used to visualize muscles, internal organs and blood vessels and to determine the size and structure of the same. The basic principle of ultrasound imaging is that a propagating wave partially reflects at the interface between different tissues. If these reflections are measured as a function of time, information is obtained on the position of tissue, assuming that the velocity of the wave in the medium is known. Ultrasound is not only used to visualize morphology or anatomy, but can also be applied to assess blood velocities. The principle of velocity measurements is based on the Doppler principle.

A sound wave is typically produced by a piezoelectric transducer encased in a probe. The sound waves have a frequency between 2 and 18 MHz. Materials on the face of the transducer enable the sound to be transmitted efficiently into the body (usually seeming to be a rubbery coating). In addition, a water-based gel is placed between the patient's skin and the probe. The sound wave is reflected or scattered at positions where transitions in acoustic impedances occur, caused by interfaces of different tissue structures. These reflections and scattered waves return to the transducer.

Ultrasound waves returned from the body have two information carriers: reflection and scattering. In case the dimension of the acoustic boundary layer is greater than the wavelength of the sound wave, the wave is reflected. If the dimension of the acoustic boundary layer is smaller than the wave transmitted, like blood particles, the ultrasound wave is scattered in all directions. The reflected power is typically 40 dB greater than scattered power. The reflected and back-scattered ultrasound pressure waves are transformed to radio frequent signals by a piezo crystal.

This radio frequent signal can be visualized in different ways. For instance, the M-mode displays the motion of tissue interfaces in one dimension as a function of time. In this way, vessel wall movement along one line through a vessel can be measured. In B-mode ultrasound imaging, a linear array of transducers scans a plane through the body. In this way a two-dimensional image, for instance a blood vessel, can be viewed on screen, see figure E.1(b).

As already mentioned, ultrasound can also be used in Doppler mode to assess blood flow velocity. The ultrasound wave is emitted with a certain frequency f into the body, where it is scattered by blood particles. The scattered wave has a different frequency than the emitted ultrasound wave, due to the Doppler effect. The difference between the ingoing and received frequency is the Doppler shift. The relation between the Doppler shift Δf of a particular sample volume and the velocity of the blood particles in this volume v is given by:

$$\Delta f = \frac{2v \cos \theta}{c} f \quad (\text{C.6})$$

Herein, c is the sound velocity of the medium and θ the angle between the emitted signal and the velocity direction. In this way, velocity as a function of time can be displayed (an example of a Doppler ultrasound image is given in figure E.1(a)). The Doppler shift falls in

the audible range and is often presented audibly using stereo speakers: this produces a very distinctive, pulsing sound.

C.4 Fat percentage

Fat percentage is determined with help of skinfold measurements. Measurements are taken with a special caliper by holding a fold of tissue with the left thumb and index finger at specific sites on the body: at the m. biceps brachii, m. triceps brachii, subscapular and suprailiacal (Durnin and Womersley, 1974). In each measurement, the thickness of a double layer of skin and its underlying adipose tissue (but not muscle tissue) is measured. Special tables are available to convert the measured tissue thicknesses to a body fat percentage.

C.5 Plethysmography

The principle of venous occlusion plethysmography is that a silicone-rubber capillary tube is filled with mercury and is attached around a limb. Venous outflow from the limb is stopped by means of a proximally placed cuff that is inflated to above venous pressure, but below arterial pressure (typically about 50 mm Hg). The increase of volume owing to venous occlusion and arterial inflow causes an increase in the girth of the limb L and a stretching of the capillary tube. This induces an increase in gauge resistance R . It is possible by this method to measure the change of girth of the limb during a certain time interval and to compute the change in cross-sectional area S and in volume of the limb segment under the gauge, assuming that the length of this segment has not been modified (Sigdell, 1969). This results in:

$$\frac{\Delta R}{R} = 2 \frac{\Delta L}{L} \simeq \frac{\Delta S}{S} \quad (\text{C.7})$$

By means of a sophisticated electrical system (Michaux et al., 1979), R and ΔR are measured at the same time. This permits the determination of the cross-sectional area change or the girth change due to arterial inflow. Often, plethysmography readings are expressed in ml blood/(100ml tissue · min).

C.6 Heart rate variability

Heart rate variability (HRV) is a measure of the beat-to-beat variations in heart rate. It is usually calculated by analyzing a time series of beat-to-beat intervals from an electrocardiographic record. A common method for analyzing heart variability data is the application of the discrete Fourier transform to the beat-to-beat interval time series. This provides an estimation of the amount of variation at specific frequencies. The heart rate variability power of a normal healthy individual shows three major peaks: 1) a very low frequency peak (<0.04 Hz) 2) a low frequency peak (0.04-0.15 Hz) and 3) a high frequency peak (0.15-0.40 Hz). The

very low frequency peaks reflect the influence of circulating neurohormones, thermoregulatory vasomotor tone and other slow variations in autonomic nerve activity. The low frequency fluctuations are mediated jointly by the parasympathetic nervous system and the sympathetic nervous system and the high frequency fluctuations are modulated by solely the parasympathetic system (Brenner et al., 1997). In this thesis, changes in the very low frequency component of the heart rate variability are studied in order to obtain information about the activity of the thermoregulatory vasomotor control system (chapter 5).

APPENDIX D

Biological zero in laser Doppler flowmetry

D.1 Introduction

The biological zero problem is a critical issue inherent in laser Doppler flowmetry. Under normal conditions the moving objects, measured with laser Doppler flowmetry, are mainly red blood cells, but white blood cell and platelets also contribute. The laser Doppler device does not react to fluid flow with a uniform refractive index such as blood plasma. On the background there is also a false movement component due to muscle cells, vessel walls and membranes. The manufacturer of the laser Doppler device used in current study (Perimed AB, Sweden) states: 'Under normal conditions, these false movement components are too small to be significant'.

However, during complete vessel occlusion when the flow of the cell drops to zero the laser Doppler signal does not reach zero. As an example, when measuring finger tip blood flow during a complete proximal occlusion, a residual perfusion value of several percent of the free-flow perfusion will be seen (Perimed, AB). In literature this effect is often referred to as biological zero.

Studies to the origin of the biological zero, point to the fact that the residual movement of the arrested blood cells are a large component of the biological zero but that movements of other aggregates in the tissue matrix may also contribute to a varying degree, depending on the circumstances under which the recordings are performed (Leahy et al., 1999). Other thoughts about the failure of flow arrest mentioned in literature are collateral circulation through bone, the continuous fluid flow into the lymphatic system or re-absorbance into the capillaries, and residual vasomotion (Kernick et al., 1999). But the general consensus remains that the biological zero signal primarily originates from Brownian motion and movement of red blood

cells (Kernick et al., 1999).

Knowledge of the biological zero is not very important when autoregulation is being assessed qualitatively. A decline in laser Doppler flux, whether corrected or not, can be interpreted as evidence of declining perfusion (Richards et al., 1995). However, when attempting to obtain quantitative changes in perfusion the signal is to some extent affected by the biological zero. When considering equation (D.1) as used in section 5.2.7 in which perfusion and temperature values were related to each other by the following equation:

$$\frac{w_{b,i}}{w_{b,i,0}} = Q_{\text{fit},i}^{\Delta T_i/10^{\circ\text{C}}} \quad (\text{D.1})$$

we see that the left hand side of the equation is affected by the biological zero signal. Instead of the $\frac{w_{b,i}}{w_{b,i,0}}$ you wanted to use, you are actually using a signal in which biological zero works as an additive:

$$\frac{w_{b,i} + w_{b,\text{zero}}}{w_{b,i,0} + w_{b,\text{zero}}} \quad (\text{D.2})$$

At low perfusion values, where $w_{b,i}$ is small, the fractional contribution of $w_{b,\text{zero}}$ to the numerator of equation (D.2) can be of interest. To get more insight in the biological zero problem and the way to deal with it, a literature survey was carried out. In addition, a pilot experiment was performed to determine the occluded perfusion values using cuff occlusion.

D.2 Literature

Experiments

Many experimental studies have been done on the question whether the biological zero flux should be subtracted from the normally measured flux signal. Abbot and Beck (1993) recommend that the biological zero should be measured wherever possible and practicable using temporary occlusion. Also Kernick et al. (1999) suggest to measure biological zero under each experimental condition by occlusion. They also found that the biological zero decreased linearly with decreasing temperature. In contrast, Janssen et al. (2007) found that the temperature effect on the biological zero was not significant in the temperature range 15°C-normal skin temperature at the forearm or palm. Richards et al. (1995) proposed a linear relation based on regression between arterial blood flow measured with ultrasound measurements and cerebral laser Doppler measurements to derive the biological zero when measuring brain perfusion.

When trying to determine the biological zero by using occlusion by cuff compression also other problems occur. The displacement of arterial blood by cuff compression may cause a transient increase in flow, while changes in interstitial fluid due to cuff compression and venous occlusion may effect the concentration of interstitial scatterers and might change the biological zero value (Kernick et al., 1999). Leahy et al. (1999) argue that when attempting to determine biological zero by occlusion, it must be ensured that arterial and venous occlusion occur at the same time in order to have similar blood volumes in the tissue as during normal

conditions.

Numerical investigation

In literature, also numerical studies were found that focussed on the biological zero problem. Zhong et al. (1998) motivated that the movement of moving blood cells is decomposed into a net translation and a random wandering (the latter representing the biological zero). With the help of Minkowski's inequality and probability density functions, he mathematically proved that the suggested subtraction of the biological zero is an invalid operation and will certainly cause underestimation of blood perfusion. Zhong et al. (1998) and later also Binzoni et al. (2004) proposed theoretical alternatives to subtract the biological zero from the laser Doppler flowmetry data, based on pure mathematical analysis. In Zhong et al.'s paper, a clinical example was shown to indicate the mistake (up to 50%) that is made when simply subtracting the biological zero (see figure D.1). The theoretical knowledge, described in their papers, should help manufacturers to improve the design of future laser Doppler flowmetry instruments.

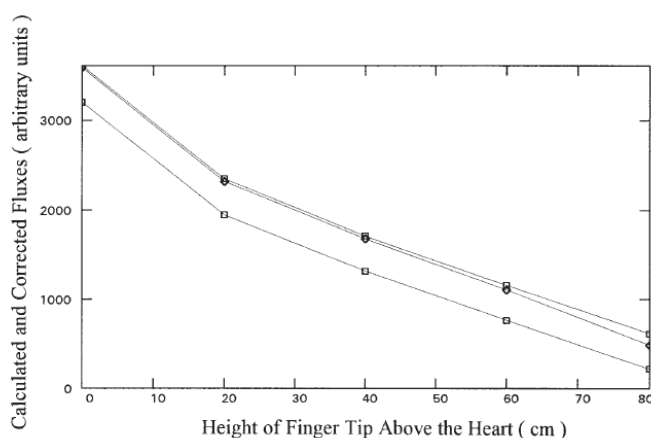


Figure D.1: From top to bottom: measured perfusion, calculated perfusion according to Zhong et al. (1998) and perfusion value when simply subtracting the biological zero. Perfusion values are taken of the fingertip while holding the hand at several distances above the heart level. The biological zero flux is measured with an inflated pressure cuff. Figure taken from Zhong et al. (1998).

D.3 Measurements

In a short experiment we measured the occluded perfusion value at two positions: 1) under the big toe and 2) at the forearm. The cuff was placed around the ankle for situation 1 and

around the upper arm for situation 2. A cuff pressure of 300 mm Hg, which was the maximal pressure in reach of the used cuff, was applied. Three subjects (2 males, 1 female) participated in this study. All of the subjects (male 1: age 34, 1.96m, 98 kg, male 2: age 25, 1.86m, 73 kg, female: age 27, 1.74 m, 63 kg) also have undergone the cooling cycle described in chapter 5. Occlusion measurements took place at room temperature. The subjects wore normal clothing. Results of the maximal and minimal observed perfusion values of the cooling cycle and the occluded perfusion value are given in table D.1.

Table D.1: Occlusion measurements results of 3 subjects: 2 males and 1 female. Maximal and minimal observed perfusion values of the cooling cycle are given as well as the occluded perfusion value.

subject	location	max. perfusion value	min. perfusion value	occluded perfusion value
1 (m)	toe	320.6	5.4	1.7
	arm	25.5	4.7	2.4
2 (m)	toe	202.0	6.0	1.6
	arm	17.8	3.0	1.7
3 (f)	toe	58.4	2.7	0.8
	arm	14.0	3.9	2.0

From table D.1 it follows that the occluded value contributes between 0.5-14.2% to the maximal perfusion signal, and between 26.7-51.2% to the minimal perfusion signal in the 3 subjects. These occluded values represent thus the overestimated upper limits of the fractional contribution of the biological zero to the laser Doppler signal. Reasons for that are:

- the pure mathematical arguments of Zhong et al. (1998) and Binzoni et al. (2004), that reject the validity of subtracting the biological zero.
- occlusion measurements took place at room temperature, while the minimal perfusion value was obtained at lower temperatures. According to Kernick et al. (1999) this might lead to overestimation of the biological zero.
- the design of the cuff only allowed gradual inflation. This means that venous occlusion started earlier than arterial occlusion, which can lead to blood accumulation and to an overestimation of the biological zero value.

D.4 Discussion

Although some investigators recommend to always subtract the biological zero from the measured value, no good working practical guidelines exist to obtain indubitable biological zero values. In literature, often raw laser Doppler signals are presented, also in more quantitatively oriented studies. We and other investigators struggle whether to subtract a polluted and

overestimated occluded perfusion value from the laser Doppler signal or only present the raw data.

In table D.1 it is seen that the occluded values that were measured ranged from 0.8-2.4 PU, while Janssen et al. (2007) observed values in the range 2.65-7.42 PU with similar measurement equipment. After studying the perfusion data in chapter 5, it was observed that one subject had a calf perfusion of 0.7 PU obtained at ambient temperature of 20°C. When subtracting the occluded perfusion values found in this study or the study of Janssen et al. (2007), it would lead to negative perfusion values, which are impossible.

Because all the unsolved obscurities about the biological zero issue, we think that it is yet not possible to subtract the biological zero in a good, consistent way. Therefore, in this thesis all laser Doppler perfusion data are the raw perfusion data, where no efforts were made to subtract artificially obtained biological zero values. But we are aware of the fact that results are subject to a deviation caused by the biological zero.

APPENDIX E

Leg blood flow calculations

E.1 Pulsatile flow

In order to derive the amount of leg blood flow with help of solely information of centerline and vessel diameter, as is the case in chapter 3, we need to go more deeply into understanding pulsatile blood flow. Womersley (1957) developed relations that describe pulsatile Newtonian flow in a rigid straight tube.

For analyzing the flow, the Navier-Stokes and mass conservation equations are considered in a cylindrical coordinate system, which yields:

$$\begin{aligned}\frac{\partial v_r}{\partial t} + v_r \frac{\partial v_r}{\partial r} + v_z \frac{\partial v_r}{\partial z} &= -\frac{1}{\rho} \frac{\partial p}{\partial r} + \nu \left(\frac{\partial}{\partial r} \left(\frac{1}{r} \frac{\partial}{\partial r} (r v_r) \right) + \frac{\partial^2 v_r}{\partial z^2} \right) \\ \frac{\partial v_z}{\partial t} + v_r \frac{\partial v_z}{\partial r} + v_z \frac{\partial v_z}{\partial z} &= -\frac{1}{\rho} \frac{\partial p}{\partial z} + \nu \left(\frac{1}{r} \frac{\partial}{\partial r} \left(r \frac{\partial}{\partial r} (v_z) \right) + \frac{\partial^2 v_z}{\partial z^2} \right) \\ \frac{1}{r} \frac{\partial}{\partial r} (r v_r) + \frac{\partial v_z}{\partial z} &= 0\end{aligned}\tag{E.1}$$

The average velocity in tangential direction equals 0, so the momentum equation and all derivatives in ϕ -direction are omitted. For fully developed flow $\frac{\partial}{\partial z} = 0$ and $v_r = 0$. This leads to:

$$\frac{\partial v_z}{\partial t} = -\frac{1}{\rho} \frac{\partial p}{\partial z} + \frac{\nu}{r} \frac{\partial}{\partial r} \left(r \frac{\partial v_z}{\partial r} \right)\tag{E.2}$$

Defining the dimensionless velocity as $v_z^* = \frac{v_z}{V}$, the dimensionless length as $r^* = \frac{r}{R}$ and $z^* = \frac{z}{R}$, the pressure can be scaled as $p^* = \frac{p}{\rho V^2}$ and the time can be scaled as $t^* = \omega t$, with V and ω characteristic flow velocity and the dominant flow frequency, respectively. Omitting

the asterix gives the equation of motion as:

$$\alpha^2 \frac{\partial v_z}{\partial t} = -\text{Re} \frac{\partial p}{\partial z} + \frac{1}{r} \frac{\partial}{\partial r} \left(r \frac{\partial v_z}{\partial r} \right) \quad (\text{E.3})$$

with Re the Reynoldsnumber given by:

$$\text{Re} = \frac{RV}{\nu} \quad (\text{E.4})$$

and α the Womersley number defined as:

$$\alpha = R \sqrt{\frac{\omega}{\nu}} \quad (\text{E.5})$$

Two dimensionless parameters are involved: the Womersley number (α) defining the ratio of the instationary inertia forces and the viscous forces and the Reynolds number (Re). In table E.1 the Womersley numbers for several sites in the arterial system are given, where the following blood properties are used in the calculation: a dynamic viscosity of $\mu = 3 \cdot 10^{-3}$ Pa · s and $\rho = 1069$ kgm⁻³. The kinematic viscosity (ν) is given by:

$$\nu = \frac{\mu}{\rho} \quad (\text{E.6})$$

The values in the table show that in the aorta and in the largest arteries the flow is expected to be inertia dominated and in the arterioles and capillaries the flow will be friction dominated.

Table E.1: Estimated Womersley number at several sites of the arterial system based on the first harmonic of the flow. Assumptions: $\mu = 3 \cdot 10^{-3}$ Pa · s, $\rho = 1.069 \cdot 10^3$ kgm⁻³ and $f=1$ Hz.

	R [mm]	α [-]
aorta	10	15
large arteries	4	6
small arteries	1	1.5
arterioles	0.1	0.15
capillaries	0.01	0.015

In case we consider the vessel wall as a rigid tube with radius R we can impose the no slip condition $v_z(R, t) = 0$ as boundary condition at the wall. Further we assume:

$$\frac{\partial p}{\partial z} = \sum_{n=0}^N \frac{\partial \hat{p}_n}{\partial z} e^{in\omega t} \quad (\text{E.7})$$

and

$$v_z = \sum_{n=0}^N \hat{v}_{z,n} e^{in\omega t} \quad (\text{E.8})$$

By substitution of equation (E.7)-(E.8) in the equation that describes the flow (E.2), analytic solutions can be derived for each harmonic. Superposition of these solutions then will give a solution for the flow velocity because (E.2) is linear in v_z .

Implementing equation (E.7) and (E.8) in equation (E.2) yields:

$$\nu \frac{\partial^2 \widehat{v}_z(r)}{\partial r^2} + \frac{\nu}{r} \frac{\partial \widehat{v}_z(r)}{\partial r} - i\omega \widehat{v}_z(r) = \frac{1}{\rho} \frac{\partial \widehat{p}}{\partial z} \quad (\text{E.9})$$

Womersley's solution (Womersley, 1957) for one component of this linear form of the Navier-Stokes equation for flow in a rigid, untapered artery reads:

$$\widehat{v}_z(r) = \frac{i}{\rho\omega} \frac{\partial \widehat{p}}{\partial z} \left[1 - \frac{J_0(i^{3/2}\alpha r/R)}{J_0(i^{3/2}\alpha)} \right] \quad (\text{E.10})$$

The end solution can be obtained by superposition of all harmonics of the signal.

According to Tarbell et al. (1982) and Tsangaris and Stergiopoulos (1988) in case the pressure gradient is not known, hemodynamic variables can be calculated from flow or from centerline velocity with the inverse Womersley method. The velocity profile in terms of the centerline velocity is then written as:

$$\widehat{v}_z(r) = \widehat{v}_c \left[\frac{J_0(i^{3/2}\alpha) - J_0(i^{3/2}\alpha r/R)}{J_0(i^{3/2}\alpha) - 1} \right] \quad (\text{E.11})$$

with \widehat{v}_c the centerline velocity in axial direction. The flowrate is then given by:

$$\widehat{q}(t) = \pi R^2 \widehat{v}_c \left[\frac{i^{3/2}\alpha J_0(i^{3/2}\alpha) - 2J_1(i^{3/2}\alpha)}{i^{3/2}\alpha J_0(i^{3/2}\alpha) - i^{3/2}\alpha} \right] \quad (\text{E.12})$$

Superposition of all flow harmonics leads to the total flow Q .

Data processing

The blood flow for each measurement was computed using the following procedure. The centerline velocity output (e.g. figure E.1(a)) was imported in MATLAB 6.5 (the Mathworks). A dedicated program was made to derive the flow rate from the measured centerline velocity. First, the velocity waveform was decomposed by Fourier analysis. The centerline velocity signal is then written in the following complex exponential Fast Fourier Transformed shape:

$$f(t) = \sum_{k=-\infty}^{\infty} F(k) e^{i\omega_k t} = \frac{A_0}{2} + \text{Re} \left[\sum_{k=1}^{\infty} 2F(k) e^{i\omega_k t} \right] \quad (\text{E.13})$$

with

$$F(k) = \frac{1}{2} (A_k - iB_k) \quad (\text{E.14})$$

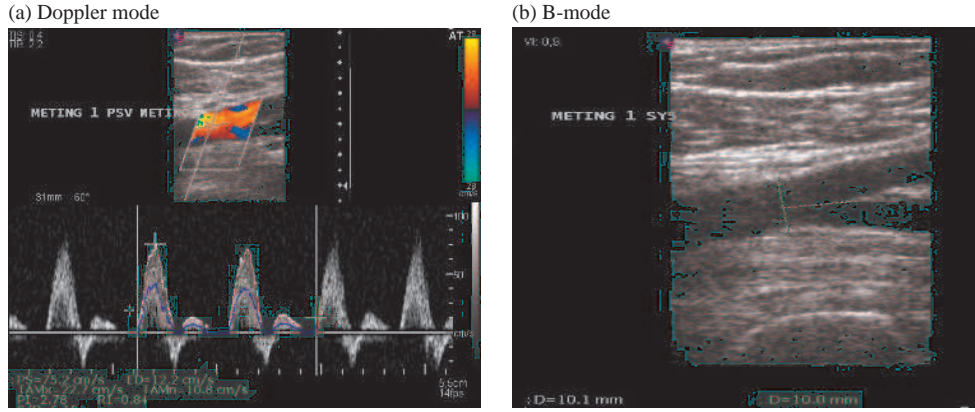


Figure E.1: (a) Centerline velocity output of the duplex device, (b) Diameter measurement of the femoral artery. Blood flow through the vessels is depicted in black. The measurements took place 1 cm from the bifurcation as is shown in the picture.

and

$$A_k = \frac{2}{T} \int_{-T/2}^{T/2} f(t) \cos(\omega_k t) dt \quad k = 0, 1, \dots \quad (\text{E.15})$$

$$B_k = \frac{2}{T} \int_{-T/2}^{T/2} f(t) \sin(\omega_k t) dt \quad k = 0, 1, \dots \quad (\text{E.16})$$

The solution of the velocity for a single harmonic pressure gradient is given by equation (E.10). However, because the pressure gradient was not measured, the velocity profile was calculated using the centerline velocity with help of the inverse Womersley method, as given by (E.11), while the flowrate was determined with help of (E.12). In figure E.2 an example is given of a flow profile (one heartbeat) in the femoral artery.

Evaluation of used assumptions

Equation (E.12) is based on rigid, straight tube walls. Only small errors are made when using this equation in our situation because the measured distension was small ($\sim 5\%$) and the tapering angle of the femoral artery is small. The distension found in the current research was in agreement with data collected from dogs by McDonald (1955), in which a maximum expansion at the end of systole was found to be less than 5%. Another finding of McDonald was that at the time of the maximal expansion (end of systole, as p is at its maximum and D is maximum) flow is at a minimum, or is retrograde. Therefore, the error that will be made by assuming the diameter of the artery constant will be small.

In the inverse Womersley theory the convective terms in (E.1) are omitted. For tapered vessels this may lead to errors (Cezeaux and Van Grondelle, 1997). Cezeaux showed that the errors

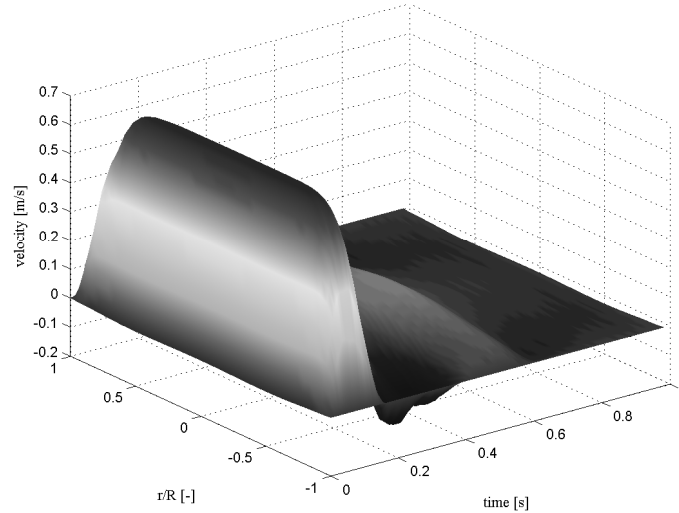


Figure E.2: Velocity profile as calculated with equation (E.11).

that are made when tapering is neglected are much smaller for the femoral artery (taper angle dog is 0.15°) than for the thoracic aorta (taper angle 0.738°). It therefore seems justified to use the relatively simple flow calculations based on the inverse Womersley methods to get estimates for the leg blood flow.

Another simplification made in our calculations is that blood viscosity was kept constant. In reality, blood is a non-Newtonian fluid, and its viscosity varies under differing shear conditions and under different temperature conditions. Furthermore, fluctuations may occur in hematocrit-level during cardiac pulmonary bypass, which also might have affected viscosity.

E.2 Non-pulsatile flow

During the main intervention to the heart, patients are connected to the heart lung machine. The heart lung machines that are used during this research use a continuous flow instead of a pulsating flow. This leads to a continuous blood pressure without systolic and diastolic stage. Consequently the second ultrasound measurements show a steady centerline velocity, with a constant vessel diameter. The following estimate is made for the Reynolds number:

$$\text{Re}_D = \frac{v_c D}{\nu} \sim 750 \quad (\text{E.17})$$

with $\mu = 3 \cdot 10^{-3} \text{Pa} \cdot \text{s} = 3 \cdot 10^{-3} \text{kgm}^{-1}\text{s}^{-1}$, $\rho = 1069 \text{kgm}^{-3}$, $\nu = 2.8 \cdot 10^{-6} \text{m}^2\text{s}^{-1}$, $D = 7 \cdot 10^{-3} \text{m}$ and $v_c = 0.3 \text{ms}^{-1}$. The flow entrance length is given by Bejan (1993):

$$\frac{X}{D} \simeq 0.05 \text{Re}_D \quad (\text{E.18})$$

This gives an entrance length of $X \sim 0.25 \text{m}$. As shown in figure E.1(b), the diameter of the vessel was measured at 1 cm before the bifurcation in the artery femoralis. This is approximately 30 cm from the position where the artery common illiac splits into the right and left femoral artery. We therefore consider the flow at the measurement position as a fully developed laminar flow. In that case the volume flow equals:

$$Q = \frac{\pi R^4}{8\mu} \frac{dp}{dz} = \pi R^2 u_{\text{bulk}} = \frac{1}{2} \pi R^2 v_c \quad (\text{E.19})$$

Samenvatting

Modelleren van Onderkoeling bij Patiënten die een Operatie Ondergaan

Door het gebruik van anesthetica wordt de warmtehuishouding van mensen verstoord. Bijna alle patiënten aan wie anesthesie is toegediend raken onderkoeld. Onder normale fysiologische condities wordt de temperatuurgradiënt tussen kern en periferie geregeld door tonische vasoconstrictie. Door toediening van anesthetica vermindert de vasoconstrictie-reactie. Zodoende vindt er warmteherverdeling plaats tussen de warme kern en de koude periferie. Dit leidt tot onderkoeling. De warmtebalans tijdens openhartoperaties verschilt van die van andere type operaties doordat bij hartoperaties het lichaam ook actief wordt gekoeld met behulp van een hart-longmachine. Op deze wijze worden het hart en de hersenen beter beschermd. Een nadeel is dat bij het opwarmen met behulp van de hart-longmachine meer warmte getransporteerd wordt naar het kerncompartiment dan naar perifeer weefsel, hetgeen leidt tot grote gradiënten tussen kern en periferie. Door interne warmteherverdeling na afkoppeling van de hart-longmachine ontstaat 'afterdrop': een temperatuur-afname van de kern. Afterdrop vertraagt het herstelproces van de patiënt. Daarom is er meer inzicht nodig in de veranderingen in thermoregulatie onder invloed van anesthesie en het effect dat diverse warmteprotocollen hebben op de temperatuurverdeling in het lichaam.

Het doel van dit proefschrift is het ontwikkelen van een computermodel dat in staat is om de warmtehuishouding tijdens anesthesie te beschrijven, waarbij de nadruk ligt op hartoperaties. Het ontwikkelde model bestaat uit drie delen: 1) het passieve gedeelte, waarin een vereenvoudigde beschrijving is gegeven van de menselijke geometrie door middel van diverse segmenten bestaande uit meer lagen en waarin alle passieve warmtewisselingsprocessen zijn verdisconteerd, 2) een actief gedeelte waarin thermoregulatie als functie van de hoeveelheid anesthesie is gemodelleerd en 3) submodellen, waardoor het mogelijk is om specifieke randvoorwaarden van de operatie en patiënt in het model mee te nemen.

Warmteoverdracht in het passieve stuk is gemodelleerd met behulp van de 'Pennes bio-

heat' vergelijking. Deze vergelijking is opgelost door gebruik te maken van ruimte-en tijds-discretisatieschema's. Er zijn randvoorwaarden geformuleerd om warmteverliezen door geleiding, convectie, straling en ademhaling te beschrijven. Verder zijn er situatie-specifieke submodellen ontworpen om de thermische invloed te beschrijven van de hart-longmachine, warmtedekens, warmtematrassen en warmteverlies door de wond.

Voor de ontwikkeling van het thermoregulatiemodel waren gegevens nodig van patiënten. Hiervoor werd een klinisch experiment uitgevoerd waarbij twee patiëntgroepen werden bestudeerd die een aortakleppoperatie ondergingen: één groep werd opgewarmd met behulp van warmtedekens en de andere zonder. De groep die opgewarmd was met warmtedekens bleek een significant kleinere afterdrop te vertonen.

Het actieve model is afgeleid door een farmacologisch model te combineren met de meetdata van de aortakleppatiënten. Het farmacologisch model is gebruikt om de propofolconcentratie (een vaak gebruikt anestheticum) in het bloed uit te rekenen. Anesthetica verlagen de drempel voor vasoconstrictie op lineaire wijze bij toenemende plasmaconcentratie. Door gebruik te maken van het farmacologisch model en de vasoconstrictiedrempel, die gevonden was in de aortakleppatiënten, is een relatie afgeleid waarin deze grootheden worden gekoppeld. Als eerste benadering zijn de versterkingsfactor en intensiteit van de vasoconstrictiereactie als een staprespons gemodelleerd. Dit model is gevalideerd door voorspelde temperaturen van het model te vergelijken met experimentele temperatuurdata.

Vervolgens is er een methode ontwikkeld om de vasoconstrictierelaties van het thermoregulatie model te verfijnen. Het bleek mogelijk te zijn om de intensiteit van de centraal overgebrachte sympathische vasoconstrictor tonus en de proportionele distributiecoëfficiënten van de verschillende lichaamsdelen te bepalen. De ontwikkelde methode is gebruikt in een studieprotocol waarin gezonde vrijwilligers deelnamen. Bij hen is op drie lichaamsdelen gemeten. Aanvullend zijn er gedetailleerde metingen bij vrijwilligers uitgevoerd om de proportionele waarden van de overige lichaamsdelen te bepalen. Het verfijnde model is geïmplementeerd in het totale thermische model van het menselijk lichaam. Het complete model is gevalideerd door het te vergelijken met experimentele data van gezonde vrijwilligers en van patiënten die een hartoperatie hebben ondergaan. In het algemeen bleken de simulaties goed overeen te komen met de metingen.

De voorspellende waarde van het ontwikkelde model is ook getest voor andere typen operaties, zoals voor orthopedische rugoperaties en diepgekoelde operaties waarbij de circulatie wordt stilgezet. Tot slot is het model gebruikt om het effect te bestuderen van diverse temperatuurprotocollen, zoals het gebruik van warmtedekens, het verhogen van de omgevingstemperatuur, het gebruik van warmtematrassen of het gebruiken van milde hypothermie in plaats van gematigde hypothermie.

Het model is in staat om temperatuurreacties te voorspellen van gezonde vrijwilligers en patiënten die een operatie ondergaan bij een temperatuur die ligt tussen gematigde hypothermie en normothermie met een huidtemperatuur tussen 30 en 34°C. Als de randvoorwaarden en begincondities goed bekend zijn voorspelt het model de kerntemperatuur met een typische afwijking van minder dan 0.5°C en huidtemperatuur met een afwijking van minder dan 1°C.

Summary

Modelling Hypothermia in Patients Undergoing Surgery

Anesthesia causes substantial perturbation in the human heat balance. Nearly all patients administered anesthesia become hypothermic. Under normal physiological conditions, the core-to-peripheral temperature gradient is maintained by tonic vasoconstriction. By the induction of anesthesia, vasoconstriction is impaired. Hence, heat redistribution takes place from the warm core to the colder periphery, leading to hypothermia. The heat balance during cardiac surgery differs from most other surgery types in that the body is also actively cooled by means of a heart lung machine to provide extra protection to the heart and the brain. A drawback of rewarming with help of the heart lung machine is that heat is transferred to the core compartment more quickly than to the peripheral tissues, leading to large core-to-periphery gradients. After decoupling the heart lung machine, internal redistribution of heat causes afterdrop: a decrease in temperature of the core. Afterdrop slows down the patient's recuperation process. Therefore, more knowledge is needed about the impaired thermoregulatory system during anesthesia and the effect of different protocols on temperature distribution.

This thesis focused on the development of a computer model that is able to describe heat transfer during anesthesia with the emphasis on cardiac surgery. The model that was developed consists of three parts: 1) a passive part, which gives a simplified description of the human geometry by means of a multi-segmental, multi-layered representation of the body, and that takes into account all passive heat transfer processes, 2) an active part that takes into account the thermoregulatory system as function of the amount of anesthesia and 3) submodels, through which it is possible to adjust the surgery and patient specific boundary conditions.

Heat transfer in the passive part was modelled with help of the Pennes' bioheat equation. This equation was solved using spatial and temporal discretization schemes. Boundary con-

ditions were formulated to account for conductive, convective, radiative and respiratory heat losses. Specific submodels were designed to model the thermal influences of the heart lung machine, forced-air heaters, heating mattress and the heat loss through the wound.

For the development of the thermoregulatory model, patient data was required. To that end, a clinical experiment was conducted. Two groups of aortic valve patients were studied: one group was rewarmed with and one group was rewarmed without using forced-air warmers. A significant reduction of afterdrop was observed in the group that was rewarmed with forced-air heating.

The active model was derived combining a pharmacological model and the data of the aortic valve patients. The pharmacological model was used to calculate the propofol (the most often used anesthetic agent) concentration in the blood. Anesthetic drugs lower the threshold for vasoconstriction in linear proportion to increased plasma concentration. A relation was derived between the anesthesia concentration calculated with help of the pharmacological model and the vasoconstriction threshold found in the aortic valve patients. As a first approach, a stepwise response was used to model the gain and intensity of the vasoconstriction response. The model was validated by comparing temperatures predicted by the computer model to experimental data.

A method was developed to refine the vasoconstriction relations of the thermoregulatory model. It was possible to determine the intensity of the centrally mediated sympathetic vasoconstrictor tone and the proportional distribution coefficients for vasoconstriction on different body parts. The method was used in a study protocol involving healthy volunteers for three body parts. In addition, detailed measurements were performed on volunteers to obtain proportionality values for the other body parts. The refined vasoconstriction model was added in the whole body thermal model. The complete model was validated against experimental data of healthy subjects and cardiac patients and showed in general good agreement.

The validity of the model was tested for other types of surgery, i.e. orthopedic back surgery and deep hypothermic surgery with circulatory arrest. Finally, the model was used to study the effect of different temperature protocols like the use of forced-air heaters, increasing the environmental temperature, using heating mattresses or using a mild hypothermia protocol instead of a moderate hypothermia protocol.

Overall, the model is able to predict temperature responses of healthy persons and patients undergoing surgery at temperatures between moderate hypothermia and normothermia, with skin temperatures ranging between 30 and 34°C. If the boundary conditions and initial conditions are accurately known, the model predicts core temperature within typically 0.5°C and skin temperature within typically 1°C.

Dankwoord

Bijna klaar! Na tien jaar studie aan de universiteit sta ik op het punt om een periode van mijn leven af te sluiten, terwijl een nieuwe periode gaat beginnen. Dit proefschrift is het resultaat van het werk dat ik de laatste vier jaar heb gedaan en waarop ik bijzonder trots ben. Ik wil dan ook graag de mensen bedanken die me de afgelopen vier jaar hebben gesteund bij de verwezenlijking van mijn proefschrift.

Ten eerste wil ik mijn promotoren Anton van Steenhoven en Bas de Mol bedanken dat ze voor mij de kans en mogelijkheid gecreëerd hebben om dit zeer uitdagende en afwisselende multidisciplinaire project aan te gaan. De maandelijkse besprekingen met Anton leidden veelvuldig tot nieuwe ideeën en tot een hogere motivatie. Ook in tijden dat het tegengaat met het onderzoek kon ik altijd rekenen op zijn steun en een duwtje in de rug om te komen tot een oplossing. Bas zorgde altijd voor een hoop enthousiasme en veel nieuwe ideeën. Zonder zijn hulp waren de experimenten, zoals beschreven in hoofdstuk 3, nooit tot stand gekomen. Voor mij was de mogelijkheid om als werktuigbouwer in de operatiekamer metingen uit te voeren bij patiënten, een unieke ervaring.

Uiteraard hebben ook de inhoudelijke discussies en aanmoedigingen van in het bijzonder Wouter, Gerard en later zeker ook Arjan bijgedragen aan de totstandkoming van dit proefschrift. Wouter's praktische ervaring, biologische kennis en enorme literatuuroverzicht gaven altijd genoeg stof tot nadenken en maakte hem een enorm goede sparringpartner. Gerard heeft me in het eerste jaar van mijn promotie een vliegende start gegeven wat betreft het model. Ook kon ik bij hem terecht met al mijn vragen. In het tweede jaar heeft Arjan de technische begeleiding overgenomen van Gerard. Zijn deur stond altijd voor mij open voor zowel inhoudelijke als niet-inhoudelijke discussies. Zelfs bij de bespreking van mijn vragen, waarbij ik soms gaandeweg zelf niet meer begreep wat de vraag was, lukte het vaak om tot nieuwe inzichten te komen.

Bij de metingen die op maar liefst vier locaties (TU/e, AMC, UM en AZM) hebben plaatsgevonden ben ik geholpen door velen: de technische staf en secretaresses van de divisie TFE

op de TU/e, de technische dienst en operatie teams van de OK van het AMC, het secretariaat cardio-thoracale chirurgie AMC, Aart Terpstra van het AMC, Boris, Sander, Loek en Paul van UM en tot slot dr. Andre van Ooij, Maurice Theunissen en het operatie team van het AZM.

Ik kijk met veel plezier terug op het contact met mijn collega's en mede-koffiedrinkers: Arjan, Gerard, Francis, Frank, Henk, Kiran, Ilhan, Srinidhi, Rudi en Pieter. De zes laatstgenoemden inclusief mezelf vormen tevens de 'event'-club. Onder de deskundige leiding van de aangewezen eventmanager hebben reeds vele leuke en gezellige activiteiten plaatsgevonden en ik hoop dat er nog vele zullen volgen. Ook op het sportieve vlak was er altijd genoeg te doen met de groep aio's van Energie Technologie: tijdens de lunchpauzes en op woensdagavond waren oorspronkelijk Ilhan en ik regelmatig te vinden in het zwembad, maar de zwemclub werd al snel uitgebreid met Kiran, Srinidhi en Pieter. En in de lunchpauzes zijn Henk en Arjan ook regelmatig van de partij geweest.

Ook mijn kamergenoten wil ik bedanken voor de fijne tijd. De eerste jaren deelde ik mijn kamer met Francis. We hebben heel wat afgekletst over de meest uiteenlopende onderwerpen, veelal onder het genot van een lekker kopje thee. Met veel plezier denk ik terug aan onze dagelijkse gesprekken en de bijbehorende lach. Later werd Kiran mijn kamergenoot. Ook hij bracht een hoop vrolijkheid mee en we hebben heel veel leuke en soms luidruchtige (sorry, Ilhan en Rudi...) discussies gevoerd over India, Nederland, taal en onderzoek doen: Dhanyaavaada. Ook Boris, die af en toe onze kamer deelde, zorgde altijd voor een welkome afwisseling. Inhoudelijk, maar ook niet-inhoudelijk was hij een verfrissende gesprekspartner. Verder wil ik hem bedanken voor zijn praktische hulp en meedenken bij de experimenten, zoals beschreven in hoofdstuk 5.

Bovenal wil ik ook de mensen bedanken uit mijn omgeving die in deze periode altijd interesse hadden in hoe het ging met mij en de voortgang van het onderzoek, in het bijzonder mijn broer Ivo en de ouders van Maurice.

Mijn speciale dank gaat uit naar mijn ouders. Ze stonden altijd klaar voor mij en hebben me mijn hele leven onvoorwaardelijk gesteund en geholpen in mijn keuzes. Last but not least: Maurice, dank je wel voor alle liefde, steun en vertrouwen dat je in me hebt.

Natascha

Veldhoven, augustus 2008

Publications

Journal papers

- Van Marken Lichtenbelt W.D., Daanen H.A.M. , Wouters L., Fronczek R., Raymann R.J.E.M., Severens N.M.W. and Van Someren E.J.W. (2006). Evaluation of wireless determination of skin temperature using iButtons. *Physiol Behav*, 88:489–497.
- Severens N.M.W, Van Marken Lichtenbelt W.D., Frijns A.J.H., Van Steenhoven A.A., De Mol B.A.J.M and Sessler D.I. (2007). A model to predict patient temperature during cardiac surgery. *Phys Med Biol*, 52:5131–5145.
- Severens N.M.W, Van Marken Lichtenbelt W.D., Van Leeuwen G.M.J., Frijns A.J.H., Van Steenhoven A.A., De Mol B.A.J.M, Van Wezel H.B. and Veldman D.J. (2007). Effect of forced-air heaters on perfusion and temperature distribution during and after open-heart surgery. *Eur J Cardiothorac Surg*, 32(6):888–895.
- Tindall M.J., Peletier M.A., Severens N.M.W., Veldman D.J. and De Mol B.A.J.M. (2008). Understanding post-operative temperature drop in cardiac surgery: a mathematical model. *Math Med Biol*, in press.

Professional publication

- Severens N.M.W. and Peletier, M.A. (2006) Brainstormen voor bruikbare wiskunde: Modelvorming van het koel- en opwarmproces van patiënten tijdens openhartoperaties. *NAW*, 5/7(1): 44-51.

Refereed proceedings

- Severens N.M.W., Van Marken Lichtenbelt W.D., Van Leeuwen G.M.J., Van Steenhoven A.A. and De Mol B.A.J.M. (2005). Heat transfer in cardiac surgery- a numerical and experimental approach, in *Abiomed/Ercoftac Workshop on Blood Flow Modelling and Diagnostics*; Editors: Kowaleski T., Warschau, Poland, LN 6: 439-450.
- Tindall M.J., Peletier M.A., Aichison J.M., Mourik S. and Severens N.M.W. (2005). The mathematical modelling of cooling and rewarming patients during cardiac surgery, in *Proceedings of the 52nd European Study Group Mathematics with Industry*; Editors: J. Bouwe van den Berg J., Bhulai S., Hulshof J., Koole G., Quant G. and Williams J.F., Amsterdam, The Netherlands: 39-52.
- Severens N.M.W., Van Marken Lichtenbelt W.D., Frijns A.J.H., Van Steenhoven A.A. and De Mol B.A.J.M. (2007). Modelling patient temperature to reduce afterdrop after cardiac surgery, in *12th International Conference on Environmental Ergonomics*; Editors: Mekjavic I.B., Kounalakis, S.N. and Taylor N.A.S., Piran, Slovenia.

Curriculum Vitae

22 December 1979	Born in Brunssum
1984–1992	Primary school, Basisschool De Tweesprong, Schinveld
1992–1998	Gymnasium (Dutch Pre-University education), R.K.S.G. Serviam, Sittard: <i>cum laude</i>
1998–2002	B.Sc. Mechanical Engineering, University of Technology Eindhoven: <i>cum laude</i>
2002–2004	M.Sc. Mechanical Engineering, University of Technology Eindhoven: <i>cum laude</i>
2004–till date	Ph.D. Student, University of Technology Eindhoven and Academic Medical Center, Amsterdam